EXAMINATION OF ABNORMAL DOLICHOL METABOLISM
IN INFANTILE BATTEN DISEASE CAUSED BY
PALMITOYL PROTEIN THIOESTERASE-1 (PPT1) DEFICIENCY

APPROVED BY SUPERVISORY COMMITTEE

Committee Chairperson's Name _____
Mark A. Lehrman, Ph.D.
Professor of Pharmacology

Committee Member (Advisor)'s Name _____
Sandra L. Hofmann, M.D., Ph.D.
Professor of Internal Medicine and Molecular Genetics

Committee Member's Name _____
Joel M. Goodman, Ph.D.
Professor of Pharmacology

Committee Member's Name _____
Paul C. Sternweis, Ph.D.
Professor of Pharmacology

DEDICATION

To our Heavenly Father, who created me to glorify His name.

To my baby sister, who is in Heaven in peace.

To my parents, who always believe in me and support me.

To my wife Judy and my children Timothy and Rachel, who are inspirations of my life.

EXAMINATION OF ABNORMAL DOLICHOL METABOLISM
IN INFANTILE BATTEN DISEASE CAUSED BY
PALMITOYL PROTEIN THIOESTERASE-1 (PPT1) DEFICIENCY

by

Steve Kyungrae Cho

DISSERTATION

Presented to the Faculty of the Graduate School of Biomedical Sciences

The University of Texas Southwestern Medical Center at Dallas

In Partial Fulfillment of the Requirements

For the Degree of

DOCTOR OF PHILOSOPHY

The University of Texas Southwestern Medical Center at Dallas

Dallas, Texas

August, 2004

ACKNOWLEDGEMENTS

There are numerous people who have helped me during my long journey here at UT Southwestern. First of all, I would like to thank my mentor, Dr. Sandy Hofmann, for her guidance and advice on my dissertation work. I have learned many things from her throughout the years in her lab. She taught me how to become a good scientist and how to think like a good scientist. I am also grateful to my dissertation committee members, Dr. Mark Lehrman, Dr. Joel Goodman and Dr. Paul Sternweis for their invaluable advice and support.

I was fortunate to have so many good friends and colleagues who believed in me. I would like to thank Hofmann lab members, Drs. Laura Lu, Amit Das, Praveena Gupta, Andrea Qiao and Hasige Sathish, for their advice, assistance, encouragement and friendship. I am particularly grateful to Dr. Ningguo Gao in Lehrman's lab who has helped me to finish my last project. I also would like to thank our collaborators, Dr. Skip Waechter and Dr. Jeff Rush at University of Kentucky, who allowed me to visit their lab to perform experiments.

I would like to thank Ms. Carla Childers, Cell Regulation Program Coordinator, for her administrative assistance during my years of graduate school.

Finally, I would like to thank my wonderful parents. They always have confidence in me and support me, and have never doubted that I would finish this journey. My wife Judy and my children, Timothy and Rachel, have stood beside me during this long journey. They have been my motivation and inspiration.

Steve K. Cho

August 2004

EXAMINATION OF ABNORMAL DOLICHOL METABOLISM
IN INFANTILE BATTEN DISEASE CAUSED BY
PALMITOYL PROTEIN THIOESTERASE-1 (PPT1) DEFICIENCY

Publication No. _____

Steve Kyungrae Cho, Ph.D.

The University of Texas Southwestern Medical Center at Dallas, 2004

Supervising Professor: Sandra L. Hofmann, M.D., Ph.D.

ABSTRACT

The neuronal ceroid lipofuscinosis (NCLs, also known collectively as Batten disease) are a group of lysosomal storage disorders characterized by the accumulation of autofluorescent storage material in the brain. Although a number of genes underlying different forms of NCL have been cloned, the underlying mechanism for the neurodegeneration is still unknown. The most severe form of NCL (infantile NCL) is caused by mutations in the *CLN1/PPT1* gene, which encodes a soluble lysosomal hydrolase (palmitoyl protein thioesterase-1) that removes fatty acids from lipid modified proteins in the lysosome. It has been postulated that abnormal dolichol metabolism might be involved in NCL pathogenesis because high levels of dolichol phosphate (Dol-P) and lipid linked

oligosaccharides (LLOs) accumulate in NCL patients including infantile NCL. Here, a possible relationship between fatty acid and dolichol metabolism in the neuropathogenesis of NCL has been explored by analyzing LLOs from mouse models of Batten disease and other non-NCL lysosomal storage diseases (LSDs), and by characterizing a unique fusion protein consisting of PPT1 and a dolichol metabolizing enzyme (DOLPP1) in *Schizosaccharomyces pombe*, which we named *pdf1* (for *ppt1-dolpp1 fusion1*).

To do this, first, I characterized *S. pombe pdf1* by ablating the *pdf1* gene and studying the function of each of the proteins (PPT1 and DOLPP1) independently. These results revealed that *PPT1* and *DOLPP1* may be co-regulated in lower organisms but the functional relationship in higher eukaryotes remains unclear.

To further explore the relationship between *PPT1* and *DOLPP1* in mammalian cells, I cloned the mammalian ortholog of *DOLPP1* and subsequently characterized the mouse Dolpp1p.

Finally, I characterized and analyzed LLOs in various mouse models of NCL by FACE (fluorophore assisted carbohydrate electrophoresis). It was shown that LLOs accumulated in PPT1-deficient mouse brain and the level of LLO accumulation was 14.5-fold higher as compared to wild type brain. Despite the striking accumulation of LLOs in PPT1-deficient brain compared to age-matched controls, I also found that the LLOs encompassed only 0.3% of the autofluorescent storage material by mass. Therefore, the abnormal dolichol catabolism is most likely a secondary phenotype to PPT1 deficiency during the pathogenesis of infantile Batten disease.

TABLE OF CONTENTS

PRIOR PUBLICATIONS

Cho, S. K., N. Gao, D. A. Pearce, M. A. Lehrman and S. L. Hofmann (2004b). "Dolichol-pyrophosphoryl oligosaccharide accumulation in mouse models of Batten Disease." *Submitted*.

Cho, S. K. and S. L. Hofmann (2004a). "pdf1, a palmitoyl protein thioesterase 1 Ortholog in Schizosaccharomyces pombe: a yeast model of infantile Batten disease." *Eukaryot Cell* 3(2): 302-10.

Rush, J. S., **S. K. Cho**, S. Jiang, S. L. Hofmann and C. J. Waechter (2002). "Identification and characterization of a cDNA encoding a dolichyl pyrophosphate phosphatase located in the endoplasmic reticulum of mammalian cells." *J Biol Chem* 277(47): 45226-34.

Hofmann, S. L., A. Atashband, **S. K. Cho**, A. K. Das, P. Gupta and J. Y. Lu (2002). "Neuronal ceroid lipofuscinoses caused by defects in soluble lysosomal enzymes (CLN1 and CLN2)." *Curr Mol Med* 2(5): 423-37.

Takeuchi, S., **S. K. Cho**, T. Seriu, M. Koike, C. R. Bartram, A. Reiter, M. Schrappe, C. Takeuchi, H. Taguchi and H. P. Koeffler (1999). "Identification of three distinct regions of deletion on the long arm of chromosome 11 in childhood acute lymphoblastic leukemia." *Oncogene* 18(51): 7387-8.

Koshizuka, K., M. Koike, H. Asou, **S. K. Cho**, T. Stephen, R. K. Rude, L. Binderup, M. Uskokovic and H. P. Koeffler (1999). "Combined effect of vitamin D3 analogs and paclitaxel on the growth of MCF-7 breast cancer cells in vivo." *Breast Cancer Res Treat* 53(2): 113-20.

de Vos, S., D. B. Kohn, **S. K. Cho**, W. H. McBride, J. W. Said and H. P. Koeffler (1998). "Immunotherapy against murine leukemia." *Leukemia* 12(3): 401-5.

Takeuchi, S., T. Seriu, T. Tasaka, M. Koike, **S. K. Cho**, S. Park, J. Slater, I. Mufti, Y. Hatta, I. Miyoshi, C. R. Bartram and H. P. Koeffler (1997). "Microsatellite instability and other molecular abnormalities in childhood acute lymphoblastic leukaemia." *Br J Haematol* 98(1): 134-9.

de Vos, S., M. I. Dawson, S. Holden, T. Le, A. Wang, **S. K. Cho**, D. L. Chen and H. P. Koeffler (1997a). "Effects of retinoid X receptor-selective ligands on proliferation of prostate cancer cells." *Prostate* 32(2): 115-21.

de Vos, S., S. Holden, D. Heber, E. Elstner, L. Binderup, M. Uskokovic, B. Rude, D. L. Chen, J. Le, **S. K. Cho** and H. P. Koeffler (1997b). "Effects of potent vitamin D3 analogs on clonal proliferation of human prostate cancer cell lines." *Prostate* 31(2): 77-83.

Said, W., K. Chien, S. Takeuchi, T. Tasaka, H. Asou, **S. K. Cho**, S. de Vos, E. Cesarman, D. M. Knowles and H. P. Koeffler (1996). "Kaposi's sarcoma-associated herpesvirus (KSHV or HHV8) in primary effusion lymphoma: ultrastructural demonstration of herpesvirus in lymphoma cells." *Blood* 87(12): 4937-43.

de Vos, S., C. W. Miller, S. Takeuchi, A. F. Gombart, **S. K. Cho** and H. P. Koeffler (1995a). "Alterations of CDKN2 (p16) in non-small cell lung cancer." *Genes Chromosomes Cancer* 14(3): 164-70.

de Vos, S., C. J. Epstein, E. Carlson, **S. K. Cho** and H. P. Koeffler (1995b). "Transgenic mice overexpressing human copper/zinc-superoxide dismutase (Cu/Zn SOD) are not resistant to endotoxic shock." *Biochem Biophys Res Commun* 208(2): 523-31.

LIST OF FIGURES

LIST OF TABLES

LIST OF DEFINITIONS

ANDS	7-amino-1, 3-naphthalenedisulfonic acid
bp	Base pair
cDNA	Complementary deoxyribonucleic acid sequence
CHO	Chinese hamster ovary
Ci	Curie
CoA	Coenzyme A
Cpm	Counts per minute
CPY	Carboxy peptidase Y
CV	Curvilinear profiles
Dol	Dolichol
Dol-P	Dolichol phosphate
Dol-P-P	Dolichol pyrophosphate
DOLPP	Dolichol pyrophosphate phosphatase
Dol-PP-OS	Dolichol pyrophosphoryl oligosaccharide
DTT	Dithiothreitol
ECL	Enhanced Chemiluminescence
EM	Electron microscopy
EMM	Edinburgh minimal media
Endo H	Endoglycosidase H
ER	Endoplasmic reticulum
EST	Expressed sequence tag
5'FOA	5-fluoroorotic acid
FACE	Fluorophore-assisted carbohydrate electrophoresis
FP	Fingerprint profiles
g	Standard earth gravitational unit
Glc	Glucose
GlcNAc	N-acetyl-$_D$-glucosamine

GPI-anchor	Glucose phosphate inositol anchor
GROD	Granular osmophilic deposits
h	Hour
HEPES	N-[2-hydroxyethyl]piperazine-N'-[2-ethanesulfonic acid]
HPLC	High pressure liquid chromatography
IgG	Immunoglobulin G
kDa	Kilodalton
LLO	Lipid linked oligosaccharide
LSD	Lysosomal storage disease
M	Molar
Man	Mannose
ME	Malt extract
MeOH	Methanol
mCi	Millicurie
mg	Milligram
min	Minute
ml	Milliliter
mM	Millimolar
M_r	Relative mobility
μg	Microgram
μl	Microliter
μM	Micromolar
NADPH	Reduced nicotinamide adenine dinucleotide
NCL	Neuronal ceroid lipofuscinosis
ORF	Open reading frame
PA	Phosphatidic acid
PAS	Periodic acid-Schiff reagent
PCR	Polymerase chain reaction
PPT	Palmitoyl-protein thioesterase

PBS	Phosphate-buffered saline
Pmole	Picomole
RL	Rectilinear complexes
rpm	Revolutions per minute
s	Second
SDS	Sodium dodecylsulfate
SDS-PAGE	Sodium dodecylsulfate polyacrylamide gel electrophoresis
Tris	Tris(hydroxylmethl)aminomethane
TUNEL	Terminal dUTP nick end-labeling
YES	Yeast extract plus supplement

CHAPTER ONE

Introduction

1.1 Hypothesis

As is true of many lysosomal storage disorders, the mechanism whereby the underlying enzyme deficiency leads to organ pathology in NCL (neuronal ceroid lipofuscinosis) is poorly understood. The storage material (granular osmophilic deposits, GROD) accumulating in infantile NCL patients' brain and other peripheral tissues is heterogeneous and complex, largely defying attempts at characterization.

PPT1 deficiency is the underlying cause of infantile NCL ((Vesa *et al.* 1995). PPT ortholog in *S. pombe* is a fusion gene with a partner gene, which is an ortholog of mouse *DOLPP1* that encodes dolichol pyrophosphate phosphatase-1 (Cho *et al.* 2004). Dolpp1p is an enzyme that is implicated in dolichol recycling during *N*-glycosylation process (Rush *et al.* 2002). Furthermore, there have been numerous reports that high level of dolichol phosphate and its oligosaccharide intermediates are accumulated in the brain tissue of NCL patients including infantile NCL (Keller *et al.* 1984; Hall *et al.* 1985; Hall *et al.* 1987; Hall *et al.* 1988; Hall *et al.* 1992). All of these observations have led me to the hypothesis that abnormal dolichol metabolism may be involved in the pathogenesis of infantile NCL.

Therefore, throughout the next three chapters of this dissertation, I will examine the function of *S. pombe* pdf1, an ortholog of *PPT1* in fission yeast, by exploring whether Ppt1p and Dolpp1p are functioning as a single polypeptide that physically interact with each other or two proteins that eventually separate to function independently of each other. I will also

investigate the possible link between these two proteins in mammalian cells by cloning and characterizing the mammalian ortholog of DOLPP1 from a mouse brain cDNA library. I will examine the subcellular localization of mammalian Dolpp1p to see whether these two proteins are able to physically interact in higher eukaryotic cells. Finally, I will analyze the accumulation of lipid linked oligosaccharides (LLOs) in infantile NCL using a PPT1 knockout mouse model, other mouse models of NCLs and non-NCL lysosomal storage disease (LSD) mouse models which cause neuronal degeneration.

1.2 Neuronal Ceroid Lipofuscinosis

1.2.1 History

The neuronal ceroid lipofuscinoses (NCL, also known collectively as Batten disease) are a group of progressive inherited neurodegenerative disorders of children characterized by the accumulation of autofluorescent inclusion bodies in the brain and other tissues (Mitchison et al. 2001; Hofmann 2002). In 1969, Zeman and Dyken first used the term 'neuronal ceroid lipofuscinosis' to distinguish the group of diseases, now known as NCL, from the gangliosidoses (Zeman et al. 1969). The historical description of the disorder was illustrated much earlier in the 19th century by Stengel (Stengel 1826) in a case report of four siblings who suffered blindness, epilepsy, and motor dysfunction (Wisniewski *et al.* 2001a).

The pathological assessments including electron microscopic (EM) studies on autopsy brain tissues from NCL patients have revealed unique pathological markers for different subtypes of NCL along with different ages of onset of symptoms. These four classical classifications are infantile, late-infantile, juvenile and adult NCLs. Each class of

NCL is represented by a unique pattern of lysosomal inclusion bodies including granular osmophilic deposits (GROD), curvilinear profiles (CV), fingerprint profiles (FP) and rectilinear complexes (RL), respectively (Wisniewski *et al.* 2001b).

In 1995, mutations in a lysosomal enzyme called palmitoyl protein thioesterase-1 were discovered to be the underlying cause of the infantile form of NCL (Vesa et al. 1995). Since the first gene (PPT1) was cloned for NCLs, rapid technical advances in molecular genetics and biochemistry allowed the identification of five more genes that are responsible for NCLs, demanding a new classification system. Therefore, a new gene designation (CLN) was introduced for NCLs including the four classical forms. To date, eight different forms of NCL are distinguished (CLN1 to CLN8) as summarized in Table 1.1.

CLN1/PPT1, CLN2/TPPI, CLN3 and CLN4 were assigned for the four classical forms of NCLs; infantile, late-infantile, juvenile and adult, respectively (Lerner et al. 1995; Vesa et al. 1995; Schriner et al. 1996; Sharp et al. 1997; Sleat et al. 1997). CLN4 is a reserved gene designation for adult-onset autosomal dominant NCL; the genetic locus has not been mapped (Kufs 1925; Das et al. 1998). The locus for CLN7, which represents the Turkish variant of late-infantile NCL, also has not been mapped, and CLN7 may be an allelic variant of one of the NCLs (Ranta et al. 1999; Mitchell et al. 2001). CLN5, CLN6 and CLN8 represent Finnish variant late-infantile NCL, Gypsy/Indian late-infantile NCL and Northern epilepsy with mental retardation, respectively (Savukoski et al. 1994; Sharp et al. 1997; Savukoski et al. 1998; Ranta et al. 1999).

1.2.2   Dolichol in NCLs

Table 1.1 Classifications of NCLs

Gene	Form	Locus	Protein encoding	Characteristics	[f,g]Ref.
CLN1	Infantile NCL	1p32	Palmitoyl protein thioesterase-1	Blindness Motor deterioration [a]GROD	
CLN2	Late-infantile NCL	11p15	Tripeptidyl peptidase-I	Seizures Motor deterioration [b]CV	
CLN3	Juvenile NCL	16p12	Lysosomal transmembrane protein	Visual loss and seizures Motor dysfunction [c]FP	
CLN4	Adult NCL	unknown	unknown	Myoclonic epilepsy Autosomal dominant Dementia, [d]RL / [e]Mixed	
CLN5	Finnish variant late-infantile NCL	13q22	Lysosomal transmembrane protein	Motor deterioration Visual loss	
CLN6	Gypsy/Indian late-infantile NCL	15q21-23	Putative transmembrane protein	Visual loss Seizures Motor	
CLN7	Turikish variant late-infantile NCL	unknown	unknown	Motor dysfunction Seizure	
CLN8	Epilepsy with mental retardation	8p23	Putative transmembrane protein	Seizure Mental deterioration	

[a]GROD: granular osmophilc deposits; [b]CV: curvilinear profiles; [c]FP: fingerprint profiles; [d]RL: rectilinear complexes; [e]Mixed: mixture of GROD, CV, FP and RL.
[f,g]Ref: reviewed in (Elleder et al. 1999; Wisniewski et al. 2001a).

Ng Ying Kin *et al* reported significant amounts of dolichol in the storage material accumulating in human cerebral cortex from infantile, late-infantile and juvenile forms of NCL patients as compared to age-matched controls, implying possible defects in dolichol metabolism in NCL patients (Ng Ying Kin *et al.* 1983). Dolichols are α-saturated, long chain polyprenols with chain length of 14-21 isoprene units, as shown in Figure 1.1 (Schenk *et al.* 2001).
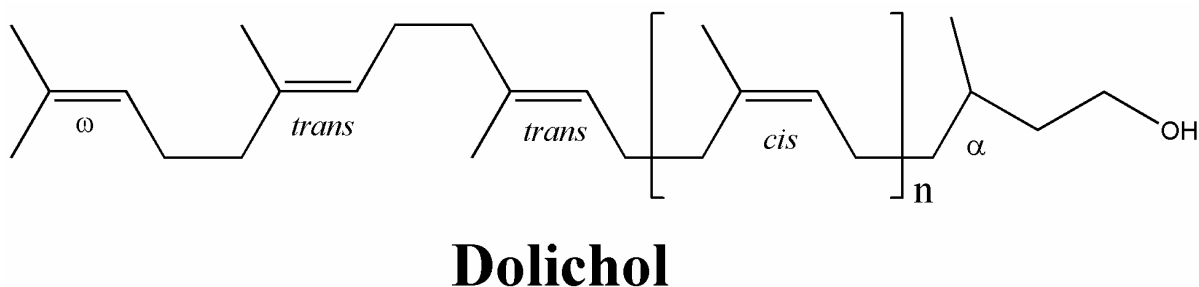
Dolichol

Figure 1.1 Structure of Dolichol

In the early 1960's dolichols were first described as a main component of unsaponifiable lipid in animal tissues during studies on the polyisoprenoid side chain of ubiquinone (Pennock *et al.* 1960). Dolichols are found in almost all membranes in eukaryotic cells and tissues, and the amount of dolichols varies from 5 to 150 μg/g depending on tissue types in different animals (Valtersson *et al.* 1985).

Dolichol exists in three different forms of in the cell: free dolichol, dolichol esterified with fatty acids and phosphorylated dolichol (Hemming 1992). The phosphorylated dolichol (Dol-P) and its oligosaccharyl derivatives (Dol-PP-OS) play a key role as a lipid carrier during the biosynthesis of asparagine (N)-linked glycoproteins in the endoplasmic reticulum

(ER). Eukaryotic cells have a very small amount of Dol-P as compared to total dolichols and the pool size of Dol-P is rate-limiting in glycosylation reactions in the ER (Carson *et al.* 1981; Eggens *et al.* 1984). Free dolichols and esterified dolichols have been postulated to be involved in the modulation of membrane fluidity, stability and permeability (Valtersson *et al.* 1985; Wood *et al.* 1986; Monti *et al.* 1987).

Elevated levels of dolichol, however, have also been reported in brains of the elderly, suggesting dolichol accumulation as a marker of aging (Pullarkat *et al.* 1982). Dolichol levels in normal human brain increases more than 10-fold from 18 μg/g (6-year-old) to 263 μg/g (68-year-old), and a similar pattern of increase has also been seen in mouse and rat brain with age (Ng Ying Kin *et al.* 1983; Pullarkat *et al.* 1984). Later, the level of dolichol in Alzheimer patients (384 ± 90.7 μg/g) has also shown to be increased significantly compared to age-matched control brains (190 ± 48.9 μg/g), implicating accumulation of dolichol in NCLs as a secondary phenotype of aging (Ng Ying Kin *et al.* 1983; Wolfe *et al.* 1983). Therefore, further work is needed to explain the precise mechanism of dolichol accumulation during NCL pathogenesis and the aging process.

1.2.3   Phosphorylated dolichol (Dol-P) in NCLs

The most metabolically active form of dolichol in cells is phosphorylated dolichol (Dol-P) (Kornfeld et al. 1985). One striking observation from the pre-genomic era was abnormally high levels of total Dol-P (measured after hydrolysis of all Dol-P containing compounds) in brain tissue of all three childhood forms of NCL, adult NCL and canine NCL, reaching concentrations 10 to 20 fold higher than those of age-matched controls (Keller et al.

1984; Hall et al. 1985; Wolfe et al. 1988). Elevated Dol-P concentrations comparable to those of NCLs were, however, also shown in some of lysosomal storage diseases (LSDs) such as GM1 gangliosidosis and Niemann Pick's Type C disease (Wolfe et al. 1988; Hall et al. 1989; Schedin et al. 1995). It turned out that dolichol levels were also shown to increase in some of these LSDs such as aspartylglucosamininuria (AGU), mannosidosis, Sanfilippo B syndrome and GM1 gangliosidosis (Humaloja et al. 1991; Jokelainen et al. 1992; Sakakihara et al. 1994; Schedin et al. 1995). These observations in LSDs imply that the high level of dolichol and/or Dol-P accumulations in cerebral cortex might be a secondary phenotype of lysosomal dysfunction in neurodegenerative disorders.

Interestingly, HPLC analysis was performed to show that the bulk of the Dol-P found in the classical childhood NCL patients was present as dolichol pyrophosphoryl oligosaccharides (lipid-linked oligosaccharides, LLO) because periodic acid-Schiff reagent (PAS) staining had suggested that the storage material contains carbohydrate (Hall *et al.* 1985; Hall *et al.* 1987; Hall *et al.* 1988; Daniel *et al.* 1992; Hall *et al.* 1992). Furthermore, oligosaccharide structure analysis suggested that the LLO were derived from catabolic rather than synthetic intermediates. These studies were, however, limited by uncertainties as to the genetic diagnosis in the clinical specimens, the use of autopsy material, the paucity of samples available for analysis, and technical limitations imposed by more cumbersome analytical methods (Schedin *et al.* 1995).

Still, early efforts at characterization of the storage material in the NCLs have led to several observations that may be of value in understanding the underlying pathophysiology of these disorders and their potential relation to changes that occur with normal aging.

1.2.4 Infantile NCL

The most severe form among NCLs is infantile NCL, with age of onset of symptoms and premature death as early as age of 2-3 years (Vesa *et al.* 1995; Hofmann *et al.* 1997; Hofmann *et al.* 1999; Das *et al.* 2001). As described above, accumulation of granular osmophilic deposits (GROD) in the lysosomal storage material in patient's brain tissues is a hallmark of INCL (Das *et al.* 1998). Although INCL patients are found worldwide, the carrier frequency of one particular mutant allele is very high in the Finnish population, which is 1 in 70 (Vesa *et al.* 1995; Lu *et al.* 1996; Hofmann *et al.* 2001a). Affected Finnish infants are homozygous for a single missense mutation (A364T or R122W), and develop visual loss, speech and motor deterioration and uncontrollable seizures beginning at the age of 6-8 months. The neurodegeneration progresses with those symptoms, and affected children show flat electroencephalogram by the age of 3 (Das *et al.* 2001).

Unlike the patients in Finland, it has been shown by Das *et al.* that those INCL patients in the U.S. and Canada exhibit a clinically and molecularly more heterogeneous nature of the disorder. A total of 19 different mutations were identified, and the two nonsense mutations (R151X and T75P) accounted for 53 % of the alleles (40% and 13 % respectively) (Das *et al.* 1998). This study has shown the broader spectrum of infantile NCL and that infantile NCL is no longer just a Finnish disease.

1.2.5 Mouse models of NCLs

Five well-defined genetic mouse models of the NCLs are available to date. As summarized in Table 1.2, all 5 mouse models reproduce the phenotypes of progressive

neuronal storage disorders that are manifest in the corresponding human NCLs. Three

models were generated by gene targeting of *CLN1* (Gupta *et al.* 2001), *CLN2* (Sleat, D.E. and

Lobel, P., manuscript submitted), and *CLN3* (Mitchison *et al.* 1999; Wheeler *et al.* 2002) and

the other two have been isolated as spontaneous mutations in *CLN6* (Gao *et al.* 2002a) and

CLN8 (Ranta *et al.* 1999).

Table 1.2 NCL mouse models

Disorder	Defective gene	Affected protein	Mouse phenotype	Ref.
Infantile NCL	CLN1/Ppt1	Palmitoyl protein thioesterase-1	Spasticity by age 5 months. Myoclonic jerking and seizures. Fatal by 10 months.	(Gupta et al. 2001; Gupta et al. 2003)
Late Infantile NCL	CLN2/Tpp1	Tripeptidyl peptidase-I	Tremor at 7 weeks and then ataxia, median survival 4.5 months.	a
Juvenile NCL	CLN3	Lysosomal transmembrane protein	Neuropathological abnormalities. Motor coordination deficits at 6 months.	(Mitchison et al. 1999), b
Variant Late-Infantile NCL	CLN6(Nclf)	Putative transmembrane protein	Progressive retinal atrophy. Gait disturbance and weakness in limbs evident by 6 months and severe paralysis by 9 months.	(Bronson et al. 1998; Gao et al. 2002a; Wheeler et al. 2002)
Epilepsy with mental retardation	CLN8(Mnd)	Putative transmembrane protein	Hindlimb weakness and ataxia at 6 to 7 months. Behavioral abnormalities.	(Bronson et al. 1993; Ranta et al. 1999; Bolivar et al. 2002)

[a]Sleat, D.E. and Lobel, P., unpublished data.
[b]Weimer, J. M. and Pearce, D. A., unpublished data.

Overall, the symptoms and the severity caused by the loss of function mutation in each mouse model are closely consistent with its human counterparts. Even though there are still many gaps to fill in our understanding of the pathogenesis of NCLs, these mouse models will serve as important tools to achieve further progress.

1.2.6   Neurodegeneration and the NCLs

In contrast to the classical lysosomal storage disorders (LSDs), biochemical analyses of the storage material in the NCLs did not provide clues as to the underlying defects, due either to the heterogeneous nature of the metabolites (proteins or lipid-modified proteins) or perhaps because the metabolites are toxic. Whereas most other LSDs are characterized by engorgement of affected organs by copious amounts of storage material, the storage in the NCLs is relatively scant and the phenotype is predominantly one of cell loss and neurodegeneration. Because of these unique phenotypes of neuronal loss and neurodegeneration caused by storage material, NCLs were not initially understood to be as lysosomal disorders. However, with the appreciation that most of the underlying genes encode lysosomal enzymes or lysosomal proteins, it is now clear that the NCLs belong to the family of lysosomal storage disease (reviewed in section 1.3).

Interestingly, all NCLs show a common phenotype, neuronal cell death, although individual defects, the age of onset of symptoms and progression of disease are all variable. Three types of mechanism for cell death are known as summarized in Table 1.3; apoptosis (type 1 cell death), autophagy (type 2 cell death) and necrosis (type 3 cell death) (Kerr *et al.* 1972; Schweichel *et al.* 1973; Clarke 1990).

Table 1.3 Summary of three different cell death mechanisms

Type	Characteristics	Ref.
Apoptosis	Cell shrinkage, plasma membrane blebbing, nuclear pyknosis, Chromatin condensation, DNA fragmentation.	(Kerr et al. 1972)
Autophagy	Formation of numerous cytoplasmic autophagic vacuoles Lysosomal degradation	(Schweichel et al. 1973)
Necrosis	Lack of lysosomal involvement Swelling of intracellular organelles Formation of empty space in the cytoplasm	(Clarke 1990)

The mechanisms of apoptotic pathways have been well documented in the last decade through identification of key components including a family of cysteine proteases called caspases, a family of adaptor proteins such as Apaf-1, and a family of mitochondria-associated proteins called Bcl-2. These proteins have been shown to control apoptosis in many different systems, including neurons (Yuan *et al.* 2000). In NCLs, apoptosis is implicated to be a major mechanism of cell death (Mitchison *et al.* 2004). However, the role of autophagy either alone or in conjunction with apoptosis, cannot be excluded. For example, no apoptotic cell death of neurons was observed in CLN3 and CLN6 knockout mice. Instead, autophagic vacuoles were discovered in the electron micrographs in CLN3 knockout mice (Mitchison *et al.* 2004).

Two major compartments for degradation of macromolecules and organelles in eukaryotic cells are the proteasome and the vacuole/lysosome. Under a variety of physiological conditions, most short-lived intracellular molecules are selectively turned over

by the ubiquitin-proteasome pathway (Hochstrasser 1996). The ubiquitin-proteasome utilizes

a series of enzymatic actions of E1 (the ubiquitin-activating enzyme), E2 (the ubiquitin

conjugating enzyme) and E3 (the ubiquitin-protein ligase) to tag the ubiquitin moiety to the

target protein via lysine residues, which are subsequently recognized by the 26S proteasome.

The 26S proteasome, which is comprised of the 20S core particle and 19S regulatory particle,

degrades the ubiquitin tagged substrates into small peptides by proteases embedded inside the

20S proteolytic core. However, the ubiquitin-proteasome pathway system functions in the

degradation of smaller and soluble proteins (cytoplasmic or nuclear), while

vacuole/lysosomal system targets the long-lived, larger and more complex substrates such as

membrane proteins, protein complexes and organelles (Mortimore *et al.* 1987; Hochstrasser

1996).

Autophagy is a Greek word and means self ("auto") eating ("phagy"). In biological

terms, autophagy is a degradation pathway to the vacuole/lysosome involving the

sequestration of cytoplasmic portions and intracellular organelles in a double membrane

vesicle called the autophagosome (Klionsky *et al.* 2000). Although the origin of

autophagocytic membrane is not yet clear, it has been suggested that the formation of

autophagic vacuoles is initiated from the membranes of rough endoplasmic reticulum (RER)

(Dunn 1990). Three types of mechanism have been suggested for autophagy:

macroautophagy, microautophagy and chaperone-mediated autophagy (Seglen *et al.* 1992;

Dunn 1994; Blommaart *et al.* 1997). Chaperone-mediated autophagy and microautophagy

have not been characterized in detail. Chaperone-mediated autophagy is suggested as a

secondary response to macroautophagy, which occurs temporally (Klionsky *et al.* 2000).

Microautophagy is triggered by invagination of vacuolar membrane to surround organelles such as occurs in the degradation of peroxisomes (Yuan *et al.* 1997; Sakai *et al.* 1998).

Macroautophagy is a conserved and well-controlled process that occurs in all eukaryotic cells. It is an important process controlling the balance between anabolism and catabolism during normal cell growth and development in response to starvation, differentiation, aging and death. At least two steps are involved in macroautophagy. Initial autophagosomes are formed after portions of cytoplasm are sequestered by membranous vesicles. By fusion of autophagosomes with pre-existing vacuole/lysosomes, the resulting autophagosomes will gain proteolytic enzymes and undergo autolysosomal degradation. The molecular mechanism of macroautophagy has been best revealed in yeast reverse genetics using *Saccharomyces cerevisiae*. Genes involved in the formation and regulation of the autophagosome were identified and characterized by genetic screening. At least 16 genes (*APG* and *AUT*) were identified that were required for formation of autophagosomes. For the docking and fusion of autophagosome and lysosome, Class C *VPS* genes are also required (Tsukada *et al.* 1993; Thumm *et al.* 1994; Sato *et al.* 2000; Seals *et al.* 2000; Khalfan *et al.* 2002). Because many of these genes have their homologous counterparts in higher eukaryotic cells, study of autophagy genes in lower organisms has led to a better understanding of the process in mammalian cells.

In mammalian cells, autophagy is induced by amino acid starvation. The autofluorescent drug monodansylcadaverine (MDC) has been used as a specific marker for autophagosomes in CHO cells. Vinblastine, a microtubule depolymerizing agent, also induces the accumulation of autophagic vacuoles by preventing their degradation, which

increases the accumulation of MDC and alters the size and distribution of autophagic

vacuoles (Munafo *et al.* 2001). It has been reported that the distribution of Rab24 is altered in

CHO cells by induction of autophagy through amino acid deprivation. GFP-tagged Rab24

stained vesicles were labeled with the specific autophagosome marker MDC and colocalized

with autophagosome protein LC3 (the mammalian ortholog of the yeast protein Apg8/Aut7),

suggesting Rab24 is involved in the autophagic pathway (Munafo *et al.* 2002).

Autophagy is a dynamic process involving remodeling of cytoplasm and organelles

by sequestering macromolecules for delivery to vacuole/lysosome so that the cargo is

degraded and recycled. The mechanism of autophagy in the mammalian system is still

unclear, although extensive studies in yeast have begun to reveal the molecular mechanism of

autophagy and vacuole/lysosomal degradation in the past decade. In Chapter 4 of this

dissertation, autophagy will be discussed as a possible mechanism of lipid-linked

oligosaccharide (LLO) accumulation in NCL mouse models.

1.3 Dolichol Metabolism

1.3.1   Dolichol biosynthesis

As briefly mentioned earlier, dolichol is a long chain polyisoprenoid with 14-21

isoprene units with the chain length varying in different species (Pennock et al. 1960; Schenk

et al. 2001). Dolichol is synthesized by the common isoprenoid pathway with other final

products such as cholesterol and ubiquinone (Hemming 1992). These pathways diverge after

the synthesis of farnesyl pyrophosphate (FPP) as shown in Figure 1.2, and *cis*-prenyl

transferase is the first enzyme in dolichol biosynthesis after the branching point (Voet et al. 1990).

Acetyl-CoA
↓
↓
HMG-CoA

│ **HMG-CoA reductase**
↓

Mevalonate
↓
↓
Mevalonate
Pyrophosphate
↓

Isopentenyl ⇌ Dimethylallyl
Pyrophosphate ⇌ Pyrophosphate

Geranyl
Pyrophosphate
↓

**Farnesyl
Pyrophosphate**

**_trans_-Prenyl
transferase**   **_cis_-Prenyl
transferase**   **Squalene
synthase**

↓   ↓   ↓ Squalene
↓   ↓   ↓
↓   ↓   ↓

Ubiquinone   **Dolichol**   **Cholesterol**
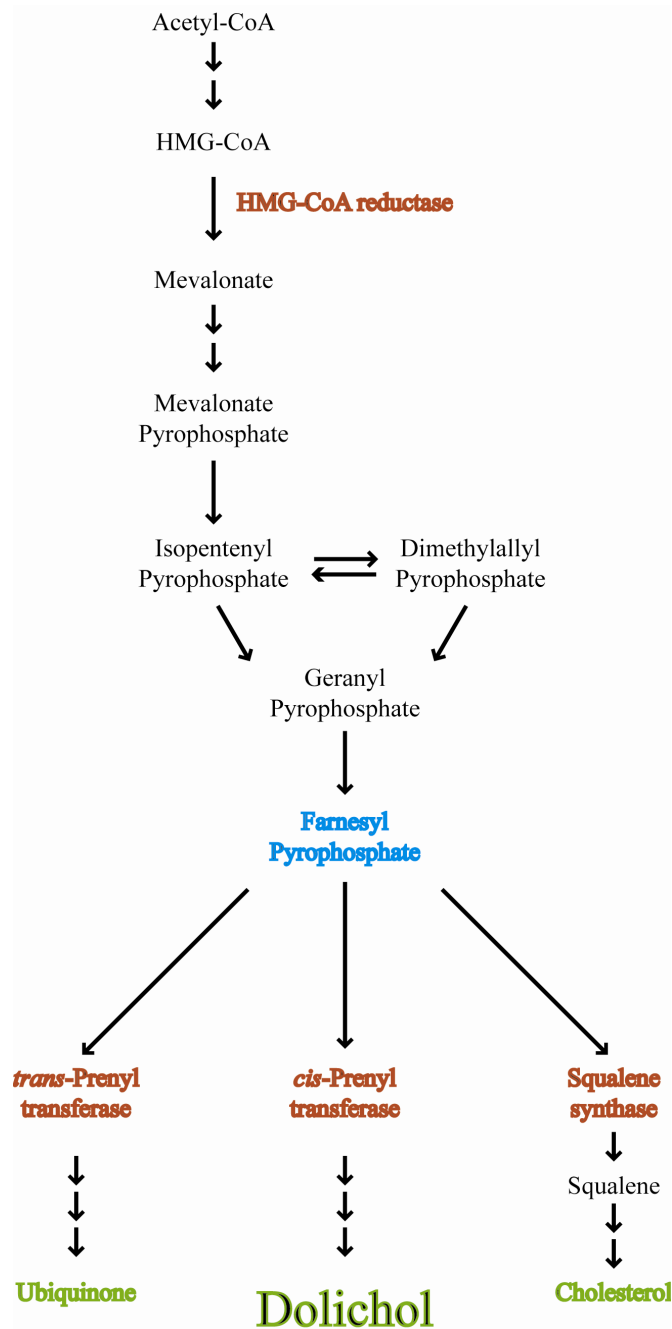
Figure 1.2 Pathway of isoprenoid metabolism

Then, a series of isopentyl pyrophosphate (IPP) additions produces polyprenyl

pyrophosphate. Isoprenoid phosphatase hydrolyzes two phosphate groups, yielding

polyprenol. Finally, polyprenol reductase converts the polyprenol to the mature

polyisoprenol, dolichol, in the presence of a cofactor, reduced nicotinamide adenine

dinucleotide phosphate (NADPH) as shown in Figure 1.3 (Grunler *et al.* 1994). All reactions

down to the synthesis of FPP in Figure 1.2 are localized in cytosol where the enzymes and

substrates are present, and the resulting cytosolic pool of FPP is then utilized as the substrate

for cholesterol and dolichol biosynthesis in the ER and for ubiquinone biosynthesis in

mitochondria (Trumpower *et al.* 1974; Wong *et al.* 1982b; Carroll *et al.* 1992; Cohen *et al.*

1992; Stamellos *et al.* 1993). *cis*-Prenyltransferase activity is also detected in peroxisomes,

implying dolichol biosynthesis is not restricted to microsomes (Appelkvist *et al.* 1989).

Interestingly, Wong and Lennarz have demonstrated by kinetic studies and

subcellular fractionation studies using rat liver that dolichol is transferred to the lysosomal

fraction and preferentially accumulated in lysosomes after being synthesized in microsomes

(Wong *et al.* 1982a; Wong *et al.* 1982b).

De novo synthesis of the most biologically active form of dolichol, Dol-P, is

catalyzed by dolichol kinase at the first carbon of the α-isoprenoid group as shown in Figure

1.3. In *S. cerevisiae*, the *SEC59* gene encodes dolichol kinase (DK). The temperature

sensitive mutant, *sec59-1*, in mutant cells has only 48% of DK activity at the permissive

temperature and less than 10% of DK activity at the restrictive temperature compared to wild

type DK. The Dol-P pool in mutant cells dries up almost instantaneously upon the

temperature shift to the restrictive temperature,
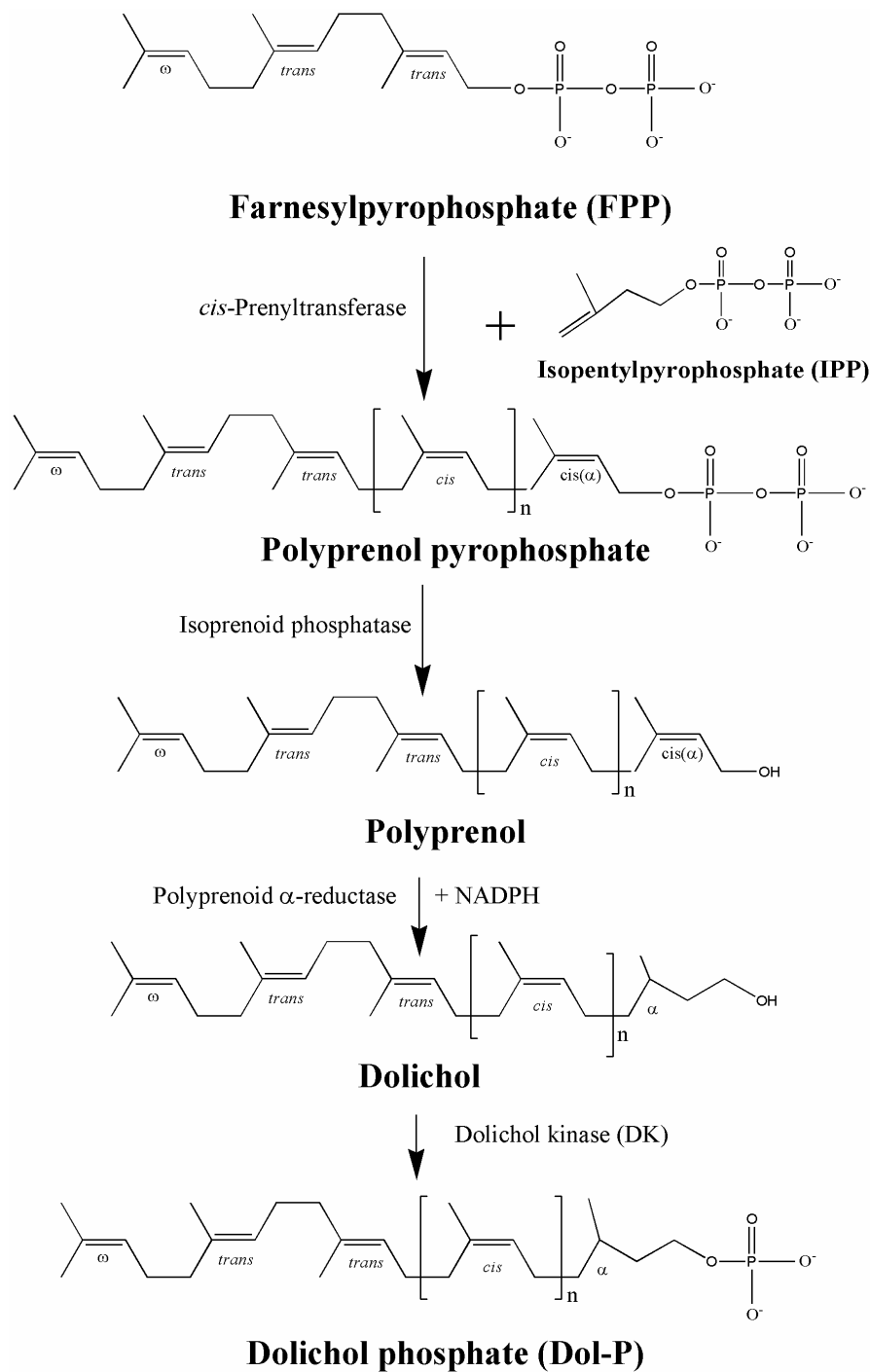
Figure 1.3 *De novo* **synthesis of dolichol phosphate (Dol-P). Other routes, such as involving reduction of polyprenol-P or dephosphorylation of Dol-P-P, are also possible.**

resulting in impairment of asparagine (N)-linked glycosylation (Bernstein *et al.* 1989; Heller *et al.* 1992). cDNA from human brain that encodes the mammalian ortholog of DK was also identified and characterized (Fernandez *et al.* 2002).

Dol-P is also utilized in biosynthesis of serine/threonine (O)-linked mannosylation, and tryptophan (C)-linked mannosylation, as well as glycosylphosphatidylinositol (GPI)-anchored proteins (Imperiali *et al.* 1995). During *N*-linked glycoprotein biosynthesis, Dol-P is the substrate for at least 3 reactions on the cytoplasmic face of the endoplasmic reticulum (ER) membrane: syntheses of GlcNAc-P-P-Dol, mannose-P-dolichol (MPD) and glucose-P-dolichol (GPD) (Gao *et al.* 2002c). As mentioned earlier, the availability of Dol-P is a rate-limiting factor in all of these lipid mediated glycosylations including *N*- and *O*-linked glycoprotein syntheses, and GPI-anchored protein synthesis.

1.3.2   Dol-P in biosynthesis of asparagine (N)-linked glycoproteins

Biosynthesis of N-linked glycoproteins involves a series of enzymatic reactions occurring on the both sides of endoplasmic reticulum (ER) membrane as shown in Figure 1.4. The rate-controlling substrate Dol-P begins the synthesis of the lipid carrier (Dol-P-P-OS) for oligosaccharide transfer to the asparagine residue of nascent polypeptides by accepting GlcNAc-1-P from one of the nucleotide-activated sugar donors (UDP-GlcNAc) (Burda *et al.* 1999). An additional unit of GlcNAc is added to produce a lipid-linked oligosaccharide (LLO) intermediate, $GlcNAc_2$-P-P-dolichol. Then, five more mannose units are added successively from GDP-Man to yield $Man_5GlcNAc_2$-P-P-

Dolichol

CTP

Dol-P → Dol-P — UDP-Glc → Glucose-P-doilchol (GPD)

GDP-Man

Mannose-P-dolicho (MPD)

UDP-GlcNAc

GlcNAc-P-P-dolichol

UDP-GlcNAc

$GlcNAc_2$-P-P-dolichol

GDP-Man

$Man_1GlcNAc_2$-P-P-dolichol (M_1)

4x GDP-Man

$Man_5GlcNAc_2$-P-P-dolichol (M_5)

OUTSIDE

INSIDE

$Man_5GlcNAc_2$-P-P-dolichol (M_5)

4x MPD

$Man_9GlcNAc_2$-P-P-dolichol (M_9)

1x GPD

$Glc_1Man_9GlcNAc_2$-P-P-dolichol (G_1M_9)

$Glc_3Man_9GlcNAc_2$-protein

2x GPD

$Glc_3Man_9GlcNAc_2$-P-P-dolichol (G_3M_9) → Dol-P-P

Dolpp1p

Dolichol ← Dol-P

?

Figure 1.4 Biosynthesis of lipid linked oligosaccharide (LLO) intermediates in the ER. The mechanism of Dol-P recycling remains uncertain.

dolichol (M_5) on the cytoplasmic face of the ER membrane. The M_5 is then flipped into the lumenal side of the ER membrane and four additional mannose units are added to produce $Man_9GlcNAc_2$-P-P- dolichol (M_9). In *S. cerevisiae*, Rft1p is found to be necessary for this flipping process on the ER membrane (Helenius *et al.* 2002). M_5 must be assembled outside of the ER because GDP- Man cannot be translocated into the ER lumen, requiring a flippase activity on the ER membrane (Burda *et al.* 1999). MPD and GPD, which are the donors of mannose and glucose onto LLO intermediates inside the ER, also have to be translocated into the lumen of the ER. However, proteins mediating translocation of MPD and GPD have not been identified (Burda *et al.* 1999). On the lumenal side of the ER, 3 more glucose units are added sequentially onto M_9, yielding $Glc_3Man_9GlcNAc_2$-P-P-dolichol (G_3M_9). Finally, from the mature LLO, G_3M_9 is transferred by oligosaccharyltransferase (OST) onto the target asparagine residue (Asn-Xxx-Ser/Thr) in the newly synthesized polypeptides in the lumen of the ER, generating *N*-linked glycoproteins (Gao *et al.* 2002c).

Gao and Lehrman have introduced a modern technique of fluorophore-assisted carbohydrate electrophoresis (FACE) to study LLO biosynthesis (Gao *et al.* 2002b; Gao *et al.* 2002c; Gao *et al.* 2003). This FACE system is a relatively simple and exceptionally sensitive method for labeling and detecting LLO intermediates from cells and tissues without using radioisotopes. In Chapter 4 of this dissertation, LLO profiles of five neuronal ceroid lipofuscinosis (NCL) mouse models, 3 lysosomal storage disease (LSD) mouse models and a PPT2 knock-out mouse using FACE analysis will be presented, and LLO accumulation in NCLs will be discussed in detail.

1.3.3   Recycling of dolichol phosphate (Dol-P)

The level of Dol-P, a rate-controlling factor in the biosynthesis of *N*-linked glycoproteins, is proposed to be maintained by *de novo* synthesis from free dolichol by dolichol kinase (DK) (Burda *et al.* 1999). There is another way of maintaining the level of Dol-P by converting from Dol-P-P to Dol-P after the oligosaccharide ($Glc_3Man_9GlcNAc_2$) transfer onto proteins (Schenk *et al.* 2001). Once the oligosaccharides are transferred onto the proteins, Dol-P-P is released on the luminal surface of the endoplasmic reticulum (ER). In order for Dol-P-P to be re-utilized as a glycosyl carrier lipid for additional rounds of LLO biosynthesis, it must be converted to Dol-P and translocated to the cytoplasmic side of the ER (Schenk *et al.* 2001).

The *S. cerevisae CWH8* locus is believed to encode this dolichol pyrophosphatase activity. *CWH8* null mutant cells are viable but grow much more slowly than wild type cells. They also show inefficient N-linked glycosylation on secretory proteins such as carboxy peptidase Y (CPY). They produce normal dolichol and a normal length of dolichol-linked oligosaccharide (LLO) intermediates at a much reduced level (20%) as compared to wild-type yeast (van Berkel *et al.* 1999). Later, it was confirmed that Cwh8p had dolichol pyrophosphate phosphatase activity *in vitro* specifically converting Dol-P-P to Dol-P on the lumenal side of the ER (it was therefore renamed as Dolpp1p) (Fernandez *et al.* 2001). Dolpp1p is recovered in crude microsomal fractions, but its subcellular location had not been established. In Chapter 3 of this dissertation, cloning of mouse *DOLPP1* will be presented and further characterization of mouse Dolpp1p including its subcellular localization will be discussed in detail.

1.4 Palmitoyl Protein Thioesterase-1 (PPT1)

1.4.1 Discovery

In 1993, Camp and Hofmann first discovered palmitoyl protein thioesterase-1 (PPT1) from bovine brain as an enzyme that cleaved the palmitate from H-Ras *in vitro* (Camp *et al.* 1993b), and the human PPT1 gene was then mapped to 1p32 to metaphase chromosomes by fluorescent in situ hybridization (FISH) (Schriner *et al.* 1996). Simultaneously, the Peltonen group in Finland assigned the locus 1p32 as a candidate gene site for an autosomal recessive disorder called infantile neuronal ceroid lipofuscinosis (INCL) by positional cloning (Jarvela 1991; Vesa *et al.* 1995). Eventually, the two groups agreed that they were studying ultimately the same gene by confirming multiple mutations in PPT1 gene in INCL patients and by showing no residual PPT activity from brain tissues and lymphoblasts derived from the patients (Vesa *et al.* 1995).

1.4.2 PPT1, a thioesterase

The substrate H-Ras was used in the enzyme assay for PPT1 during the purification from bovine brain tissues, because H-Ras is palmitoylated via S-acylation at the two C-terminal cysteine residues (Cys$_{181}$ and Cys$_{184}$) (Kato *et al.* 1992). S-acylation is a post-translational modification of proteins that utilizes a thioester bond between the carboxyl end of the fatty acid and the sulfhydryl group of the cysteine residue (Casey 1995). In addition to palmitoylation, H-Ras also has a site for carboxy methylation and farnesylation (Cys$_{186}$) at the C-terminus (Kato *et al.* 1992). For farnesylation, a thioether linkage to the cysteine residue is used instead of thioester linkage. Therefore, it has been demonstrated that PPT1

specifically cleaves off palmitate groups from H-Ras leaving farnesyl group intact (Camp *et al.* 1993b).

In mammals, the PPT1 cDNA encodes 306 amino acids and contains an N-terminal leader sequence (first 25 amino acids). PPT1 is a classical globular monomeric enzyme, which possesses an α/β hydrolase fold typical of lipases and a classical catalytic triad consisting of serine, aspartic acid and histidine residues (Camp *et al.* 1993b; Bellizzi *et al.* 2000). PPT1 also has three potential sites for asparagine (N)-linked glycosylation (Asn_{197}, Asn_{212} and Asn_{232}). Mutations of those glycosylation sites cause a reduction of enzyme activity and mutations of all three sites inactivate PPT1 completely *in vitro* due to effects on protein folding and stability (Bellizzi *et al.* 2000). An *in vivo* substrate for PPT1 has not been identified but in addition to palmitoylated proteins, PPT1 hydrolyzes long chain fatty acyl CoAs with fatty acid chain length of 14 to 18 carbons *in vitro* (Camp *et al.* 1994). The crystal structure for PPT1 has shown that PPT1 cannot bind lipid chains less than 10 carbons because they are not long enough to make contact with the critical residues of PPT1 (Calero *et al.* 2003). This observation has explained why PPT1 had almost no activity with acyl CoA substrates of six carbons or less (Camp *et al.* 1993b).

1.4.3 PPT1, a lysosomal enzyme

PPT1 has been demonstrated to be a lysosomal enzyme by Verkruyse and Hofmann, although recombinant PPT1 showed a broad neutral pH optimum (Verkruyse *et al.* 1996). The experiments showed that recombinant PPT1 was taken up by COS cells via the mannose 6-phosphate receptor pathway, a hallmark of lysosomal enzyme trafficking. PPT1 activity

also fractionated with lysosomal markers by Percoll density gradient analysis, strongly suggesting its lysosomal localization (Verkruyse *et al.* 1996). Lysosomal localization of PPT1 was also confirmed by immunofluorescence studies (Hellsten *et al.* 1996).

Defective PPT1 initiates an accumulation of [^{35}S]cysteine-labeled lipid thioesters in lymphoblasts derived from INCL patients (Lu *et al.* 1996). The accumulation of lipid thioesters is time dependent and requires prior protein synthesis, indicating that the cysteine containing lipid thioesters probably originated from fatty acylated proteins. The accumulation is corrected by incubating the cells with recombinant PPT1, which was taken up via the mannose 6-phosphate receptor mediated pathway (Lu *et al.* 1996). It also has been shown that the accumulated radiolabeled lipid thioesters cosedimented with lysosomal markers, confirming that the accumulated lipid esters were PPT1 substrates *in vivo* (Lu *et al.* 2002).

1.4.4   *PPT1* **knock-out mouse**

Using a gene targeting strategy, a PPT1 null mutant mouse was engineered and its phenotypes were well characterized and documented (Gupta *et al.* 2001; Bible *et al.* 2004). PPT1 knock-out mice are viable and fertile. However, the mice show severe cortical atrophy, spontaneous seizures and premature death by 10 months. PPT1 knock-out mice exhibit a lack of grooming, frequent myclonic jerks and seizures from 3-4 mo of age. PPT1 deficiency also affects motor functions such as a progressive gait abnormality and spasticity (a "clasping" phenotype) beginning at 5 months of age which progresses to hind-limb paralysis (Gupta *et al.* 2001).

Autofluorescent storage material accumulation is evident in brain tissues from all PPT1 knock-out mice examined (the earliest age of mice examined were 4 wk-old). Neuronal GROD (granular osmophilic deposits), a hallmark of INCL, are also identified in PPT1 knock-out brain and they are indistinguishable from GROD seen in human patients (Das *et al.* 1998; Gupta *et al.* 2001). In PPT1 knock-out brain, a 46% reduction of volume in thalamus as well as a 35% and a 30 % reduction in the cortex and striatum are observed, respectively. Cortical thinning probably due to neuronal loss is also observed in different regions of the PPT1 knock-out brain (Bible *et al.* 2004). Terminal dUTP nick end-labeling (TUNEL) assay shows apoptotic neurons in the Purkinje layer of the cerebellum in PPT1 knock-out brain, implying apoptosis as a cell death mechanism in PPT1 knock-out mouse brain (Gupta *et al.* 2001).

1.4.5 *PPT1* ortholog in *Schizosaccharomyces pombe*

cDNAs for *PPT1* have been cloned and characterized from human, bovine, rat, mouse, fruit fly and fission yeast (Camp *et al.* 1994; Schriner *et al.* 1996; Salonen *et al.* 1998; Glaser *et al.* 2003; Cho *et al.* 2004). The 25 amino acid-long N-terminus leader sequences are less obvious in *PPT* orthologs in *Drosophila* and *S. pombe* but the classical "catalytic triad" residues of Ser-Asp-His in the active site of typical thioesterases are very well conserved in all the species from human to fission yeast (Glaser *et al.* 2003; Cho *et al.* 2004). The *Drosophila* ortholog of *PPT1* is 55% identical and 72% similar to human *PPT1*, and flies with a homozygous deletion of *PPT1* show almost complete abolition of PPT1 activity using the fluorometric substrate 4-methylumbelliferyl-6-thiopalmitoyl-β-D-

glucoside, but no apparent phenotype was observed (Glaser *et al.* 2003). Overexpression of a *PPT1* ortholog in *Drosophila,* however, was reported to cause apoptotic cell death in the visual system, suggesting that tight regulation of PPT1 might be important in neuronal cell survival (Korey *et al.* 2003).

S. pombe is a single-celled free living archiascomycete fungus sharing many features associated with more complex eukaryotic cells. Because the genome of *S. pombe* can be manipulated experimentally, it has served as an excellent model organism for many studies, particularly those involving cell-cycle control, mitosis and meiosis (Davis *et al.* 2001), and DNA repair and recombination (Humphrey 2000). *S. pombe* is also increasingly used for investigating the functions of human disease genes. About 50 genes (out of a total complement of approximately 4,800) are orthologous to known human disease genes, including those underlying various metabolic, cardiac, renal, and neurological diseases, and cancer. Most of these genes are also found in *Saccharomyces cerevisiae* (another common fungal model). However, two known disease-associated genes (SPAC630.13c and SPBC530.12c) are found only in *S. pombe,* and not in *S. cerevisiae* (Wood *et al.* 2002). One of the genes, SPBC530.12c, encodes the *S. pombe* ortholog of the human *PPT1* gene. (The other encodes a gene associated with tuberous sclerosis (*TSC2*)).

Interestingly, examination of SPBC530.12c reveals that it is a fusion gene consisting of the *S. pombe PPT1* ortholog followed by a single in-frame open reading frame (ORF), which is an ortholog of *DOLPP1,* a gene encoding dolichol pyrophosphate phosphatase-1 (Dolpp1p), an enzyme also implicated in dolichol metabolism as reviewed earlier. In Chapter

2 of this dissertation, the cloning and characterization of this *S. pombe* ortholog gene

(SPBC530.12c) will be presented in detail.

CHAPTER TWO

PPT1 ortholog in *Schizosaccharomyces pombe*

2.1 Introduction

As described in the introduction, *S. pombe* is fission yeast, a single-celled free living archiascomycete fungus sharing many features associated with more complex eukaryotic cells. Because the genome of *S. pombe* can be manipulated experimentally, it has served as an excellent model organism for many studies. Bioinformatics screening using amino acid sequence of human *PPT1* has resulted in identification of an uncharacterized gene (SPBC530.12c) as the *PPT1* ortholog in the *S. pombe* genome. Interestingly, examination of SPBC530.12c reveals that it is a fusion gene consisting of the *S. pombe PPT1* ortholog followed in the same open reading frame (ORF) by sequence encoding an ortholog of *DOLPP1*, a dolichol pyrophosphate (Dol-P-P) phosphatase-1 (Dolpp1p), an enzyme implicated in dolichol metabolism. Dolpp1p is a transmembrane protein that catalyzes the conversion of Dol-P-P to Dol-P, and is postulated to play a role in the recycling of dolichol utilized in the synthesis of the dolichol pyrophosphate oligosaccharides (Dol-P-P-OS) in the ER.

Dol-P-P-OS are intermediates in the asparagine (N)-linked glycosylation of proteins (Rush et al. 2002). Dolpp1p null mutant alleles in *S. cerevisiae* produce normal dolichol and dolichol-linked oligosaccharide intermediates at a reduced level (20%) as compared to wild-type yeast. The presence of a putative fusion protein containing both *PPT1* and *DOLPP1*

orthologs in *S. pombe* suggests coordinate regulation of the synthesis of the two polypeptides

in *S. pombe*.

In this chapter, I have ablated the SPBC530.12c gene (hereafter referred to as *pdf1*,

ppt1-dolpp1 fusion 1) and determined the consequences of inactivating mutations in the

Ppt1p and Dolpp1p domains through plasmid complementation assays. I have also produced

a polyclonal antibody against the C-terminus of Pdf1p to examine possible post-translational

processing.

2.2 Experimental Procedures

2.2.1 Yeast strains, media and genetic methods

Genotypes of *S. pombe* strains used in this study are listed in Table 2.1. All strains

were maintained on yeast extract plus supplement (YES) agar plates or under selection on

Table 2.1 *S. pombe* strains used in this study and their genotypes

Strain	Genotype	Source
SC 247	h^+ *his3-D1 ade6-M210 ura4-D18 leu1-32*	Rokeach, L.
SC 248	h^- *his3-D1 ade6-M216 ura4-D18 leu1-32*	Rokeach, L.
SC 2478	h^+/h^- *his3-D1/his3-D1 ade6-M210/ade6-M216 ura4-D18/ ura4-D18 leu1-32/leu1-32*	This study
SC 41	h^+/ h^- *pdf1Δ:: his3$^+$/ pdf1$^+$ his3-D1/ his3-D1 ade6-M210/ade6-M216 ura4-D18/ura4-D18 leu1-32/leu1-32*	This study
SC41R	h^+ *pdf1Δ:: his3$^+$ his3-D1 ade6-M210 ura4-D18 leu1-32 pREP1[pdf1$^+$-LEU2$^+$]*	This study
SC 41U	h^+ *pdf1Δ:: his3$^+$ his3-D1 ade6-M210 ura4-D18 leu1-32 pAAU[pdf1$^+$-ura4$^+$]*	This study
SC 41L	h^+ *pdf1Δ:: his3$^+$ his3-D1 ade6-M210 ura4-D18 leu1-32 pAAL[pdf1$^+$-LEU2$^+$]*	This study

Edinburgh minimal media (EMM) with appropriate supplements as described (Moreno et al.

1991).Yeast cells were transformed using lithium acetate (Alfa et al. 1993). Standard

molecular biological techniques were employed (Sambrook et al. 1989).

2.2.2   Identification and subcloning of *pdf1*+

The SPBC530.12c gene of *S. pombe* was identified as containing sequences

corresponding to a potential human PPT1 ortholog through a BLAST search of GenBank[TM]

using the human PPT1 amino acid sequence (NP_000301) as the query. *S. pombe* cosmid

530 (GenBank[TM] accession number: AL023634), which contains the SPBC530.12c gene,

was obtained from the Sanger Center (http://www.sanger.ac.uk). Polymerase chain reaction

(PCR) was carried out using pfu polymerase (Stratagene) and cosmid 530 DNA as a

template DNA with primers 5'-TAAGAATTCGACTCAAGACAACAATCACT-3' and 5'-

CTTGGATCCCCTTGGGTAATTTTCTGAAC-3'. The amplified product was digested with

*EcoR*I and *BamH*I (underlined in the forward and reverse primers, respectively) and

subcloned into the plasmid vector pGEM-T-Easy (Promega) to create pGPD1. The entire

open reading frame (ORF) was sequenced on both strands and corresponds exactly to

nucleotides 37983 through 39794 of AL023634.

2.2.3   Construction of the *pdf1* disruption

Disruption of *pdf1* was performed by removal of a large portion of the open reading

frame (Figure 2.1, corresponding to amino acids 69 through 565) of pGPD1 and insertion of

a *his3*+ gene. Briefly, pGPD1 was digested with *Bbs*I and *Blp*I to remove most of the open

reading frame and the remaining 3.5 kb fragment (containing vector and flanking sequence)

was rendered blunt-ended. The *his3*⁺ gene from pJB1 (a gift from Dr. Luis Rokeach, University of Montrėal) (Burke et al. 1994) was amplified using pfu polymerase and primers 5'-CAACGTTTTCTTTACTATTGCAC-3' and 5'-ACGCGTGAATGGACTGTTGGCTG-3' and ligated into pGEM-T-Easy (Promega). A 2.1 kb *Not*I fragment containing the *his3*⁺ gene was rendered blunt-ended and ligated to the 3.5 kb fragment of pGPD. The resultant plasmid (pGPDH1) was digested with *Not*I and the 2.6 kb insert was transformed into a wild-type diploid strain SC2478. *His*⁺ diploids were selected and designated as SC41. Replacement of the wild-type allele by the disrupted gene was confirmed by Southern analysis using a randomly primed labeled probe generated by PCR amplification of a 300 bp portion of pGPD using primers 5'-CCCTTGGGTAATTTTCTGAAC-3' and GTCTTCAAATTCGTTGTCACC-3'. The correct targeting of the deletion cassette into the genomic locus was also verified by PCR. Primers were designed that were specific to the upstream, downstream and internal regions of the ORF, and to the internal region of the *his3*⁺ cassette. To determine the effect of the gene disruption on spore viability, SC41 cells were plated on malt extract (ME) plates to induce sporulation. After 36 to 48 hours, the presence of asci was confirmed under the light microscope and tetrad dissection was performed using a micromanipulator as described previously (Alfa et al. 1993).

2.2.4 Expression Plasmids

The ORF of pdf1+ was amplified by PCR using pGPD1 as a template and the amplified product was subcloned into three plasmid vectors; pREP1, pAAU (a gift from Steven Marcus, MD Anderson Cancer Center) and pAAL. The pAAL vector was created by

replacing the ura4+ marker with *LEU2*^{+} in pAAU by digestion with *Hind*III and ligation.

Point mutations were introduced in the *pdf1*[+] ORF using the QuickChange Site-Directed

Mutagenesis Kit (Stratagene). Oligonucleotide sequences used in the construction of point

mutations are available upon request. The truncation mutation (Δ373-602) was constructed

by PCR using pGPD1 as template.

2.2.5 Isolation of haploid *pdf1Δ* strains complemented by *pdf1*[+]

SC41 cells were transformed with pAAU-*pdf1*[+], and *his*[+] and *ura*[+] transformants

were selected on medium lacking adenine, histidine and uracil. Transformants were induced

to sporulate on ME plates, the ascus walls were digested with glusulase (Sigma), and the

individual spores were germinated on plates lacking histidine and uracil. The resulting

colonies were examined as *his*[+], *ade*[-] haploids only if they were also *ura*[+], indicating plasmid

rescue of the disruption phenotype. Loss of the wild-type allele was confirmed by Southern

analysis. The haploid strains were designated SC41R, SC41U or SC41L, for strains

complemented by pREP1- *pdf1*[+], pAAU- *pdf1*[+] and pAAL- *pdf1*[+], respectively.

2.2.6 Structure-function analysis of *pdf1*[+] by plasmid shuffling

SC41U cells were transformed with wild type pAAL- *pdf1*[+] or with plasmids

containing mutations as indicated in the Figure Legends. Transformants were selected on a

medium lacking leucine and uracil. Each transformant was then streaked onto medium

containing 0.1% 5-fluoroorotic acid (5'FOA) and 50 µg/ml uracil (Liang et al. 2001) and was

grown at 30°C for 4 days to promote the loss of the ura4+ plasmid. The growth of cells in the

presence of 5'FOA was scored to assess the ability of the wild type or mutated pAAL- *pdf1*[+] to promote viability of the haploid *pdf1Δ* strain.

2.2.7   Vanadate and extracellular pH sensitivity

Sodium orthovanadate (Sigma) was added to medium from a filter-sterilized stock solution (100 mM) after autoclaving. For pH sensitivity experiments, 50 mM MOPS and 50 mM MES was included in the medium and the pH was adjusted by dropwise addition of 10 N NaOH.

2.2.8   Affinity-purified polyclonal antibodies

Three New Zealand White rabbits were each immunized with 300 μg of a synthetic peptide corresponding to amino acid residues 583 to 603 of Pdf1p that was coupled to keyhole limpet hemocyanin using methods described previously (Rush et al. 2002). The antigen was injected intradermally in Freund's complete adjuvant, and rabbits were boosted three times at 3-week intervals with 300 μg of peptide in Freund's incomplete adjuvant. An IgG fraction was prepared from preimmune and immune serum by specific binding to Protein A-Sepharose CL-4B (Pharmacia). The IgG was affinity-purified by specific binding to a column consisting of the peptide cross-linked to SulfoLink coupling gel (Pierce).

2.2.9   Protein extraction and immunoblotting

Cells were grown to mid-log phase in EMM with appropriate amino acids. The harvested cells were washed twice with distilled water and cell lysates were prepared by glass bead lysis in homogenization buffer (20 mM HEPES, pH 7.0, 50 mM potassium

acetate, 5 mM magnesium acetate, 100 mM sorbitol) with the addition of 1 mM dithiothreitol

(DTT) and a cocktail of protease inhibitors (2 µg/ml each of leupeptin, pepstatin and

aprotinin and 1 mM phenylmethylsulfonyl fluoride) (Liang et al. 2001). Lysates were cleared

by centrifugation at 500 x g for 1 min at 4 °C, and resulting supernatants were centrifuged at

20,000 x g for 30 min at 4 °C in a Beckman Optima TLX ultracentrifuge. The supernatant

fraction was reserved and the membrane pellet was washed once with homogenization buffer

and resuspended in 8 M urea for immunoblotting. Samples were analyzed by electrophoresis

in 12.5% SDS-PAGE gels and immunoblotting essentially as described (Rush et al. 2002).

Filters were blocked for 1 h with Sea Block (East Coast Biologics) and washed in PBS-T

(0.25% (v/v) Tween 20 in phosphate-buffered saline) followed by incubation for 1 h with

rabbit anti-peptide polyclonal antibody (0.1 µg/ml). The filters were washed with PBS-T and

incubated for 45 min in a solution containing horseradish peroxidase-conjugated secondary

antibody (sheep anti-rabbit IgG, Amersham) diluted 1:2500 in PBS-T. The filters were

washed and developed using ECL chemiluminescence reagents (Amersham).

2.3 Results

2.3.1   Cloning of the fission yeast *pdf1* gene

A BLAST search of the *S. pombe* genome database using the human PPT1 amino

acid sequence yielded a gene (SPBC530.12c) that encodes a 603-amino acid residue protein

that contains a Ppt1p domain (31% identical to human Ppt1p), a linker region, and a domain

that shares 33% sequence identity to mouse Dolpp1p (Figure 2.1). Residues of human Ppt1p

A

```
Sp Pdf1p   MKS------FAIPIISLDKVRLAINDGA-SEQLPVVIWHGLGDTPTS-FT   42
Hs Ppt1p   MASPGCLWLLAVALLPWTCASRALQHLDPPAPLPLVIWHGMGDSCCNPLS   50

Sp Pdf1p   LTEVSQRVQKLTKGA-VYAIRVGDNEFEDIKAGYLGKLEDQLDEVCDLIG   91
Hs Ppt1p   MGAIKKMVEKKIPGIYVLSLEIGKTLMEDVKNSFFLNVNSQVTTVCQALA  100

Sp Pdf1p   NEDSLSNGFYALGLSQGGLFLRALAQTCDAAKIISLITLGSPHSGINTIP  140
Hs Ppt1p   KDPKLQQGYNAMGFSQGGQFLRAVAQRCPSPPMINLISVGGQHQGVFGLP  150
                         *
Sp Pdf1p   GC-SPTNLICKAVVHSILGLGIWHSWIQNHVVQAQYYRTEKQYDKYLENN  190
Hs Ppt1p   RCPGESSHICD-FIRKTLNAGAYSKAIQERLVQAEYWHDPIREDVYRNHS  199
                                                    *
Sp Pdf1p   KFITHLNNE-VLHDNYTRNIEKLKELDNLVAVSFERDDIVEPPYSTGFGW  238
Hs Ppt1p   IFLADINQERGVNESYKKNLMALKK---FVMVKFLNDSIVDPVDSEWFGF  246

Sp Pdf1p   INE-TTGENLEMEDFVLY--ESLGLKDLVNQGKLETISFPGRHLQMRWGD  286
Hs Ppt1p   YRSGQAKFTIPLQETSLYTQDRLGLKEMDNAGQLVFLATEGDHLQLSEEW  296

Sp Pdf1p   FDALVLKYFKDEKEEKTELEESTRPSNFLSTYFVSPLVSAIDGTVDYLHG  336
Hs Ppt1p   FYAHIIPFLG.                                         306
                    **          ***
Sp Pdf1p   KSLFPEKRNFKELTMRKRSIVTPEDSEEVYPYISEFVAASNVSEEKGPKS  386
Mm Dolpp1p                                         MAA------DGQCS    8

Sp Pdf1p   FANLAFITIFSHFFYHIDDMWRSTLGLFSLIPQIIGIIYLTVMFTGRELD  436
Mm Dolpp1p LPASWRPVTLTHVEYPAGDLSGHLIAYLSLSPIFVVVGFLTLIIFKRELH   58
                                                         *
Sp Pdf1p   TFMQFGGQVVNEFINYVVKVSLKYPRFA---DIEYGVGYGMPSSHSQFMG  483
Mm Dolpp1p TISFLGGLALNRGVNWLIKHVIQEPRFCGGPHTAVGTKYGMPSSHSQFMW  108

Sp Pdf1p   FFSAYMIAWDY----KYRRSQCFSMLSFAKYAIYITLSTFVCS-SRYLLD  528
Mm Dolpp1p FFSVYSFLFLYLRMHQTNNARFLDLLWRHVLSLGLLTAAFLVSYSRVYLL  158

Sp Pdf1p   FHYLTQVVYGYMIGFGVGLFWVYLVGKLRSLGVTKWLLSLPPLQFFYIKD  578
Mm Dolpp1p YHTWSQVLYGGVAGGLMAVAWFIITQEILTPLFPR-IAAWPVSEFFLIRD  207

Sp Pdf1p   TIPHSKDNHKRQWLESKQFKNQKSN.                          603
Mm Dolpp1p TSLIPNVLWFEYTVTRAEARNRQRKLGTKLQ.                    238
```

B

S^{106} D^{226} KR^{344} RKR^{354} H^{478}

Ppt1p   Dolpp1p
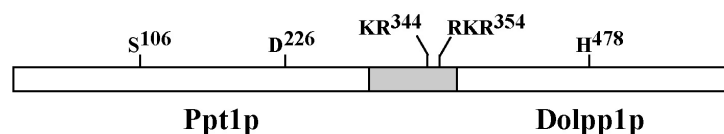
Figure 2.1 Amino acid sequence alignment (A) and domain structure (B) of proteins encoded by *S. pombe* pdf1, human PPT1, and mouse DOLPP1. Gaps in the sequences are indicated by dashes. Identical amino acid residues are shaded dark gray; similar residues are light gray. The linker region contains two distinct clusters (*) of basic amino acids, which are putative cleavage sites of serine endopeptidase Krp1. Amino acids that participate in catalysis and that were mutated to catalytically inactive residues for the purposes of this study are indicated (✴). An acidic linker region of 76 amino acids between the Ppt1p and Dolpp1p domains is indicated by a shaded bar.

and mouse Dolpp1p known to participate in catalysis (i.e., catalytic triad residues Ser115, Asp233 and His289 of human PPT1) (Bellizzi et al. 2000) and the consensus lipid-phosphate phosphatase motif of mouse Dolpp1p (Lys455, His478 and His530) (Rush et al. 2002) are conserved in Pdf1p.(Figure 2.1A). The linker region (Figure 2.1B) contains sequences that conform to cleavage recognition sites for a kex-related processing protease, Krp1 (Powner et al. 1998).

2.3.2   Disruption of fission yeast *pdf1* is lethal

To investigate the function of *pdf1*, I constructed and examined the phenotypes of *S. pombe* strains in which *pdf1* was deleted. The *pdf1* gene is 1812 base pairs in length and contains no predicted intron sequences (Figure 2.2A). One copy of the *pdf1* open reading frame (comprising amino acids 69 to 565) was replaced with the *his3*[+] selectable marker in a diploid *S. pombe* strain and chromosomal deletion of the gene was confirmed by Southern analysis (Figure 2.2B), which yields a 2.2 kb band in wild type (lane 1), 2.2 and 1.8 kb bands in heterozygous diploids (lane 2), and a single band of 5.5 kb in the disruption strain rescued by a plasmid (pREP1- *pdf1*[+]) in the haploid state (lane 3). Correct targeting of the deletion cassette into the genomic locus was also confirmed by PCR as described in Experimental Procedures. Sporulation and tetrad analysis of independently derived heterozygous diploid strains (*Δ pdf1:: his3*[+]/ *pdf1*[+]) resulted in only two viable spores, showing a 2:0 segregation (Figure 2.2C). All of the viable spores were his- and *pdf1*[+], indicating that *pdf1* is an essential gene in *S. pombe*.
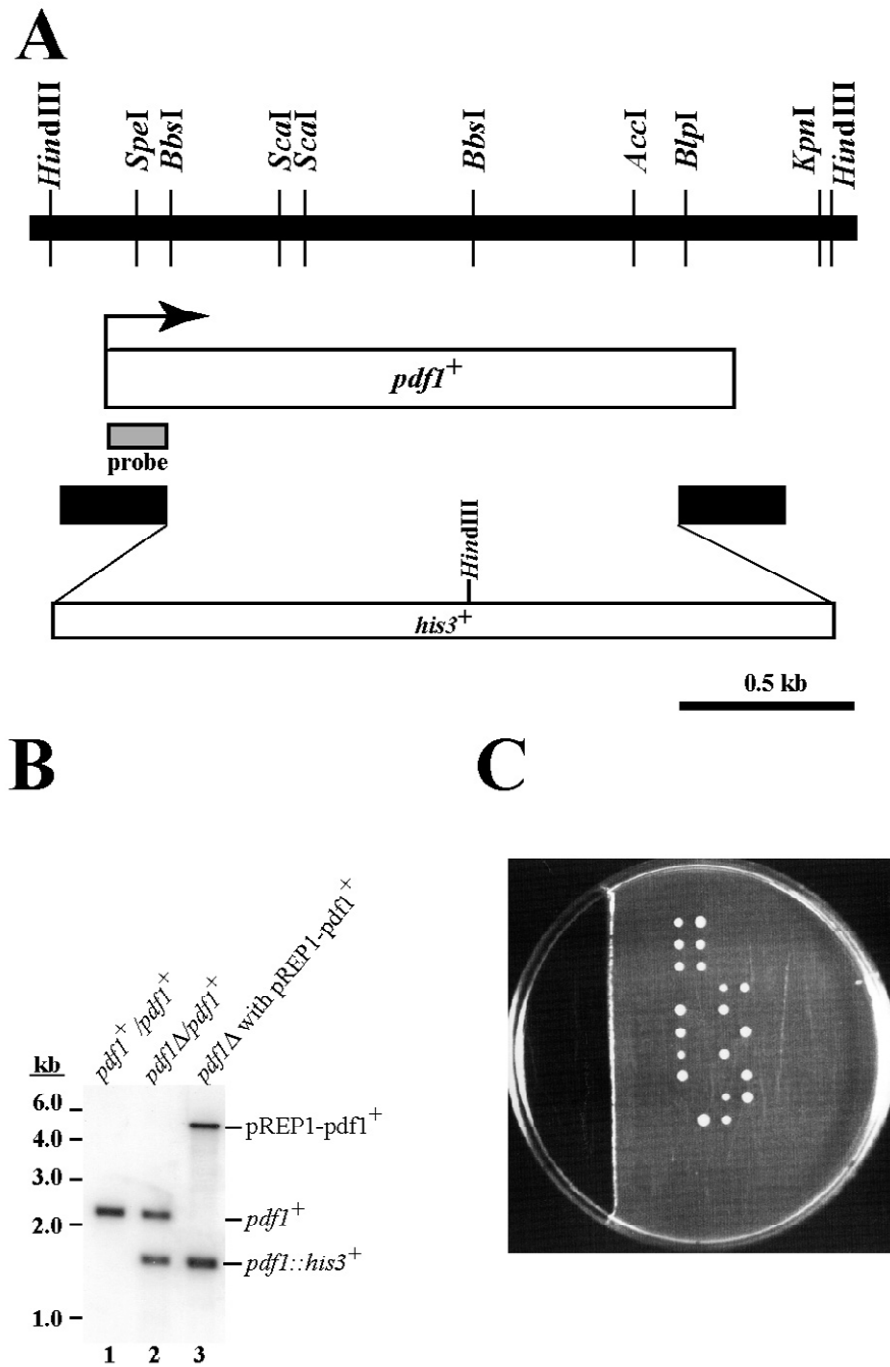
Figure 2.2 Disruption of *pdf1*[+]. (A) Restriction map and schematic of the *pdf1*[+] locus. The direction and location of the *pdf1*[+] ORF are indicated. The position of the probe used for Southern blot analysis is indicated as a shaded box. The location of the *his3*[+] gene in the *pdf1*Δ::*his3*[+] disruption construct is shown. An additional *Hind*III site is located within the

his3⁺ gene. (B) Southern blot analysis of the chromosomal *pdf1*⁺ deletion. Genomic DNA was digested with *Hind*III, resolved on a 1% agarose gel, and probed with the 0.3-kb fragment indicated in panel A. Lane 1, homozygous wild type *pdf1*⁺/*pdf1*⁺; lane 2, heterozygous *pdf1*Δ/*pdf1*⁺ strain; lane 3, homozygous *pdf1*Δ/*pdf1*Δ strain rescued with a plasmid bearing *pdf1*⁺. (C) Tetrad analysis of the *pdf1*⁺ gene disruption. A 2:0 segregation ratio resulted from microdissection of heterozygous diploid (*pdf1*Δ::*his3*⁺/*pdf1*⁺) cells after sporulation. The spores that formed colonies in any tetrad were *his*⁻ and hence *pdf1*⁺.

2.3.3   The Dolpp1p domain of Pdf1p is essential for viability whereas the Ppt1p domain is dispensable

To gain a further insight into the role of two domains of the *pdf1*, I analyzed a *pdf1*Δ strain complemented by various plasmids as shown in Figure 2.3. Of note, the analysis was complicated by an inability to express the *S. pombe* Dolpp1p domain alone in the absence of upstream sequences, presumably due to the need for a signal sequence or other sequences needed for proper Dolpp1p membrane insertion and folding.

A structure-function analysis was performed using a plasmid shuffling technique. First, I isolated a haploid strain SC41U which contains the *pdf1* deletion and harbors the wild type *pdf1*⁺ gene within a complementing plasmid (pAAU). Because *pdf1* is an essential gene, only haploid cells containing the plasmid were viable. The SC41U cells were transformed with a second plasmid (pAAL) containing a series of mutant constructs, or *S. cerevisiae* *DOLPP1* or human *PPT1* cDNAs. Those plasmids included specific point mutants, deletion and nonsense mutants within the *pdf1* coding sequences on the plasmid. The growth of each transformant in the presence and absence of 5'FOA was scored (Figure 2.3). As a result, I observed that plasmids bearing inactivating mutations in the Ppt1p domain (Hofmann et al. 2002) (S106A and D226A) that contained an intact Dolpp1p domain complemented the
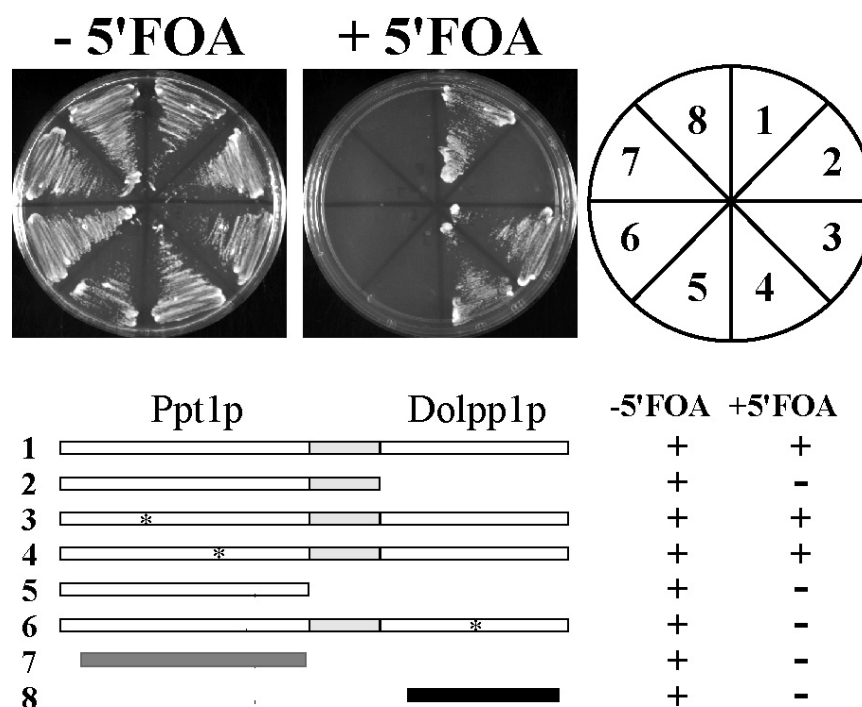
Figure 2.3 Plasmid shuffling by counterselection on 5-FOA reveals that the Dolpp1p domain is essential for viability. The ability to grow in the presence of 5-FOA indicates complementation of *pdf1*Δ by the indicated plasmid in SC41U haploid cells. The schematic (1 to 8) indicates the amino acid sequences encoded by the complementing plasmid with inactivating point mutations, deletions, or nonsense mutations as indicated: 1, wild-type Pdf1p; 2, Pdf1pΔ 373 to 602; 3, Pdf1p (S106A); 4, Pdf1p (D226A); 5, Pdf1p (K302Stop); 6, Pdf1p (H478A); 7, human Ppt1p; 8, *S. cerevisiae* Dolpp1p. The transformants were streaked to EMM plates supplemented only with adenine (−5'FOA) or adenine, uracil, and 5-FOA (+5'FOA). The growth of each transformant on the plates was scored. +, growth; −, no growth.

lethal phenotype (Figure 2.3, sectors 3 and 4), whereas plasmids truncated before the

Dolpp1p domain or bearing a mutation in a highly conserved residue in the phosphate

binding pocket of Dolpp1p (Studdert et al. 1991) (H478A) did not rescue the phenotype

(Figure 2.3, sectors 2, 5 and 6). Therefore, it is clear that loss of the Dolpp1p domain is

responsible for the lethal phenotype. Interestingly, neither human Ppt1p nor *S. cerevisiae*

Dolpp1p expression plasmids alone complemented the lethal phenotype.

2.3.4   Phenotype of Ppt1p-deficient mutants

I observed that while *pdf1Δ* mutants rescued by functional Dolpp1p alone were

viable, the growth rate of these cells was somewhat slower than that of the haploid cells

containing the wild type *pdf1*⁺ gene (Figure 2.4, left panel). This growth retardation

phenotype was reversed by a second plasmid encoding a wild type Ppt1p domain (Figure 2.4,

right panel) and an inactivated Dolpp1p domain, suggesting that the growth retardation was

caused by the lack of Ppt1p function. Therefore, I have further examined the phenotype of

these strains. (Of note, Ppt1p enzymatic activity in these strains could not be measured due

to interfering activities or substances in the yeast that raised background signals in the assay).

None   **pAAU-pdf1(H478A)**   **pAAU**
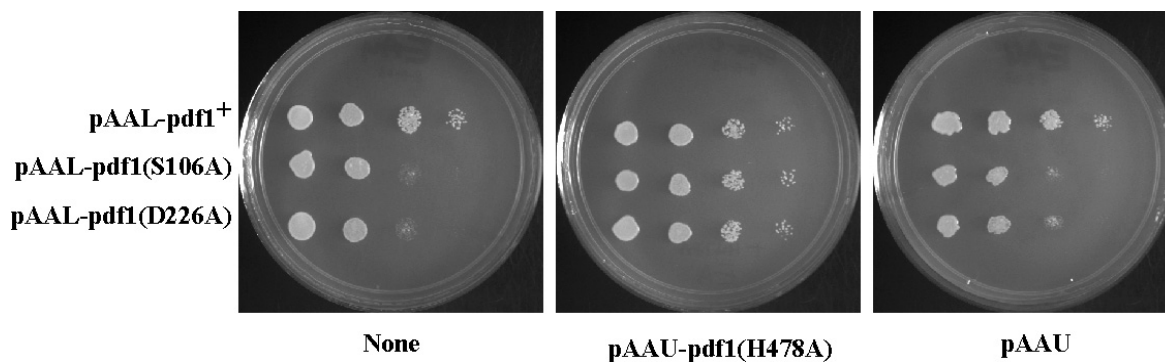
Figure 2.4 Growth retardation of cells harboring point mutants in the Ppt1p domain.
(Left panel) *pdf1Δ::his3*⁺ haploids were rescued by plasmids containing wild-type *pdf1*⁺ or
plasmids bearing mutations in active site residues of the Ppt1p domain (S106A and D226A).
(Middle panel) Rescue of growth retardation by a second plasmid containing a wild-type
Ppt1p domain and catalytically inactive Dolpp1p domain. Serial 10-fold dilutions were
spotted onto plates containing the relevant amino acid supplement.

2.3.5   Ppt1p-deficient mutants are abnormally sensitive to vanadate and elevated extracellular pH

As Ppt1p is a lysosomal enzyme in mammalian cells and as the fungal vacuole is the equivalent organelle of mammalian lysosome, I thought that it would be of interest to see whether deficiency of Ppt1p function would lead to phenotypes normally associated with vacuolar mutants in fungi, such as sensitivity to sodium orthovanadate or external pH (Banta et al. 1988; Kitamoto et al. 1988; Klionsky et al. 1990; Takeshige et al. 1992; Iwaki et al. 2003). As shown in Figure 2.5A, cells harboring a wild type *pdf1* gene were not affected by vanadate, while cells harboring inactivating mutations in Ppt1p are sensitive to vanadate in a concentration dependent manner (sectors 2 and 3). This sensitivity was reversed when the cells were transformed with a second plasmid containing the wild type Ppt1p domain and an inactive Dolpp1p domain (Figure 2.5A, center column). Inactivating mutations in the Ppt1p domain were also associated with an abnormal sensitivity to elevated extracellular pH, as shown in Figure 2.5B. At pH 5.5, cells complemented with either wild type or plasmids bearing mutations in the Ppt1p domain grow normally. However, when the external pH was elevated above pH 6.0, the haploid cells lacking functional Ppt1p did not grow. This pH sensitivity was reversed when the cells were transformed with a second plasmid containing a wild type Ppt1p domain and an inactive Dolpp1p domain (Figure 2.5B, center column).

Transformation of cells with an empty plasmid vector had no effect on the phenotype (Figure 2.5A and B, third column). These results strongly suggest that Ppt1p activity is required for normal vacuolar function in *S. pombe.*
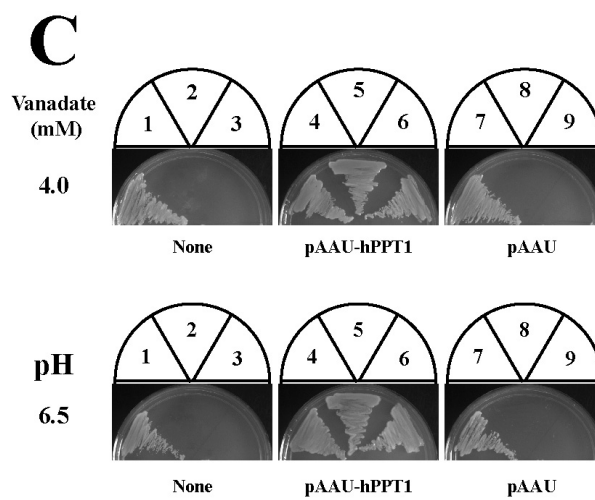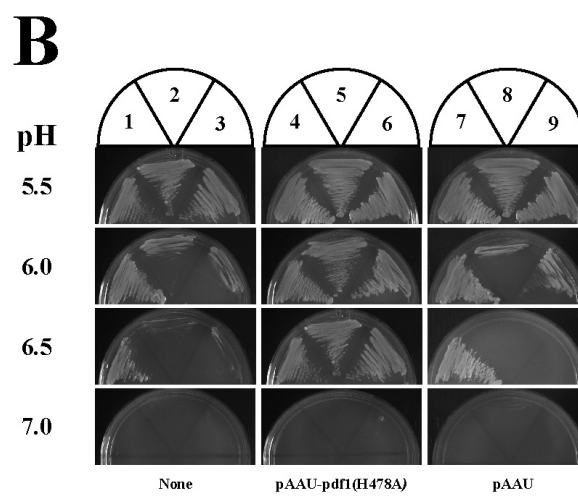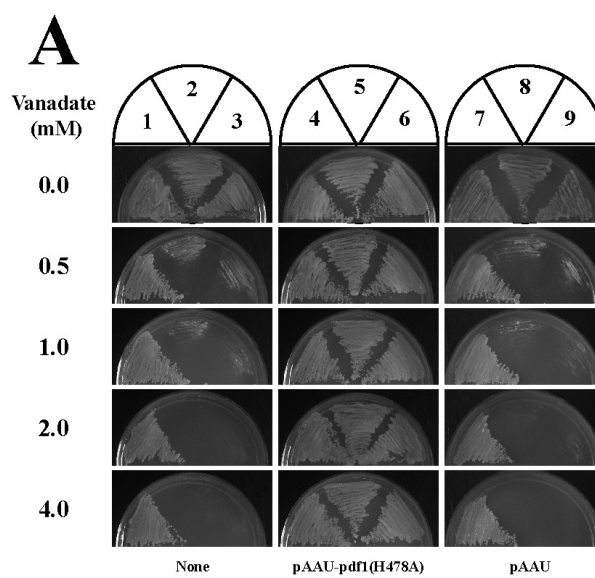
Figure 2.5 Sensitivity of PPT-deficient cells to sodium orthovanadate and to extracellular pH. (A) Normally inviable *pdf1Δ::his3*[+] haploids rescued by wild-type pAAL-pdf1[+] (1), mutated pAAL-pdf1(S106A) (2), or pAAL-pdf1(D226A) plasmids with mutations in the Ppt1p domain (3) were exposed to various concentrations of sodium orthovanadate for 4 days at 30°C. Mutations in the Ppt1p domain conferred sensitivity to sodium orthovanadate in a concentration-dependent manner. The sensitivity was reversed when the cells were transformed with a second plasmid, pAAU-pdf1(H478A), containing wild-type PPT and an inactivating mutation in the Dolpp1p domain (sectors 4 to 6). Empty vector controls are shown in sectors 7 to 9. (B) Yeast cells were incubated at 30°C for 4 days on EMM adjusted to the indicated pH. Ppt1p-inactivating mutations conferred an abnormal sensitivity to high pH to the cells. The sensitivity to higher pH was reversed when the cells were transformed with a second plasmid containing a wild-type PPT domain and an inactivating point mutation in the Dolpp1p domain (sectors 4 to 6). This suggests that the pH sensitivity is due solely to the absence of wild-type Ppt1p activity in the cells. Note that even normal *S. pombe* cells were unable to grow at pH 7.0. Empty vector controls are shown in sectors 7 to 9. (C) The human PPT1 gene activity was able to complement the phenotypes of PPT-deficient mutants. A second plasmid containing a human PPT1 cDNA (pAAU-hPPT1) was transformed into the cells. Transformants were streaked onto plates containing either 4 mM sodium orthovanadate or medium buffered to pH 6.5.

I also tested for a number of other phenotypes, especially those associated with defects in cell wall integrity, as is seen in Dolpp1p (CWH8) mutants in *S. cerevisiae* (van Berkel et al. 1999; Fernandez et al. 2001). Ppt1p deficient growth was unaffected in the presence of calcofluor white (up to 1 mg/ml), sorbitol or glucose (2 M), potassium chloride (0.9 M) or glycerol (as a sole carbon source). In addition, staining with the dye FM4-64, which reveals defects in endocytosis in *S. pombe vps* mutants (Takegawa et al. 1995), was unaffected, when observed after 30 minutes of incubation and up to 16 hours after incubation. Addition of vanadate (4 mM) or upward adjustment of extracellular pH to 6.5 for 3 h prior to staining had no effect. Evaluation of wild-type and Ppt1p deficient cells by electron microscopy revealed no significant differences in vacuolar morphology, and no clear accumulations of granular osmiophilic deposits were noted. In addition, heat sensitivity (as

assessed by growth at 37°C) and cold sensitivity (growth at 23°C) were indistinguishable

from wild-type.

2.3.6 Functional equivalence of human and *S. pombe* Ppt1p domains

The presence of vacuolar phenotypes in the cells lacking Ppt1p function allowed

testing of whether the human PPT1 ortholog would substitute for the *S. pombe* gene to

complement these phenotypes. As shown in Figure 2.5C, a human PPT1 cDNA

reestablished *S. pombe* cell viability in the presence of vanadate and at elevated extracellular

pH. These results indicate that *S. pombe* can be used as a model organism for the study of

Batten disease.

2.3.7 Posttranslational processing of Pdf1p.

In order to determine whether the two functional domains of Pdf1p remain associated

as a single polypeptide or whether they are subject to post-translational proteolytic

processing, I made an antibody that recognizes the carboxyl terminus of Pdf1p, and used it to

examine the molecular masses of proteins produced from plasmid-derived expression of

Pdf1p (Figure 2.6). Membrane fractions were prepared from the yeast and solubilized

samples were subjected to SDS-PAGE and transferred onto nitrocellulose membranes for

immunoblotting. In Figure 2.6A, lane 1 (wild type), one major band at 31 kDa and two minor

bands at 101 kDa and 33 kDa are seen. The major band corresponds precisely to the

predicted molecular mass of the Dolpp1p domain (in the absence of the linker region),

whereas the upper minor band at 101 kDa corresponds to the full-length unprocessed Pdf1p.

The Pdf1p linker region contains two putative cleavage sites for the kex-related

A

B

$$\text{SLFPEKR}^{344}\text{NFKELTMRKR}^{354}$$

R α Pdf1p

Ppt1p   Dolpp1p
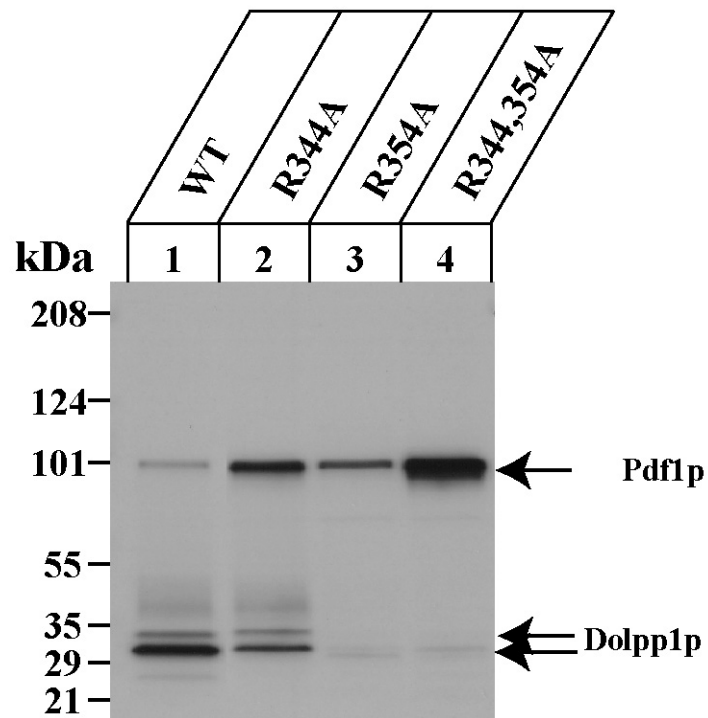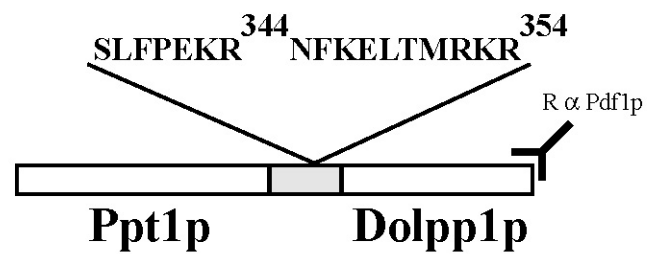
C

Pdf1p	SLFPEKR[344]NFKELTMRKR[354]
Krp1p	SSIRKR[82]GIDAGILELERQTRPRWRYKR[102]

Figure 2.6 Posttranslational processing of Pdf1p at dibasic cleavage sites. (A) Membrane fractions of cell lysates were prepared, separated by SDS-PAGE, and transferred to

nitrocellulose for immunoblotting with an antibody that recognizes the carboxyl terminus of Pdf1p. Cells were expressing either wild-type Pdf1p or Pdf1p that contained point mutations in the linker domain (R344A, R354A, or both mutations). Substitution of alanine for arginine at position 354 blocks the proteolytic cleavage, suggesting that arginine 354 is crucial for the posttranslational processing. (B) Schematic of Pdf1p cleavage sites. Two clusters of dibasic motifs, KR^{344} and RKR^{354}, are indicated. (C) Comparison of known cleavage sites for Krp1p within Krp1p itself (autocatalytic sites) versus putative Krp1p cleavage sites within the Pdf1p linker region. Note that the order of internal and primary sites for Krp1p (Davey *et al.* 1994; Powner *et al.* 1998) along the polypeptide is reversed and the number of intervening amino acids between the two sites is smaller in Pdf1 (10 versus 20). In addition, the arginine in the primary site of Krp1 is replaced by leucine in Ppt1p.

endopeptidase designated Krp1p (Davey et al. 1994; Powner et al. 1998). Mutation at one of

the two putative Krp1p cleavage sites (R344A) did not prevent cleavage of the linker domain

(Figure 2.6A, lane 2) but did increase the ratio of the unprocessed to the processed form.

However, mutation of the dibasic motif at the internal site (R354A) (Figure 2.6B, C)

essentially abolished cleavage (Figure 2.6A, lane 3). Mutation of the dibasic motifs at both

the primary and internal sites also prevented the processing of Pdf1p and increased the level

of precursor Pdf1p (Figure 2.6A, lane 4). These results suggest that Pdf1p is proteolytically

cleaved to form distinct Ppt1p and Dolpp1p domains and that Arg354 is crucial for the

posttranslational processing.

2.4 Discussion

In the present study, I demonstrated that an ortholog of human PPT1 is present in the

genome of *S. pombe* as a fusion gene with a partner, *DOLPP1*. The entire open reading

frame of the *pdf1* gene is translated as a unit and subjected to post-translational proteolytic

processing. Mutation at either one of two consensus sequences for the endopeptidase Krp1p

inhibits processing whereas mutation at both sites abolishes it. I found that Dolpp1p function

is absolutely essential for viability in *S. pombe*. However, lack of Ppt1p function causes hypersensitivity to elevated extracellular pH and to sodium orthovanadate. The human *PPT1* cDNA complements these phenotypes, suggesting that the function of *PPT1* has been conserved throughout evolution.

Abnormalities in lysosomal pH homeostasis in the juvenile-onset form of Batten disease were first uncovered through the study of a yeast model of the disease (Pearce et al. 1997; Pearce et al. 1998; Pearce et al. 1999a; Pearce et al. 1999b; Pearce 2000). Juvenile onset Batten disease is caused by mutations in *CLN3*, which encodes a multi-membrane spanning intrinsic lysosomal membrane protein of unknown function (Lerner et al. 1995). The orthologous *S. cerevisiae* gene, *BTN1*, is an intrinsic vacuolar protein. In contrast to Ppt1p-deficient *S. pombe*, *BTN1Δ* cells do not exhibit an overt phenotype referable to defective vacuolar function (in over 100 experimental conditions screened (Pearce et al. 1999a)), with the exception that the cells are resistant to a primary amine growth inhibitor, D-(-)-threo-2-amino-1[p-nitrophenyl]-1, 3-propanediol (ANP). The ANP resistance of *BTN1Δ* cells was shown to be related to a subtly enhanced acidification of the external medium, and *BTN1Δ* strains have a slightly more acidic vacuolar pH in early phases of growth (Pearce et al. 1999a). The human *CLN3* cDNA complements this phenotype and substitutes functionally for *BTN1* (Pearce et al. 1998; Pearce et al. 1999b; Chattopadhyay et al. 2000). Observations of more robust phenotypes in Ppt1p vs. Cln3p deficiency appears to hold in yeast, mice (Katz et al. 1999; Mitchison et al. 1999; Gupta et al. 2001) and humans (Goebel 1995).

The phenotypes I observed in Ppt1p loss of function mutations in *S. pombe* (hypersensitivity to elevated extracellular pH and vanadate), while not seen in the yeast model of late-onset Batten disease, do overlap some of those previously described in the *vma* (vacuolar membrane ATPase) and class C and D *vps* (vacuolar protein sorting) mutants of *S. cerevisiae* and *vps33* mutants of *S. pombe* (Bankaitis et al. 1986; Robinson et al. 1988; Nelson et al. 1990; Oluwatosin et al. 1998; Yoshida et al. 2000; Iwaki et al. 2003). *Vma* mutants carry mutations in subunits of the vacuolar H^+-ATPase (an enzyme responsible for the acidification of vacuolar contents and maintenance of intracellular pH) and class C and class D *vps* mutants display defects in vacuole morphogenesis (Rothman et al. 1986; Robinson et al. 1988). These mutants are also sensitive to environmental manipulations such as external pH and sodium orthovanadate (Banta et al. 1988; Kitamoto et al. 1988; Klionsky et al. 1990; Takeshige et al. 1992; Iwaki et al. 2003). Therefore, the data in *S. pombe* suggest that Ppt1p functions in the vacuole, just as it functions in the analogous structure (lysosome) of mammalian cells.

The observed proteolytic processing of the Pdf1p fusion protein in *S. pombe* is also entirely consistent with the known subcellular compartmentalization of Ppt1p and Dolpp1p in mammalian cells. As described earlier, Ppt1p is a resident soluble lysosomal enzyme in higher organisms that traffics through the classical mannose 6-phosphate receptor pathway (Verkruyse et al. 1996), whereas Dolpp1p is a resident ER protein (Fernandez et al. 2001; Rush et al. 2002). Therefore, the data are consistent with a model that in *S. pombe*, the Pdf1p fusion protein is directed into the secretory pathway by virtue of the Ppt1p signal sequence, with appearance of the Ppt1p domain on the lumenal side, followed by cotranslational

incorporation of Dolpp1p into the ER membrane. The fusion protein would then become available for processing by Krp1p (or a related enzyme) and the Ppt1p domain would be free for transport to the vacuole.

Whether Pdf1p is indeed a physiological substrate for Krp1p remains to be determined experimentally. Deletion of *Krp1* in *S. pombe* is lethal (Powner et al. 1998), and as deletion of Dolpp1p is also lethal, one may speculate that lack of processing of Dolpp1p by Krp1p is responsible for the lethality in *Krp1* null strains. (Of note, Dolpp1p processing mutants created in this study were viable, but the mutants appeared to be leaky, because small amounts of processed Ppt1p were detectable on longer exposures).

The translation of Pdf1p as a single polypeptide suggests that there may be an advantage in coordinately regulating levels of Ppt1p and Dolpp1p in *S. pombe*. In mammalian cells, a number of lysosomal enzymes are coordinately upregulated in a compensatory fashion under conditions of lysosomal dysfunction (Cataldo et al. 1991; Kopacek et al. 2000; Tyynela et al. 2000).

Studies in lower organisms, particularly yeast, have provided surprising insights into human biology, even in the area of human neurodegenerative disease (Sherman et al. 2003). The two yeast models of Batten disease have provided evidence for abnormal vacuolar function due to lack of the relevant disease proteins and have begun to implicate abnormalities in pH homeostasis in the pathogenesis of these disorders, with implications for therapy. Future work in these genetically tractable organisms may therefore provide further insights into the pathogenesis of Batten Disease.

CHAPTER THREE

Cloning and characterization of mammalian *DOLPP1*

3.1 Introduction

The multisubunit oligosaccharyltransferase (OST) complex (Silberstein *et al.* 1996) catalyzes the transfer of $Glc_3Man_9GlcNAc_2$ from dolichyl pyrophosphate (Dol-P-P) to asparagine residues of the *N*-glycosylation in the consensus sequence (Asn-Xxx-Ser/Thr) during the co-translational *N*-glycosylation of nascent polypeptides in yeast and mammalian cells (Herscovics *et al.* 1993; Burda *et al.* 1999; Schenk *et al.* 2001). During the process, Dol-P-P is released on the luminal surface of the endoplasmic reticulum (ER). In order for Dol-P-P to be re-utilized as a glycosyl carrier lipid for additional rounds of lipid intermediate biosynthesis, it has to be converted to dolichyl phosphate (Dol-P) and translocated to the cytoplasmic face of the ER (Schenk *et al.* 2001). Although it is possible that Dol-P-P, or perhaps Dol-P, diffuses transversely from the luminal leaflet to the cytoplasmic face by a protein-mediated mechanism, it is hypothesized that it is dephosphorylated on the luminal surface to form free dolichol that could more readily diffuse back to the cytoplasmic leaflet. Then, free dolichols in the cytoplasm would be re-phosphorylated by dolichol kinase (Allen *et al.* 1978; Fernandez *et al.* 2001). It has been shown that the *CWH8* gene in *Saccharomyces cerevisiae* encodes a Dol-P-P phosphatase that actively converts Dol-P-P to Dol-P (Fernandez *et al.* 2001). Moreover, the yeast Dol-P-P phosphatase is recovered in crude microsomal fractions, but its subcellular location has not been established. Although it has been reported that crude microsomal fractions from a variety of mammalian cells contain

enzymes that can hydrolyze exogenous Dol-P-P, the identity, specificity and exact subcellular location of the enzymes catalyzing the hydrolysis of Dol-P-P have not been established (Scher *et al.* 1984a; Wolf *et al.* 1991; Toke *et al.* 1998; Faulkner *et al.* 1999; Toke *et al.* 1999; Fernandez *et al.* 2001; Schenk *et al.* 2001).

In this chapter, I will present the data of cloning and characterization of mammalian ortholog of *CWH8*, including a subcellular localization study. The identification of the mammalian ortholog of *CWH8* as a Dol-P-P pyrophosphate phosphatase is based on its ability to complement defects in growth and protein *N*-glycosylation in the *cwh8Δ* mutant and to prevent the accumulation of Dol-P-P in the mutant cells (van Berkel *et al.* 1999; Fernandez *et al.* 2001). These studies were done in collaboration with Dr. Skip Waechter's group at University of Kentucky. The mammalian ortholog gene of *CWH8* is then renamed as mouse *DOLPP1* (dolichol pyrophosphate phosphatase 1). Polyclonal antibody against a synthetic peptide corresponding to amino acid residues (86-105) of mouse *DOLPP1* has been generated. This polyclonal antibody (anti-mDOLPP1) was utilized in subcellular localization studies.

3.2 Experimental Procedures

3.2.1 Materials

Plasmid YEp352 containing the yeast gene *CWH8* coding sequence and 240 bp of 5'-flanking sequence was a gift from Drs. Fabiana Fernandez and Markus Aebi (ETH, Zurich, Switzerland). Yeast strains W303-1A, *cwh8Δ*, and *lpp1Δ/dpp1Δ* were the generous gifts from Dr. George Carman, Department of Food Science, Rutgers University, New Brunswick,

NJ. *n*-Octyl-β-D-glucopyranoside was purchased from Calbiochem-Novabiochem. Triton X-100 was from Pierce. Trichloroacetonitrile, tetrabutylammonium hydroxide, and anhydrous acetonitrile were obtained from Aldrich. Nycodenz, dioleoylphosphatidic acid (lot number 129F8359), and diolein (D-8894) were obtained from Sigma. Dolichol (C95) was a generous gift from Dr. M. Mizuno, Kuraray Chemical Co. (Okayama, Japan). Carrier-free [^{32}P] phosphoric acid was purchased from American Radiolabeled Chemicals (St. Louis, MO). Econo-safe^{TM} biodegradable scintillation counting mixture is a product of Research Products International (Mount Prospect, IL). Yeast nitrogen base, yeast extract, and BactoPeptone are products of BD Biosciences. Casamino acid is a product of Fisher. Antibodies were obtained from the following commercial sources and used according to instructions from the supplier: rabbit anti-calnexin polyclonal antibody and mouse anti-KDEL monoclonal antibody (StressGen Biotechnologies, Victoria, British Columbia, Canada); mouse anti-KDEL receptor monoclonal antibody, mouse anti-β-COP monoclonal antibody, horseradish peroxidase-conjugated sheep anti-rabbit IgG, horseradish peroxidase-conjugated sheep anti-mouse IgG (Amersham Biosciences); and fluorescein isothiocyanate-conjugated goat anti-rabbit IgG and Texas Red-conjugated goat anti-mouse IgG (Molecular Probes, Eugene, OR). Anti-CPY antiserum was generously provided by Dr. Neta Dean, State University of New York, Stony Brook, NY. All other chemicals and reagents were purchased from standard commercial sources.

3.2.2   Affinity-purified rabbit anti-Dolpp1p antibodies and immunoblotting

Three New Zealand White rabbits were each immunized with 300 µg of a synthetic peptide corresponding to amino acid residues 86-105 of mouse Dolpp1p coupled to keyhole limpet hemocyanin as described previously (Camp *et al.* 1994). The antigen was injected intradermally in Freund's complete adjuvant, and rabbits were boosted three times at 3-week intervals with 300 µg of peptide in Freund's incomplete adjuvant. An IgG fraction was prepared from preimmune and immune serum by specific binding to protein A-Sepharose CL-4B (Amersham Biosciences). IgG was affinity-purified by specific binding to a column consisting of the Dolpp1p peptide cross-linked to SulfoLink coupling gel (Pierce). For analysis of *DolPP1* expression by immunoblotting, samples were analyzed by electrophoresis in 15% SDS-PAGE gels and immunoblotting essentially as described (Verkruyse *et al.* 1997). Filters were blocked for 1 h with Sea Block (East Coast Biologics, North Berwick, ME) and washed in PBS-T (0.25% (v/v) Tween 20 in phosphate-buffered saline) followed by incubation for 2 h with rabbit anti-Dolpp1p polyclonal antibody (1 µg/ml). The filters were washed with PBS-T and incubated for 45 min in a solution containing horseradish peroxidase-conjugated secondary antibody (sheep anti-rabbit IgG, Amersham Biosciences) diluted 1:2500 in PBS-T. The filters were washed and developed using ECL chemiluminescence reagents (Amersham Biosciences).

3.2.3 Preparation of radiolabeled phosphorylated lipid substrates

$[^{32}P]PA$, $[^{32}P]Dol-P$, $[\alpha,\beta^{-32}P]Dol-P-P$, and $[\beta^{-32}P]Dol-P-P$ were chemically synthesized in anhydrous acetonitrile from the appropriate lipid using $[^{32}P]$tetrabutylammonium phosphate and trichloroacetonitrile as described by Danilov *et al.*

(Danilov *et al.* 1989). Unlabeled polyisoprenyl phosphates were synthesized using tetrabutylammonium phosphate. Synthetic substrates were purified by preparative thin layer chromatography on Baker Si250 thin layer plates developed in $CHCl_3/CH_3OH/H_2O/NH_4OH$ (65:35:6:1, v/v).

3.2.4 Northern blotting

Plasmid and genomic DNA preparation, restriction enzyme digestion, and DNA ligations were performed by standard methods (Sambrook *et al.* 1989). Transformation of yeast and *Escherichia coli* were performed as described(Sambrook *et al.* 1989; Schiestl *et al.* 1989). For blot hybridization of RNA, total RNA was isolated from mouse tissues as described (Gupta *et al.* 2001). Blots were pre-hybridized for 30 min at 65 °C in Rapid-Hyb buffer (Amersham Biosciences), followed by hybridization with a random hexamer-primed ^{32}P-labeled mouse cDNA fragment corresponding to the entire 717-bp coding region of DolPP1 for 3 h at 65 °C. The blots were washed in 2× SSC (1× SSC = 150 mM NaCl and 15 mM sodium citrate (pH 7)), 0.1% SDS at ambient temperature for 30 min, followed by stringent washes in 0.5× SSC, 0.1% SDS at 65 °C for 15 min and in 0.1 × SSC, 0.1% SDS at 65 °C for 15 min.

3.2.5 Yeast culture

Yeast cultures were grown at 30 °C in either 1% yeast extract, 2% BactoPeptone, and 2% dextrose or in yeast nitrogen base (6.7 g/liter), 50 mM sodium succinate (pH 5.0), 2% dextrose, amino acids (25 mg/liter), and purine and pyrimidine bases (25 mg/liter) as required to meet auxotrophic requirements for selective growth. Yeast transformants were screened on

2% agar plates containing 6.7 g/liter yeast nitrogen base, 0.5% casamino acids, 50 mM

sodium succinate (pH 5.0), 2% dextrose, and 25 mg/liter adenine or leucine as required.

Yeast microsomal fractions for the routine analysis of lipid phosphatase activities

were prepared exactly as described previously (Fernandez *et al.* 2001). Assays of Dol-P-P,

Dol-P, and PA phosphatase activities were performed as described previously (Scher *et al.*

1984a; Scher *et al.* 1984b).

3.2.6   Measurement of cellular levels of Dol-P and Dol-P-P in yeast cells

Yeast cells (1 liter) were grown in YPD containing 2% dextrose to 1-4 A_{600} and

collected by centrifugation at 1,000 × g, 20 min. The cells were resuspended in distilled

water, sedimented again, resuspended in distilled water to 200 A_{600}/ml, and incubated for

30 min at 30 °C in 50 mM Tris-HCl (pH 7.4), 10 mM $MgCl_2$ containing 1 mg/ml lyticase

(Sigma). The yeast spheroplasts were sedimented at 1,000 × g for 20 min; the supernatant

was decanted, and the pellet was mixed vigorously with 40 volumes of $CHCl_3/CH_3OH$ (2:1,

v/v). Dol-^{32}P and Dol-P-^{32}P (5,000 cpm of each) were added as recovery markers, and the

insoluble material was sedimented in a clinical centrifuge. The organic layer was removed

and reserved on ice. The insoluble pellet was sequentially extracted twice with 5 ml of

$CHCl_3/CH_3OH$ (2:1 v/v) and twice with 5 ml of $CHCl_3/CH_3OH/H_2O$ (10:10:3, v/v). The

organic extracts were combined, taken to dryness by rotary evaporation under reduced

pressure at 30 °C, and then saponified in 1 ml of toluene/CH_3OH (1:1, v/v) containing 0.1 M

KOH on ice for 30 min. Following saponification, the reaction was neutralized with acetic

acid, diluted with 5 ml of $CHCl_3/CH_3OH$ (2:1 v/v), and partitioned with 1 ml of water. The

aqueous layer was discarded, and the organic phase was subsequently partitioned twice with

1 ml of $CHCl_3/CH_3OH/H_2O$ (3:48:47, v/v). The organic phase was dried under a stream of N_2

gas and redissolved in 0.2 ml of $CHCl_3/CH_3OH/H_2O$ (10:10:3, v/v). Dol-P and Dol-P-P in the

organic extracts were separated by ion exchange chromatography on a 20-ml column of

DEAE-650M (Toyopearl, Supelco, Bellefonte, PA) equilibrated with $CHCl_3/CH_3OH/H_2O$

(10:10:3, v/v) and eluted with a linear gradient of 0 to 0.2 M ammonium acetate (60 ml). The

fractions containing Dol-P and Dol-P-P were pooled separately and supplemented with

$CHCl_3$ and water to give a final composition of $CHCl_3/CH_3OH/H_2O$ (3:2:1, v/v). The phases

were separated by a brief centrifugation, and the aqueous layer was discarded. The organic

layer was then partitioned once with 1/5 volume of $CHCl_3/CH_3OH/H_2O$ (3:48:47, v/v), taken

to dryness under a stream of N_2 gas, and redissolved in a small volume of

$CHCl_3/CH_3OH/H_2O$ (10:10:3, v/v). Aliquots representing equivalent portions of the initial

extracts were spotted on 10 × 20-cm Baker Si250 Silica Gel thin layer plates and developed

in $CHCl_3/CH_3OH/H_20/NH_4OH$ (65:35:6:1,v/v). Following chromatography, the thin layer

plates were allowed to air dry and were visualized by staining with anisaldehyde (Dunphy *et*

al. 1967). The migration positions of radioactive standards were determined with a Bioscan

System 200 Imaging Scanner (Bioscan Inc. Washington, D. C.).

3.2.7   Expression of pCHA7/*DOLPP1* in COS cells

To construct a Dolpp1p transient expression plasmid for mammalian COS cells, the

expressed sequence tag division of GenBank[TM] was searched for clones homologous to

S. cerevisiae Cwh8p, and yielded IMAGE clone 1974625, GenBank[TM] accession number

AI876279. (This clone was obtained independently of gene 2-23 sequence described above.)

Both strands of the cDNA were sequenced, which revealed that the clone was incomplete at

the 5' end. Therefore, a 5'-RACE procedure was employed using 1 μg of mouse total brain

mRNA and a SMART RACE cDNA Amplification Kit (Clontech Laboratories, Inc., Palo

Alto, CA). Briefly, Moloney murine leukemia virus-reverse transcriptase Superscript II

(Invitrogen) was used to perform the reverse transcription according to the supplier's

protocol. PCR was performed using the supplied universal primer mix, a gene-specific primer

(5'-CTGGGAATGGCTGGAGGGCATCCCG-3'), and a nested primer (5'-

CGCCCTGATTCAGTGCCAGTCCCCC-3') to obtain the 5' terminus of mouse *DOLPP1*

cDNA. The PCR was performed using a PerkinElmer Life Sciences GeneAmp System

9600 using the Advantage 2 PCR kit (Clontech Laboratories, Inc., Palo Alto, CA) under

conditions suggested by the supplier. The resulting fragment was subcloned into the plasmid

pGEM-T-Easy (Promega, Madison, WI), sequenced, and shown to be complete at the 5' end.

The entire open reading frame was then amplified from total mouse brain cDNA using

primers corresponding to sequences within the 5'-RACE product and mouse expressed

sequence tag IMAGE clone 1974625 (5'- ATGGCAGCGGACGGACAGTGC-3' and 5'-

TCACTGCAGTTTTGTTCCAAG-3'). PCR conditions for the amplification consisted of the

following: 95 °C, 5 min, one cycle; 94 °C, 30 s, 68 °C to 58 °C ("touch down" protocol),

30 s, 72 °C, 1 min for 10 cycles; 94 °C, 30 s, 58 °C, 30 s, 72 °C, 1 min for 25 cycles; 72 °C,

10 min. The resulting PCR product was subcloned into pCHA7 using *Sal*I and *Bam*HI

restriction sites at the 5' and 3' ends of the insert, respectively (Cha *et al.* 2000). The construct

was verified by sequencing, and the open reading frame was found to be 100% identical to GenBank^{TM} AB030189, which was deposited subsequently (Inoue *et al.* 2000).

Simian COS-7L cells were maintained in Dulbecco's modified Eagle's medium (high glucose), supplemented with 10% (v/v) fetal bovine serum, 100 units/ml penicillin, 100 µg/ml streptomycin, and 0.25 µg/ml amphotericin B. Cells were plated on Day 0 in 100-mm dishes and were transiently transfected on Day 1 using 6 µg of DNA (pCHA7/DOLPP1) and 18 µl of FuGEN 6 reagent (Roche Molecular Biochemicals) per plate. The cells were harvested 48 h post-transfection into ice-cold phosphate-buffered saline and pelleted at low speed. Cell pellets were resuspended in a homogenization buffer containing 50 mM Tris-HCl (pH 7.5), 0.25 mM sucrose, 5 mM EDTA, and 5 mM 2-mercaptoethanol and sonicated briefly. Nuclei and intact cells were removed by centrifugation at $500 \times g$ for 5 min at 4 °C. The postnuclear supernatant was further centrifuged at $100,000 \times g$ for 1 h at 4 °C in a Beckman Optima TLX ultracentrifuge. The resulting supernatant (S100) was reserved, and the membrane pellet (P100) was washed once and resuspended in homogenization buffer for immunoblotting or in 10 mM HEPES (pH 7.0), 0.25 M sucrose at a concentration of 10 mg of protein per ml for analysis of enzyme activity.

3.2.8   Subcellular localization of Dolpp1p

COS-7L cells (six 100-mm dishes) were transfected using pCHA7/DOLPP1 as described above and washed twice in a buffer consisting of 10 mM triethanolamine, 10 mM acetic acid, 250 mM sucrose, 1 mM EDTA, and 1 mM dithiothreitol. Cells were harvested with a rubber policeman in 800 µl of buffer containing 10 µg/ml each of chymostatin,

leupeptin, and pepstatin and homogenized by 15 passages through a 25-gauge needle on a 1-ml syringe. Nuclei and intact cells were removed by microcentrifugation at $1,200 \times g$ for 5 min at 4 °C. The postnuclear supernatant was loaded on preformed Nycodenz gradients prepared exactly as described (Rickwood *et al.* 1982). Briefly, linear Nycodenz gradients were prepared for the Beckman SW 41 Ti rotor from initial discontinuous gradients (24, 19, 15, and 10% Nycodenz in 10 mM Tris-HCl (pH 7.4), 3 mM KCl, and 1 mM EDTA) that were allowed to diffuse in a horizontal position for 45 min at room temperature and then centrifuged for 4 h at 37,000 rpm in a Beckman L8-M ultracentrifuge to generate a nonlinear density gradient profile. The postnuclear supernatant was loaded on top of the gradients and centrifuged for 1.5 h at 37,000 rpm. Fifteen fractions were collected, and aliquots of each fraction were subjected to electrophoresis on SDS-PAGE gels. The distribution of Dolpp1p, calnexin (ER marker), KDEL receptor (Golgi marker), and β-COP (Golgi marker) in the gradients was determined by immunoblotting using ECL chemiluminescence reagents (Amersham Biosciences).

3.2.9   Immunofluorescence

COS-7L cells were grown on 12-mm diameter coverslips and transfected with pCHA7/DOLPP1 using FuGEN 6 as described above. At 48 h post-transfection, the cells were fixed for 15 min in 4% formaldehyde and permeabilized for 10 min with 0.05% Triton X-100 at room temperature. The cells were doubly stained using the rabbit anti-Dolpp1p antibody and either the anti-KDEL monoclonal antibody or anti-KDEL receptor monoclonal antibody. The secondary antibodies used were fluorescein isothiocyanate-conjugated goat

anti-rabbit IgG and Texas Red-conjugated goat anti-mouse IgG. Immunofluorescence was visualized under a Zeiss Axiophot immunofluorescence microscope.

3.2.10 Preparation of sealed microsomal vesicles and general analytical methods

Sealed microsomal vesicles were prepared from the pertinent yeast strains and evaluated for integrity as described previously (Rush *et al.* 1998; Fernandez *et al.* 2001). Protein was determined by the method of Rodriquez-Vico *et al.* using a commercial protein assay reagent (BCA, Pierce) and bovine serum albumin as standard. Lipid-phosphorus analysis was according to Bartlett (Bartlett 1959; Rodriguez-Vico *et al.* 1989). Radioactivity was measured by liquid scintillation spectrometry in a Packard Tri-Carb TR-2100 Liquid Scintillation Analyzer (Packard Instrument Co., Meriden, CT) in the presence of Econo-Safe Biodegradable Counting Mixture (Research Products International, Mount Prospect, IL).

3.3 Results

3.3.1 Mammalian cells express an ortholog of the yeast *CWH8* gene

To find a mammalian ortholog of *CWH8*, the GenBank[TM] expressed sequence tag division was searched for clones orthlogous to *S. cerevisiae* Cwh8p, yielding IMAGE clone 1974625, GenBank[TM] accession number AI876279. As described in Experimental Procedures, the full length cDNA clone of mouse *DOLPP1* was obtained. Its deduced amino acid sequences are 29.8% identical and 49.4% strongly similar to sequences of yeast Cwh8p. In addition, Dolpp1p contains the consensus lipid-phosphate phosphatase motif, suggesting that Dolpp1p is the mammalian ortholog of yeast *CWH8* (Stukey *et al.* 1997).
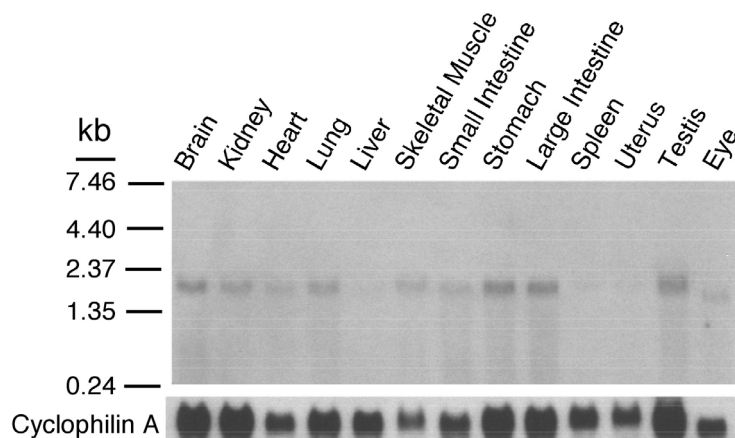
Figure 3.1 RNA blot hybridization of *DOLPP1* RNA from mouse tissues. Total RNA (20 μg) from various tissues was subjected to electrophoresis and transferred to a nylon membrane. Hybridization was performed using a ^{32}P-labeled *DOLPP1* cDNA probe (*upper panel*) followed by washing as described under "Experimental Procedures." The filter was exposed to Amersham Biosciences Hyperfilm MP film with an intensifying screen at −85 °C for 4 days. The integrity of RNA in each lane was demonstrated by stripping and reprobing the filter with a ^{32}P-labeled cDNA probe encoding mouse cyclophilin A (*lower panel*).

The *DOLPP1* mRNA was found to be widely expressed in various mouse tissues as assessed by RNA blotting (Figure 3.1). A single transcript migrating at 2.0 kb was observed in all tissues examined, with highest expression in brain, kidney, lung, and intestine and low but detectable levels in liver, spleen, and uterus. The broad tissue distribution is consistent with the ER Dol-P-P phosphatase having an essential function in the lipid intermediate pathway for protein *N*-glycosylation in all mammalian cells.

3.3.2   Overexpression of Dolpp1p corrects defects in growth rate and N-glycosylation of CPY in the *cwh8Δ* mutant

The mutant yeast strain, *cwh8Δ*, grows at an abnormally slow rate and exhibits a defect in protein N-glycosylation (van Berkel *et al.* 1999; Fernandez *et al.* 2001). To

determine whether expression of mammalian *DOLPP1* corrects the growth deficiency of the

cwh8Δ yeast strain, the *DOLPP1* gene was subcloned into YEp352 under the control of the

putative yeast *CWH8* promoter and transformed into *cwh8Δ*. The effect on rate of growth in

complete media was then assessed. As shown in Table 3.1, the cell density of wild type yeast

cultures typically doubles approximately every 2 h, whereas the doubling time ($T_{2\times}$) for

cwh8Δ was ~4 h. Overexpression of *DOLPP1* in c*wh8Δ* reduces the doubling time to 3 h,

similar to the effect of transformation with YEp352 containing the yeast *CWH8* gene

($T_{2\times}$ = 2.5 h).

Table 3.1 Overexpression of either *DOLPP1* or *CWH8* partially restores the normal rate

of growth in the *cwh8Δ* yeast mutant

Yeast strain	Doubling time (h)
Wild type	1.9
cwh8Δ	4.0
cwh8Δ/DOLPP1	3.0
cwh8Δ/CWH8	2.5

As reported previously, mutation of the *CWH8* gene in yeast results in defects in

protein *N*-glycosylation, as assessed by *N*-glycosylation of carboxypeptidase Y (CPY) (van

Berkel *et al.* 1999; Fernandez *et al.* 2001)(Figure 3.2). Although SDS-PAGE of wild type

yeast extracts revealed a single protein band corresponding to mature, fully *N*-glycosylated

CPY (Figure 3.2, *lane 1*), extracts from the *cwh8Δ* mutant contain several bands

corresponding to underglycosylated isoforms of CPY (Figure 3.2, *lane 2*). (The migration

positions of CPY lacking 1-4 oligosaccharide chains are indicated by the *arrows*.) Expression

of YEp352 carrying either the *DOLPP1* gene or the yeast *CWH8* gene restored full

glycosylation to CPY (Figure 3.2, *lanes 3* and *4*, respectively).
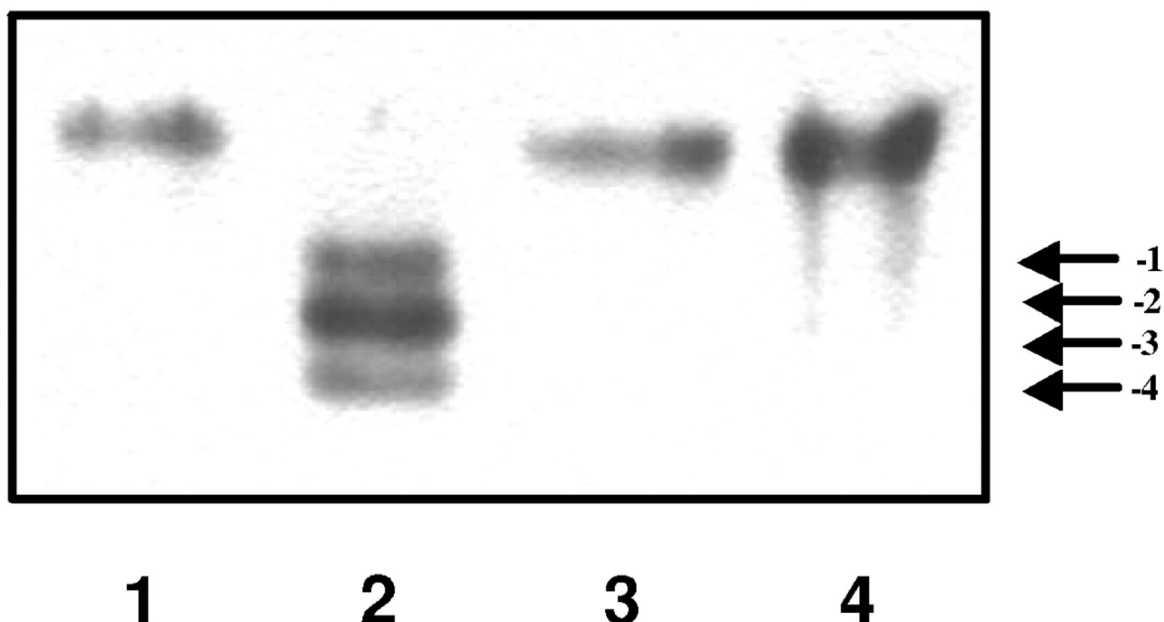
Figure 3.2 Overexpression of DOLPP1 cDNA corrects hypoglycosylation of CPY in the yeast cwh8Δ mutant. Total cell extracts from the various yeast strains were separated by SDS-PAGE and analyzed by Western blotting using α-CPY serum as described previously (56). Lane 1, wild type; lane 2, cwh8Δ; lane 3, cwh8Δ/DOLPP1; and lane 4, cwh8Δ/CWH8. The positions of mature CPY and underglycosylated isoforms are indicated.

3.3.3 Overexpression of either Dolpp1p or Cwh8p reverses the accumulation of Dol-P-P in the *cwh8Δ* mutant

Abnormally high levels of Dol-P-P accumulate in *cwh8Δ* yeast cells, due to a lack of

the Dol-P-P phosphatase activity responsible for the hydrolysis of the Dol-P-P released

during the transfer of the precursor oligosaccharide from $Glc_3Man_9GlcNAc_2$-P-P-Dol to

nascent polypeptides in the lumen of the ER (Fernandez *et al.* 2001).
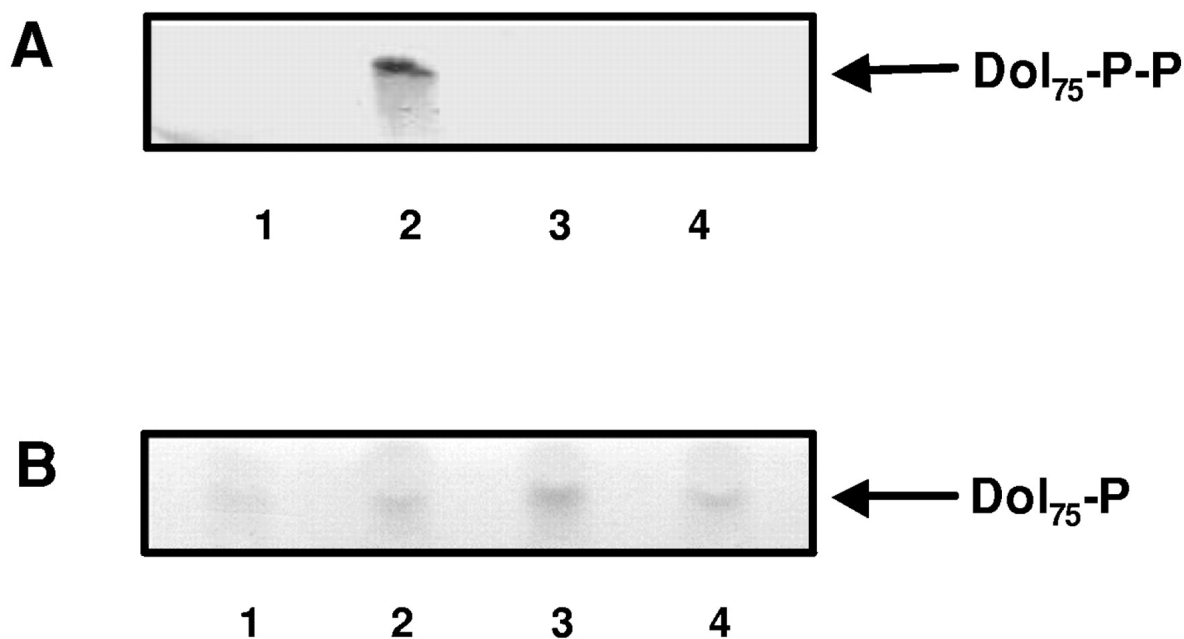
Figure 3.3 Overexpression of Dolpp1p corrects Dol-P-P accumulation in the yeast *cwh8Δ* mutant. Dol-P-P was extracted from either wild type (lane 1), *cwh8Δ* (lane 2), *cwh8Δ/DOLPP1* (lane 3), or *cwh8Δ/CWH8* yeast strains and chromatographed on Baker Si250 Silica Gel thin layer plates as described under "Experimental Procedures." Dol-P-P was visualized by anisaldehyde staining (Dunphy et al. 1967).

To determine whether overexpression of Dolpp1p in *cwh8Δ* will restore normal Dol-P-P levels, total lipid extracts were prepared from either wild type, *cwh8Δ* plus YEp352, *cwh8Δ* plus YEp352/yPro-*DOLPP1*, or cwh8Δ plus YEp352/*CWH8* yeast cells and analyzed for Dol-P-P (Figure 3.3, panel A, lanes 1-4). As reported earlier (Fernandez et al. 2001), the lipid extracts from *cwh8Δ* cells (Figure 3.3, panel A, lane 2), contained a prominent anisaldehyde-positive compound with the chromatographic mobility of standard Dol75-P-P.

In contrast to this result, virtually no Dol-P-P was detected in extracts from wild type cells (Figure 3.3, panel A, lane 1) or from *cwh8Δ* yeast cells expressing either the *DOLPP1* gene (Figure 3.3, panel A, lane 3) or the *CWH8* gene (Figure 3.3, panel A, lane 4). To confirm the identity of the anisaldehyde-positive compound as Dol-P-P, this lipid was quantitatively converted to a product chromatographically identical to Dol75-P by mild acid hydrolysis (2 h at 80 °C in CHCl$_3$, CH$_3$OH, 2 N HCl, 10:10:3, v/v). It should be noted that the levels of Dol-P in the various yeast strains were not significantly different (Figure 3.3; panel B, lanes 1-4).

3.3.4 Increase in Dol-P-P phosphatase activity upon overexpression of Dolpp1p in COS cells

The results described above (obtained from collaborative work with Dr. Waechter's group) indicate that the *DOLPP1* gene encodes a functional ortholog of the yeast Cwh8p. To explore the properties of the *DOLPP1* expressed in mammalian cells, the full-length mouse brain *DOLPP1* cDNA was inserted into the eukaryotic expression vector pCHA7 to yield the plasmid pCHA7/*DOLPP1*. Microsomal fractions were prepared from the COS cells after transient transfection with either pCHA7/*DOLPP1* or vector alone. Phosphatase reaction mixtures contained microsomes from COS cells (10 μg of protein), 10 mM EDTA, 0.6% n-octylglucoside, 25 mM citrate-sodium phosphate (pH 7), and 20 μM of substrate in a total of 0.02 ml. Three different substrates were assayed; [β-^{32}P] Dol-P-P, [^{32}P] Dol-P or [^{32}P] PA. The reaction mixture was incubated with the substrate for 5 min at 30 °C and the rates of dephosphorylation of each substrate were assayed as described previously (Scher et al. 1984a; Scher et al. 1984b). As shown in Table 3.2, a substantial increase (12-16-fold) of Dol-

P-P phosphatase activity was seen compared with identical microsomal fractions from cells transfected with the empty vector alone. It is noteworthy that no concomitant increase in Dol-P or PA dephosphorylation was observed, corroborating the specificity for Dol-P-P.

Table 3.2 Dol-P, Dol-P-P and PA phosphatase activities assayed in microsomes from COS cell lines expressing Dolpp1p.

Yeast strain	Phospholipid substrate (nmol/min/mg)		
	Dol-P-P	Dol-P	PA
COS cells	1	<0.01	0.03
COS cells	0.8	<0.01	0.06
COS(DOLPP1)	16.2	0.03	0.09
COS(DOLPP1)	12.2	<0.01	0.08

3.3.5 Expression and Subcellular Localization of Dolpp1p in COS Cells

Although mutations in the *CWH8* gene affect the rate of lipid intermediate synthesis and protein *N*-glycosylation in the ER, the precise subcellular location of the yeast enzyme had not been firmly established. Soluble (S100) and particulate (P100) fractions from *DOLPP1*-transfected COS cells were analyzed by SDS-PAGE and immunoblotting using a rabbit polyclonal antibody raised against a Dolpp1p peptide (Figure 3.4). This analysis revealed a single band in the P100 fraction (Figure 3.4, *lane 4*) at a M_r of 27 kDa in accord with the molecular mass of Dolpp1p predicted from the *DOLPP1* cDNA sequence

(27.1 kDa). No bands were visible in the S100 fraction or the fractions from the vector-

transfected cells (Figure 3.4, *lanes 1-3*).
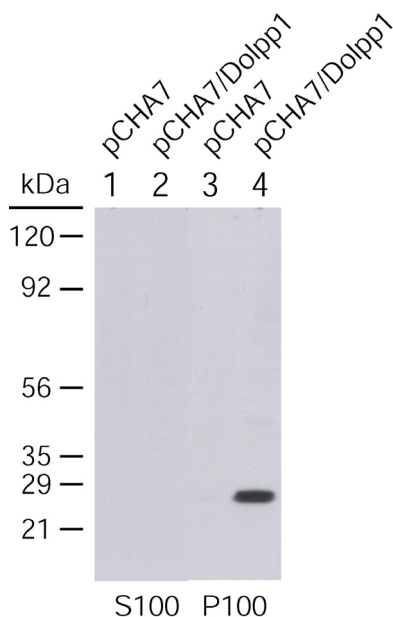
Figure 3.4 Dolpp1p expressed in COS cells is membrane-associated. COS-7L cells were
transfected with pCHA7 (*lanes 1* and *3*) or pCHA7/DOLPP1 (*lanes 2* and *4*) and harvested
48 h later. Cells were sonicated briefly and centrifuged at 100,000 × *g* to obtain a soluble
fraction (*S100, lanes 1* and *2*) and a particulate fraction (*P100, lanes 3* and *4*). A single band
appears exclusively in the particulate fraction (*lane 4*) as visualized by immunoblotting using
a rabbit anti-Dolpp1p peptide antibody. The visualized band corresponds to the predicted
molecular mass of Dolpp1p (27 kDa).

To determine further the subcellular location of Dolpp1p, transfected COS cells were

fractionated on nonlinear Nycodenz gradients, using a method previously developed to

provide effective separation of ER and Golgi complex proteins (Rickwood *et al.* 1982). As

shown in Figure 3.5, >95% of the immunoreactivity sedimented to the bottom of the gradient

(*upper panel*), co-sedimenting with calnexin, a well established ER marker. A much smaller

amount was found at the top of the gradient co-fractionating with the Golgi markers, KDEL

receptor and β-COP (Figure 3.5). The minor immunoreactivity in Golgi shown in Figure 3.5

was not observed in every experiment and seemed to correlate with higher levels of Dolpp1p

expression.
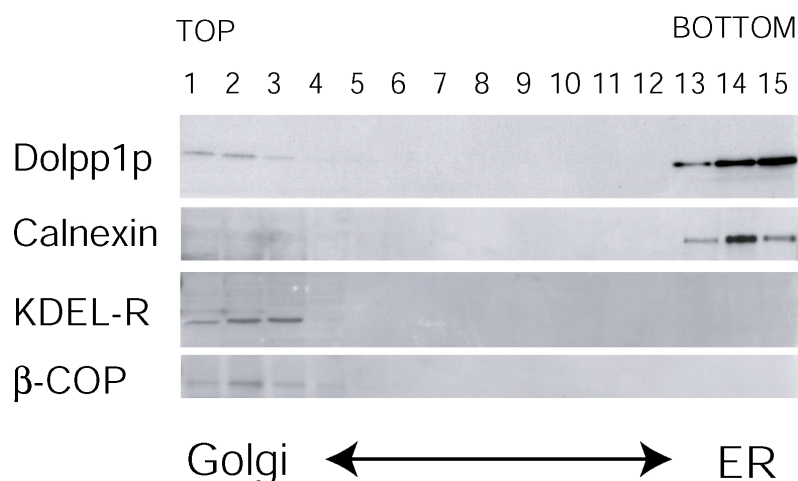
Figure 3.5 Subcellular localization of Dolpp1p on Nycodenz density gradients. COS-7L
cells were transfected with pCHA7/DOLPP1 and cell homogenates separated on preformed
Nycodenz gradients. Fractions along the gradient were analyzed by immunoblotting using
anti-Dolpp1p anti-peptide antibodies and other markers as indicated. Marker proteins were
calnexin (ER membrane marker), β-COP (Golgi marker), and KDEL receptor (Golgi
marker). A predominantly ER localization for Dolpp1p was observed (top panel). The results
illustrated in this figure are representative of three separate experiments.

A reticular and nuclear envelope pattern, which is characteristic of ER localization,

was observed when COS cells overexpressing *DOLPP1* were examined by immuno-

fluorescence microscope using a specific Dolpp1p antibody (Figure 3.6). This pattern

essentially completely overlapped with the ER marker (KDEL, *upper panel*) and showed no

overlap with a Golgi marker (KDEL receptor, *lower panel*).

| Dolpp1p | ER Marker | Merge |
| Dolpp1p | Golgi Marker | Merge |
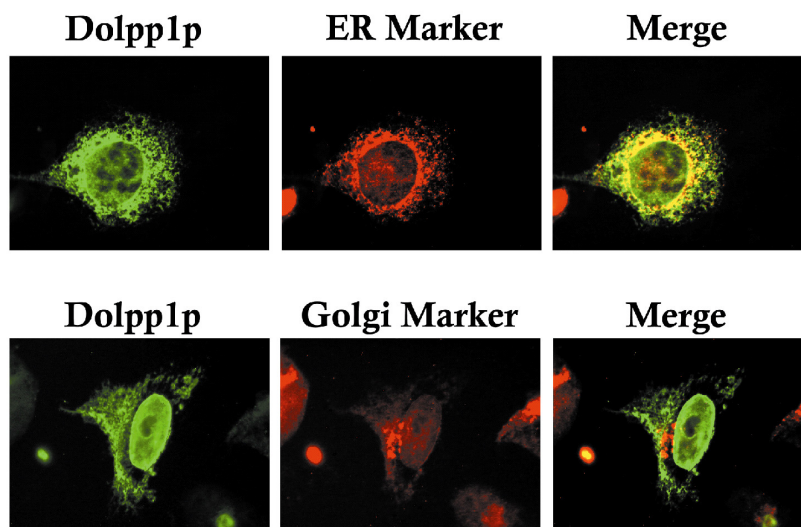
Figure 3.6 ER localization of Dolpp1p by immunofluorescence in fixed and permeabilized COS-7L cells. COS-7L cells were transfected with pCHA7/DOLPP1 and simultaneously stained with anti-Dolpp1p antibodies (*green, A* and *D*) and one of two markers, anti-KDEL antibody (ER marker, *red, B* and *C*) or anti-KDEL receptor (Golgi marker, *red, E* and *F*). Dolpp1p (*green*) shows a reticulated and nuclear envelope pattern typical of ER localization, an impression that is confirmed by the overlapped images (*merge, C*). Dolpp1p staining was distinct from Golgi staining (*F*). Weak nuclear labeling was evident in some preparations and was deemed nonspecific because it appeared in the presence of either anti-Dolpp1p or non-immune antibodies (not shown). Experiment shown is one of two yielding similar results.

3.3.6 Topological Orientation of the Active Site of Dolpp1p

To determine whether the active site of Dolpp1p faces the lumen of the ER or the cytoplasm, protease-sensitivity studies were conducted on the Dol-P-P phosphatase activity in intact and unsealed ER vesicles from the *lpp1Δ/dpp1Δ/DOLPP1* yeast strain. When detergent-disrupted ER vesicles (Table 3.3) were treated with trypsin, the Dol-P-P phosphatase activity was extensively inactivated (74.8% of control). However, the phosphatase activity was found to be relatively resistant to proteolysis in intact ER vesicles

(87.5% of control). Separate pilot experiments employing latency of glucosidase I/II established that the sealed vesicles used in this experiment were >98% intact throughout the time of incubation and that 0.2% Triton X-100 was sufficient to unseal >95% of the yeast ER vesicles (Rush *et al.* 1998). Thus, it appears that the mammalian Dol-P-P phosphatase has a trypsin-sensitive site, perhaps part of the reactive site of the enzyme, which is luminally oriented, as in the yeast enzyme.

Table 3.3 Effect of trypsinization on Dol-P-P phosphatase activity in intact and disrupted microsomal vesicles from *lpp1Δ/ dpp1Δ/DOLPP1* yeast

Vesicle treatment	Time of exposure to trypsin (min)	Dol-P-P phosphatase activity	
		(nmol/min/mg)	(% control)
None	0	3.3	100
None	60	2.9	87.5
Unsealed with 0.2% Triton X-100	0	3.7	100
Unsealed with 0.2% Triton X-100	60	0.98	26.2

3.3.7   Dolpp1p activity in *PPT1* knockout mouse brain

To further explore the functional relationship between PPT1 and DOLPP1, I prepared microsomal fractions from brain tissues of wild type, PPT1 and PPT2 knockout mice and assayed Dol-P-P phosphatase activity. Three different substrates were assayed; $[\beta\text{-}^{32}P]$ Dol-P-P, $[^{32}P]$ Dol-P or $[^{32}P]$ PA. The reaction mixture was incubated with the substrate for 10 min at 30 ˚C except for $[\beta\text{-}^{32}P]$ Dol-P-P which was incubated for 3 min at 30 ˚C, and the

rates of dephosphorylation of each substrate were assayed as described previously (Scher *et al.* 1984a; Scher *et al.* 1984b).

As shown in Table 3-4, Dolpp1p activity was decreased in the brain microsomes of *PPT1* knockout mouse compared to wild type and *PPT2* knockout mouse, indicating loss of PPT1 activity somehow affected the Dolpp1p activity in the brain.

Table 3.4 Dol-P, Dol-P-P and PA phosphatase activities assayed in microsomes from wild type, *PPT1* and *PPT2* knockout mice brain.

Mouse strain	Phospholipid substrate (nmol/min/mg)		
	Dol-P-P	Dol-P	PA
Wild type brain	0.128	0.107	0.129
PPT1 knockout brain	0.025	0.138	0.160
PPT2 knockout brain	0.089	0.101	0.131

3.4 Discussion

The *CWH8* gene in *S. cerevisiae* has been shown to encode a Dol-P-P-specific pyrophosphate phosphatase that was proposed to function in a model for the recycling of the carrier lipid (Fernandez *et al.* 2001). This chapter describes the identification and characterization of a mammalian ortholog of the yeast *CWH8* gene, *DOLPP1*, from the GenBank[TM] expressed sequence tag (EST) division.

Although there have been reports describing Dol-P-P/Dol-P phosphatase activities in crude microsomal fractions from various mammalian tissues, the exact number, location, and

specificity have not been rigorously defined (Scher *et al.* 1984a; Wolf *et al.* 1991; Faulkner *et al.* 1999; Fernandez *et al.* 2001). Previous studies have been complicated by an inability to study the enzymatic properties of these proteins independent of the activities of other contaminating phosphatases. Expression of Dolpp1p in the *lpp1Δ/dpp1Δ* yeast strain has allowed characterizing the brain Dol-P-P phosphatase in the absence of other endogenous lipid phosphatase activities hydrolyzing Dol-P-P and Dol-P. As collaborative work with Dr. Waechter's group at University of Kentucky, the comparisons reported in Tables 3.2 show that expression of Dolpp1p in COS cells results in a substantial and highly specific increase in Dol-P-P phosphatase activity.

DOLPP1 shares a high degree of sequence identity with *CWH8* and is shown to be a functional ortholog in the *cwh8Δ* mutant yeast strain. This conclusion is based on the following observations that overexpression of mouse *DOLPP1* in *cwh8Δ* yeast cells: 1) complements the growth defect; 2) corrects the deficiency in protein *N*-glycosylation; and 3) reverses the accumulation of Dol-P-P resulting from defective Dol-P-P phosphatase activity. Moreover, as noted above, expression of the *DOLPP1* gene in the *lpp1Δ/dpp1Δ* yeast strain, or mammalian COS cells produces large increases in Dol-P-P phosphatase activity, indicating that Dolpp1p is an essential component of the brain enzyme. The presence of a consensus lipid phosphatase motif within the amino acid sequence and the observations that overexpression of *DOLPP1* in yeast and COS cells produces dramatic increases in the level of Dol-P-P phosphatase activity strongly suggest that Dolpp1p contains the catalytic site. Whether other components may be needed for full activity is a question that will only be

answered upon successful solubilization, isolation, and reconstitution of the recombinant enzyme in active form.

Although the effects of mutations in the *CWH8* gene on protein *N*-glycosylation, lipid intermediate synthesis, and the accumulation of Dol-P-P are consistent with the yeast enzyme being located in the ER, these observations are only indirect support for this conclusion. The immunofluorescence microscopy and subcellular fractionation studies described in this chapter represent the first direct evidence that Dolpp1p is located in the ER in COS cells. In addition, protease sensitivity studies indicate that the mammalian Dol-P-P phosphatase has a critical domain that is luminally oriented. It is clear from these studies that the *DOLPP1* gene product is predominantly localized in the ER, the site of lipid intermediate biosynthesis, and protein *N*-glycosylation.

The specificity, location in the ER, and luminally oriented active site of Dolpp1p meet all the criteria for a role in the recycling of Dol-P-P released during primary protein *N*-glycosylation reactions on the luminal surface. There is substantial evidence that cellular levels of Dol-P are a rate-controlling factor in the regulation of lipid intermediate biosynthesis (Harford *et al.* 1977; Lucas *et al.* 1977; Harford *et al.* 1980; Spiro *et al.* 1986). The induction of *cis*-isoprenyltransferase activity correlates closely with the onset of developmental increases in Dol-P and $Glc_3Man_9GlcNAc_2$-P-P-Dol biosynthesis, suggesting that *de novo* synthesis is an important source of Dol-P for lipid intermediate synthesis (Crick *et al.* 1994a; Crick *et al.* 1994b). However, considering the impressive effect (~80% reduction in $Glc_3Man_9GlcNAc_2$-P-P-Dol synthesis) produced by mutations in *CWH8* (van

Berkel *et al.* 1999; Fernandez *et al.* 2001), it seems likely that recycling of Dol-P-P plays an important role in maintaining Dol-P supplies for $Glc_3Man_9GlcNAc_2$-P-P-Dol biosynthesis.

The decrease in Dolpp1p activity in PPT1 knockout mouse brain suggests there is possible co-regulation of PPT1 and DOLPP1. These preliminary results prepared on a single set of samples would have to be repeated to be meaningful. Because PPT1 and DOLPP1 are localized in different subcellular compartments (lysosome vs. ER), it is impossible that the two proteins physically interact. Then, it has been shown PPT1 did not interact with any other proteins co-expressed from cDNA library derived from human cerebellum *in vivo* using the two-hybrid system (Cottone *et al.* 2001).

CHAPTER FOUR

Lipid linked oligosaccharide (LLO) accumulation in mouse models of neuronal ceroid lipofuscinosis (NCL)

4.1 Introduction

As stated earlier, the neuronal ceroid lipofuscinoses are a group of lysosomal storage disorders characterized by the accumulation of autofluorescent storage material in the brain and other tissues (Mitchison *et al.* 2001; Hofmann 2002). Although vigorous efforts have been made in the last a couple of decades, the underlying basis for the neurodegeneration is still unknown. Previously, abnormally high levels of dolichol pyrophosphoryl oligosaccharides were demonstrated in brain tissue from several NCL patients (in the era before the genetics of the NCLs were defined) but the specificity of the effect for the NCLs has been unclear.

In this chapter, I present data that lipid-linked oligosaccharide (LLO) accumulation is selective for the NCLs, with particularly striking accumulation in CLN1, CLN6 and CLN8 models using modern fluorophore assisted carbohydrate electrophoresis (FACE). The accumulated LLO in brain and liver tissues are rigorously characterized using the *CLN1/PPT1* (the most severe form of NCL) null mutant mouse model. The accumulation of dolichol pyrophosphoryl oligosaccharides is postulated to result from inhibition of late stages of lysosomal degradation of autophagosomes, which may be enriched in these metabolic precursors.

75

4.2 Experimental Procedures

4.2.1 Rodent tissues

Gene-targeted *CLN1/PPT1 -/-*, *PPT2 -/-*, and littermate control mice were maintained on a mixed C57BL/6J X 129S6/SvEv background in the animal facility of the University of Texas Southwestern Medical Center, Dallas, Texas, as described previously (Gupta *et al.* 2001; Gupta *et al.* 2003). The *CLN1/PPT1 -/-* and *PPT2 -/-* mice used in this study resulted from four to six generations of backcrosses from 129S6/SvEv onto C57BL6J. Frozen brain tissues derived from *CLN3* knockout mice (20-months of age) were a kind gift of Dr. Beverly Davidson, University of Iowa College of Medicine. Frozen brain tissues derived from CLN2/TPPI knockout mice (129SvEv) were a kind gift of Drs. Peter Lobel and David Sleat, University of Medicine and Dentistry of New Jersey. Mouse models of juvenile-onset NCL/*CLN3* (7-months of age, 129S6-*Cln3*^{tm1Nbm}/J, stock#: 004072), variant late-infantile NCL, *CLN6/nclf* (B6.Cg-^{Cln5nclf}/J, stock#: 003605), Northern epilepsy, *CLN8/mnd* (B6.KB2-*Cln8*^{mnd}/MsrJ, stock#: 001612), Niemann-Pick Type C/*Npc1*^{spm} (C57BLKS/J-*Npc1*^{spm}/J, stock#: 002760) (Loftus *et al.* 1997), Sanfilippo Type B/*Naglu* (B6.129S6-*Naglu*^{tm1Efn}/J, stock#: 003827) (Li *et al.* 1999) and Krabbe disease/*Galc*^{twi} (B6.CE-*Galc*^{twi}/J, stock#: 000845) (Luzi *et al.* 2001) were obtained from Jackson Laboratory stocks and maintained at the University of Rochester. All of the animals were euthanized in accordance with NIH and institutional guidelines. Tissues were harvested immediately and frozen under liquid nitrogen, except tissues used for the microsomal preparation and subcellular localization studies, which were freshly prepared.

4.2.2 FACE analysis

FACE (fluorophore-assisted carbohydrate electrophoresis) analysis of LLOs derived

from mouse tissues was performed essentially as described (Gao *et al.* 2002b; Gao *et al.*

2003). Briefly, tissues were homogenized in ice-cold methanol using a Polytron (Brinkmann)

and dried under a stream of nitrogen. The dried pellet was extracted sequentially with

chloroform/methanol 2:1(v/v), water and chloroform/methanol/water, 10:10:3 (v/v/v)

(CMW). The organic phase from the final extraction was loaded onto a column containing 1

ml DEAE-cellulose (Whatman) in the acetate form equilibrated with CMW. The column was

washed to remove contaminating glycogen fragments with 10 ml of CMW followed by 10 ml

of CMW containing 3 mM ammonium acetate. LLOs were eluted with 10 ml of CMW

containing 300 mM ammonium acetate. Chloroform (4.4 ml) and water (1.4 ml) were then

added to remove ammonium acetate and the lower phase (containing LLOs) was recovered

after centrifugation and dried under nitrogen gas. The oligosaccharides were released from

dolichol lipid by mild acid treatment with 0.1 N HCl in 50% isopropanol for 1h at 50˚C.

Residual ammonium acetate was removed by desalting with Dowex (Biorad) ion exchange

resins AG50-X8 (hydrogen form) and AG1-X8 (formate form). The released

oligosaccharides were labeled with 150 mM ANDS (7-amino-1, 3-naphthalenedisulfonic

acid, Molecular Probes) and 1 M sodium cyanoborohydride solution, and then resolved on an

oligosaccharide profiling gel as described previously (Gao *et al.* 2003). The gel was imaged

with a Biorad Fluor-S MultiImager using a 530DF60 filter. Electronic gel images were

generated, and individual ANDS-positive species were quantified using software supplied

with the scanner. The linearity and sensitivity of oligosaccharide detection by FACE was determined with known quantities of α1, 4-linked glucose oligomers as described previously (Gao *et al.* 2003).

4.2.3 Enzymatic digestion of ANDS-labeled oligosaccharides

ANDS-oligosaccharides were dissolved in 100 mM sodium acetate (pH 5.0) and incubated with 0.1 U per reaction (typical reaction, 50 μl) of jack bean α-mannosidase (Glyko) or dissolved in 100 mM Na-MES (pH 6.5) containing 0.2 % Triton X-100 and incubated with 270 ng recombinant Golgi endomannosidase (a gift of Dr. Robert Spiro) at 37 ˚C for 18 hours. For endoglycosidase H (Endo H) digestions, ANDS-oligosaccharides (or unlabeled oligosaccharides) were incubated with 0.1 U Endo H (New England Biolabs) in 50 mM sodium citrate (pH 5.0) containing 5% glycerol and 0.1% Triton X-100 at 37˚C for 30 minutes to 18 hours as indicated in the Figure Legends.

4.2.4 Microsomal preparation, LLO synthesis and oligosaccharide transfer assays

To prepare microsomes, fresh tissues from *CLN1/PPT1 -/-* and age-matched wild type mice were pooled (two animals from each group) and homogenized in ice-cold buffer containing 50 mM Tris-HCl (pH 7.5) and 250 mM sucrose using a motor driven Dounce homogenizer. The homogenate was centrifuged at 1,000 X g at 4 ˚C for 15 min to remove nuclei and cell debris. The supernatant was subjected to centrifugation at 100,000 X g at 4˚C for 1 h to sediment the microsomal pellet. The microsomes were resuspended in Buffer A (50 mM K-HEPES (pH 7.5), 25 mM KCl and 5 mM $MgCl_2$) and incubated with 0.2 μCi per ml

of GDP-[2-³H] mannose, 1 μM UDP-GlcNAc and 400 μM acceptor peptide (Ac-Asn-Tyr-Thr-CONH₂) or control peptide (Ac-Gln-Tyr-Thr-CONH₂). The reaction mixture was incubated for 30 min at 37°C and LLOs were recovered by extraction into chloroform/methanol/water (CMW, 10:10:3, v/v/v) as described previously (Pan *et al.* 1990; Zeng *et al.* 1990; Gao *et al.* 2002b). The incorporation of [2-³H] mannose into newly-synthesized LLOs was determined by counting a portion (5 %) of the organic phase from the CMW extraction. The remaining organic phase was dried under nitrogen gas and the oligosaccharides were released by mild acid, labeled with ANDS, and analyzed by FACE as described above.

4.2.5   Isolation of autofluorescent storage material

Storage material was isolated as described previously (Palmer *et al.* 1986; Tyynela *et al.* 1993) with modifications. Briefly, *CLN1/PPT1 -/-* and age-matched wild type mouse brains were homogenized in Milli-Q water using a Polytron (Brinkmann). The homogenate was filtered through glass wool and sonicated for 1 min. The resulting homogenate was centrifuged at 500 X g for 20 min and the pellet was resuspended in 16.75% CsCl (w/v, ρ = 1.13 g/cm³) and centrifuged at 1,500 X g for 20 min. The pellet was washed twice with CsCl and resuspended with Milli-Q water. The isolation was monitored visually using a Zeiss Axiophot epifluorescence microscope.

4.2.6   Differential fractionation of mouse brain tissue

Microsomes were prepared from fresh brain tissue from *CLN1/PPT1 -/-* and age-matched wild type mice (two mice per group) by Dounce homogenization in sucrose buffer as described above and subjected to a series of stepwise centrifugations (1,000 X g for 10

min, 3,000 X g for 10 min, 6,000 X g for 10 min, 9,000 X g for 15 min, and 100,000 X g for

1 h). Each pellet was washed once with Buffer A and subjected to fluorescence microscopy

and FACE analysis.

4.3 Results

4.3.1   LLO accumulates in *CLN1/PPT1* -/- mouse brain and peripheral tissues

Lipid linked oligosaccharides (LLOs) corresponding to the structure

$Glc_3Man_9GlcNAc_2$-P-P-dolichol are typically the precursors of asparagine-linked glycans in

mammalian cells. The steady state concentrations of LLOs are normally low in biological

systems, in the range of 1 nmol/gm tissue. Fluorophore-assisted carbohydrate electrophoresis

(FACE) analysis allows for the sensitive detection and structural characterization of

monosaccharides and oligosaccharides in biological samples without the need for radioactive

metabolic labeling (Gao *et al.* 2002b). Therefore, I applied this technique to the

characterization of LLOs extracted from *CLN1/PPT1* -/- mouse tissues in collaboration with

Dr. Ningguo Gao, who developed this method. Briefly, tissues were homogenized rapidly in

methanol, dried under nitrogen, and the dried pellets extracted with chloroform/methanol 2:1

(vol/vol) and water sequentially to remove contaminants. The resulting pellets were extracted

again with chroloform:methanol:water 10:10:3 (vol/vol/vol) to recover the LLOs, and the

LLOs were treated with mild acid to cleave the pyrophosphate linkage. The released

oligosaccharides were then reacted with the fluorophore 7-amino-1, 3-naphthalenedisulfonic

acid (ANDS), resolved by gel electrophoresis and visualized with a fluorescence scanner

(Gao *et al.* 2003).

As shown in Figure 4.1, striking accumulations of LLO intermediates were observed in brain, kidney and liver (the three tissues chosen for examination) from *CLN1/PPT1 -/-* mice. In brain (Figure 4.1A), the accumulation appeared to be relatively specific for LLOs migrating as $Man_{5-9}GlcNAc_2$, with little or no increase in $Glc_{1-3}Man_9GlcNAc_2$ species. In contrast, in the kidneys of *CLN1/PPT1 -/-* mice, all species of LLO were increased to about the same extent (Figure 4.1B). The pattern of accumulation in liver was similar to that of brain, but the accumulation was not nearly as striking (Figure 4.1C). Of note, the liver is particularly poor in storage material accumulation in different forms of Batten disease (Hofmann *et al.* 2001b).

To estimate the composition of accumulated LLOs from *CLN1/PPT1 -/-* and normal mouse brains, LLOs were derivatized with ANDS as described and varying amounts of labeled LLOs were loaded onto FACE gels and quantitated in comparison with known standards. Of note, the dry weight of *CLN1/PPT1 -/-* mouse brain (75.9 ± 4.0 mg) was 23% less than that of wild type brain (98.0 ± 5.0 mg), presumably due to massive neuronal loss during the progression of the disease (Bible *et al.* 2004). As suggested by the results in Figure 2.1D, the increase in LLOs in the *CLN1/PPT1 -/-* mouse brain is confined to the non-glucosylated intermediates ($Man_{5-9}GlcNAc_2$), which were accumulated to an overall level that was 14.5-fold higher as compared to wild type brain. The mature species ($Glc_3Man_9GlcNAc_2$), which is the major species in the wild type brain, estimated at about 1 nmol per gram of dry weight, is actually decreased (to 47% of the wild type level) in *CLN1/PPT1 -/-* brain (asterisk in Figure 4.1).
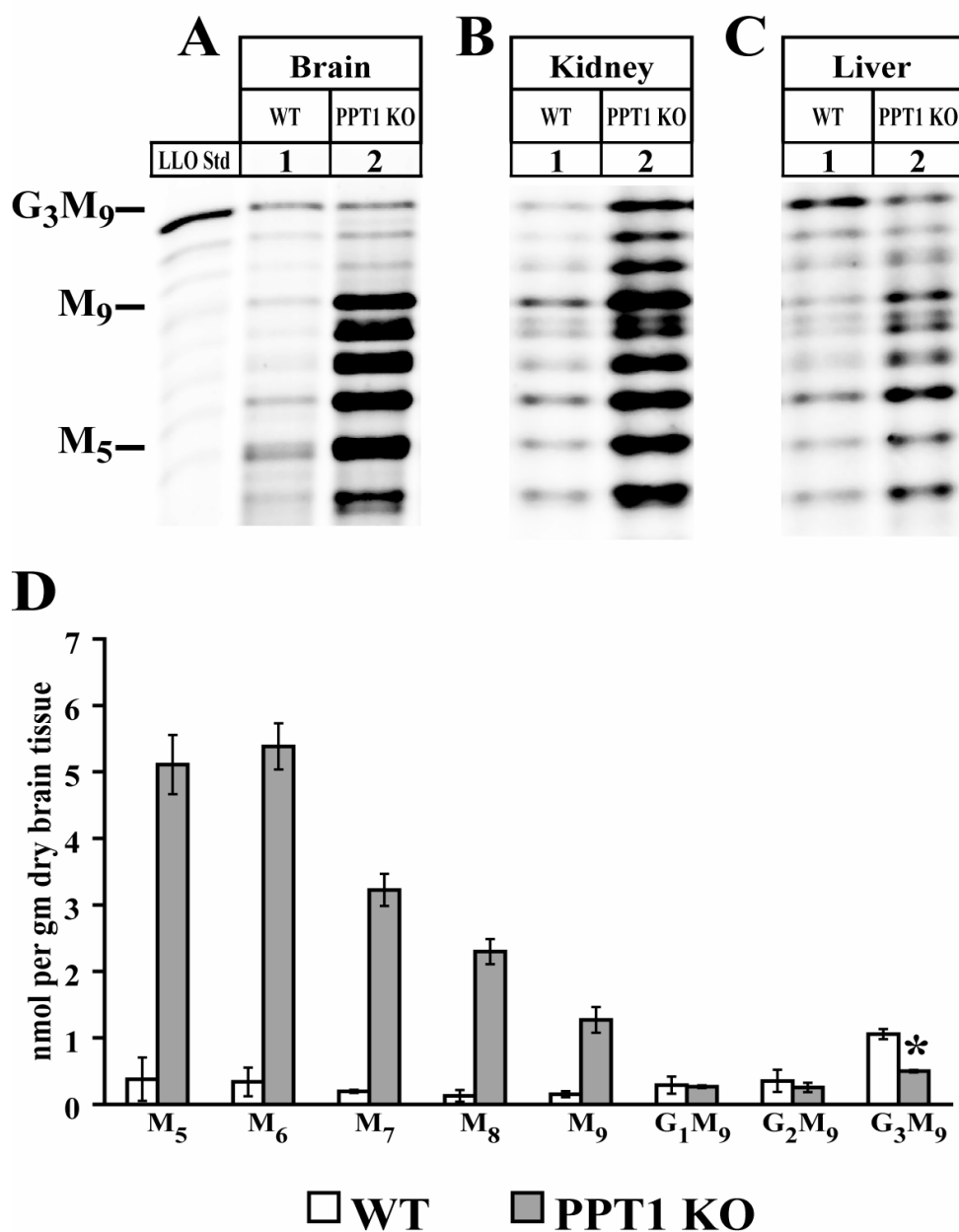
Figure 4.1 Lipid-linked oligosaccharide intermediates (LLOs) accumulate in
CLN1/PPT1 -/- mouse tissues. (A), brain; (B), kidney; and (C), liver. LLOs were extracted
and processed for fluorophore-assisted carbohydrate electrophoresis (FACE) analysis as
described under *Material and Methods*. LLO standards were prepared from wild type mouse
liver as described (Gao *et al.* 2002b). The positions of $Glc_3Man_9GlcNAc_2$-ANDS,
$Man_9GlcNAc_2$-ANDS and $Man_5GlcNAc_2$-ANDS are indicated as G_3M_9, M_9, and M_5,
respectively. Lane 1 and lane 2 in each panel corresponds to the ANDS-labeled LLOs from

wild type and PPT1 knockout mice, respectively. One tenth of the total derivatized extract from one organ was loaded. Results shown represent one of 3 experiments giving similar results. (D) The quantities of each ANDS-labeled LLO intermediate extracted from *CLN1/PPT1 -/-* and wild type mouse brains (nmol per g dry weight) were shown. Values shown represent mean ± S.D. (n=3). The asterisk (*) in panel D indicates that this result for $Glc_3Man_9GlcNAc_2$ in the PPT1 knock-out mouse was repeatable.

4.3.2   Structural characterization of LLOs from *CLN1/PPT1 -/-* mouse brain

To characterize the composition and structure of LLOs that accumulate in the tissues

of *CLN1/PPT1 -/-* mice, several analytical enzyme treatments were performed. Jack bean α-

mannosidase hydrolyzes exposed α-mannosyl residues on oligosaccharides. One or more

glucosyl residues on the " α 1, 3" arm of the oligosaccharide have two effects: they block

digestion of the α 1,3 arm by mannosidases, and they retard digestion of exposed mannosyl

residues on the α 1,6 arm by jack bean α -mannosidase (Beeley 1985; Cacan *et al.* 2001).

Therefore, the enzyme may be used to test for the presence of glucosylated Glc_{1-}

$_3Man_{5-9}GlcNAc_2$ species. As shown in Figure 4.2A, ANDS-labeled oligosaccharides from a

standard LLO mix prepared from normal mouse liver (which appears largely as

$Glc_3Man_9GlcNAc_2$ plus various unglucosylated LLOs) was converted to the relatively

protected $Glc_3Man_6GlcNAc_2$-ANDS (Figure 4.2A, lane 2, asterisk) and $Man_1GlcNAc_2$-

ANDS (containing a β-mannosyl residue) as the result of digestion of the unglucosylated

species (Figure 4.2A, lane 2) (Gao *et al.* 2003). The mannosyl residues most likely removed

by jack bean mannosidase to generate $Glc_3Man_6GlcNAc_2$-ANDS are indicated in Figure 4.3

(cleavage sites labeled "a"). In contrast, all of the ANDS-labeled LLOs from the

CLN1/PPT1 -/- mouse brain were converted to a product that migrated as $Man_1GlcNAc_2$-

ANDS after digestion with jack bean α-mannosidase (Figure 4.2A, compare lanes 4 and 5).

This result suggests that LLOs from the *CLN1/PPT1 -/-* brain consist of oligomers of
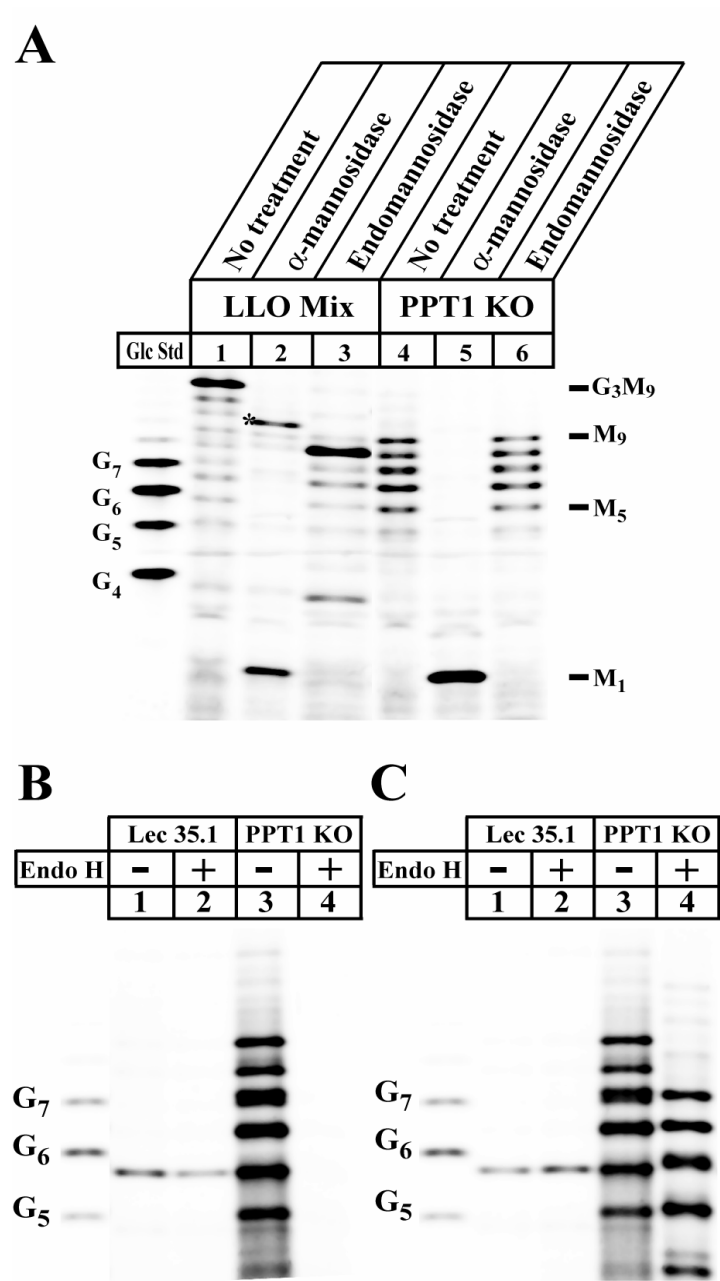
mannose units that are not capped by glucose units.

Figure 4.2 Characterization of ANDS-labeled LLO intermediates from *CLN1/PPT1 -/-* mouse brain. (A) α-mannosidase and Golgi endomannosidase treatment. Glc Std, oligomerized glucose standards (G_4 through G_7). LLOs extracted from *CLN1/PPT1 -/-* mouse brain (lanes 4-6) and control LLOs prepared from normal mouse liver (lanes 1-3) were treated with buffer alone (lane 1 and lane 4) or were digested with either jack bean α-mannosidase (lane 2 and lane 5) or Golgi endomannosidase (lane 3 and lane 6). The asterisk (*) denotes $Glc_3Man_6GlcNAc_2$-ANDS. (B) Endo H treatment after ANDS labeling. (C) Endo H treatment before ANDS labeling. LLOs extracted from a *CLN1/PPT1 -/-* mouse brain (lanes 3, 4) or control Lec35.1 cells (lanes 1, 2) were treated with endoglycosidase H (Endo H) at 37˚C for 30 min (B) and 18 hours (C). Subsequently, the LLOs were resolved and analyzed by FACE.

Golgi endomannosidase specifically converts $Glc_{1-3}Man_9GlcNAc_2$-ANDS to $Man_8GlcNAc_2$-ANDS (Figure 4.3; cleavage site marked as "b") (Spiro *et al.* 2000; Gao *et al.* 2002b). The result of enzyme treatment of the normal mouse liver LLO mix was consistent with this specificity, shifting the glucosylated species to $Man_8GlcNAc_2$-ANDS (Figure 4.2A, compare lanes 1 and 3) without affecting other intermediates. Treatment of LLOs from the *CLN1/PPT1 -/-* brain caused no changes in migration (Figure 4.2A, compare lanes 4 and 6); again suggesting that the accumulated LLO intermediates lack glucosyl residues. LLO biosynthesis occurs in a well-ordered series of reactions in which mannose residues are added sequentially to the growing oligosaccharide chain (Figure 4.3). Endoglycosidase H (Endo H) recognizes a particular mannose residue (Figure 4.3, shaded circle) that is added only after the "core" five mannose residues have been added (Figure 4.3, M_5) and then cleaves the growing chain at the $\beta_{(1\rightarrow4)}$ linkage between the two GlcNAc molecules already present on the molecule (Figure 4.3, cleavage site marked as *c*). Therefore, "authentic" $Man_5GlcNAc_2$ (M_5) derived from the biosynthetic pathway is insensitive to Endo H, because it does not contain the sixth mannose residue recognized by the enzyme (Figure 4.3, shaded

circle). This is illustrated in Figure 4.2B, lanes 1 and 2, in which authentic $Man_5GlcNAc_2$ prepared from CHO-K1 mutant Lec35.1 cells (which lacks a factor required for the addition of the sixth mannose) (Camp *et al.* 1993a; Anand *et al.* 2001) is shown to be resistant to Endo H treatment. In contrast, the species migrating as $Man_5GlcNAc_2$ in *CLN1/PPT1 -/-* brain (Figure 4.2B, lane 4) as well as the species migrating as $Man_4GlcNAc_2$ were sensitive to Endo H (lane 4). This result suggests that $Man_{4-5}GlcNAc_2$ (M_4/M_5) LLO in *CLN1/PPT1 -/-* brain contain the sixth mannose residue, and that rather than being "authentic" intermediates in the biosynthetic pathway, they are atypical LLOs that have gained the sixth mannose and subsequently lost residues via degradation by a catabolic pathway.

Because Endo H treatment removes the ANDS group from labeled oligosaccharides (thereby precluding an examination of the oligosaccharide products of the Endo H reaction), we performed experiments in which we incubated the LLOs with Endo H prior to ANDS labeling. In these experiments, we demonstrated that Endo H causes a shift of oligosaccharides corresponding to a loss of one GlcNAc residue (Figure 4.2C, lane 3 and lane 4), confirming the presence of the expected products of the Endo H reaction.

The absence of glucose (as indicated by α-mannosidase and endomannosidase digestion results) together with the observation of Endo H sensitivity provide strong evidence that the LLOs accumulating in *CLN1/PPT1 -/-* mouse brain are derived from a catabolic, rather than from the normal biosynthetic pathway.

4.3.3   LLO synthesis is normal in *CLN1/PPT1 -/-* mouse brain microsomes
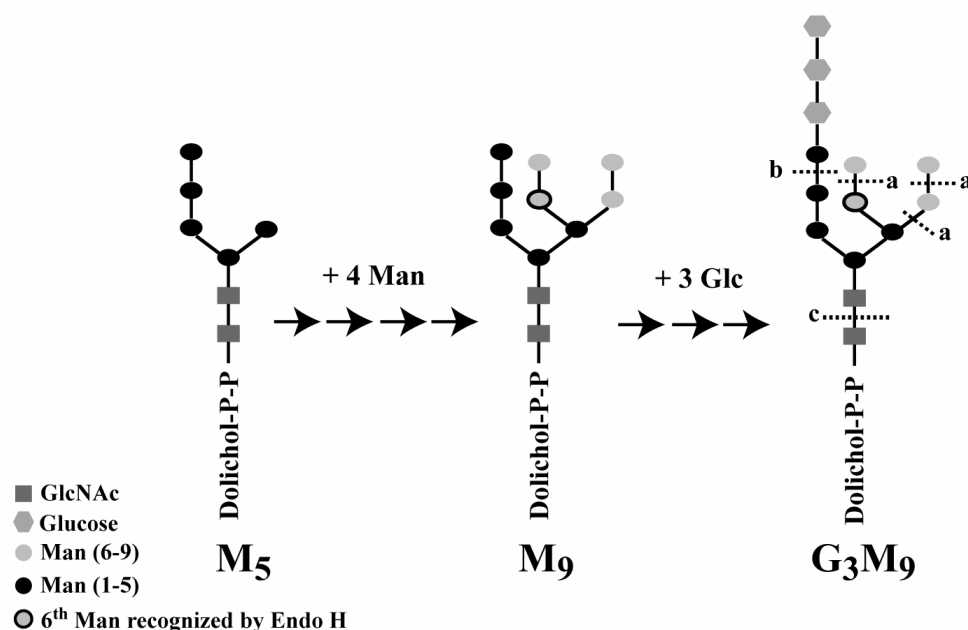
Figure 4.3 Schematic representation of LLO intermediate synthesis in the lumen of endoplasmic reticulum (ER). $Man_5GlcNAc_2$-P-P-dolichol is synthesized on the cytosolic side of the ER and then flipped into the luminal side. Four more mannose units and three glucose units are sequentially added to produce the mature species $Glc_3Man_9GlcNAc_2$-P-P-dolichol (Helenius *et al.* 2002). Likely cleavage sites in $Glc_3Man_9GlcNAc_2$ for jack bean α-mannosidase (a) and Golgi endomannosidase (b) are indicated. Endoglycosidase H (Endo H) recognizes specifically 6th mannose (closed circle) added onto the "core" M_5, and cleaves the $\beta_{(1\rightarrow4)}$ linkage between two GlcNAc molecules (c).

To determine whether LLO synthesis proceeds normally in *CLN1/PPT1 -/-* mouse brain, incorporation of [2-^{3}H]mannose into LLOs was measured using an *in vitro* quantitative assay as previously described (Gao *et al.* 2002c). Microsomal fractions were prepared from *CLN1/PPT1 -/-* and wild type brain and liver as described in *Material and Methods*. In short, brain (Figure 4.4A) and liver (Figure 4.4B) microsomes were incubated with 0.2 μCi/ml GDP-[2-^{3}H] mannose, 1 μM UDP-GlcNAc for 30 min at 37 ˚C and LLOs recovered by extraction into chloroform/methanol/water (CMW, 10:10:3). GDP-[2-^{3}H]-

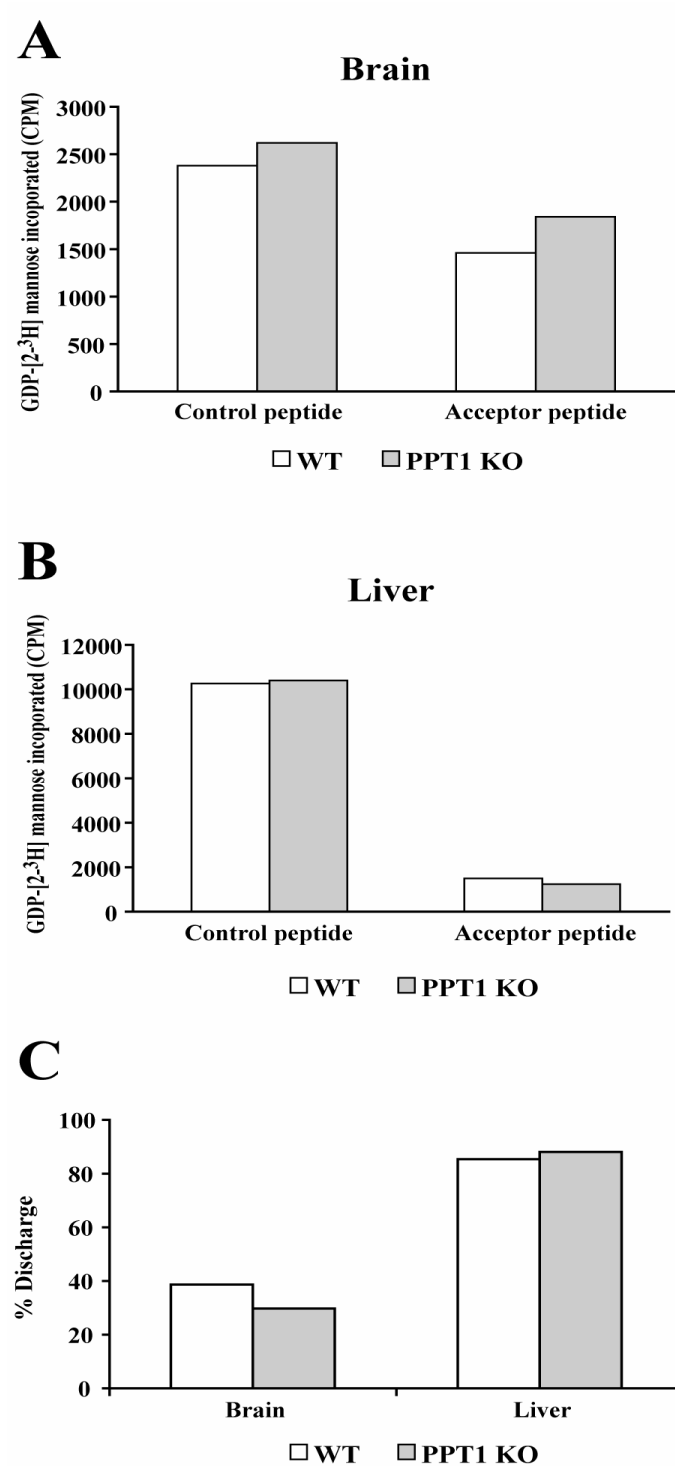**Figure 4.4 LLO synthesis in liver and brain of *CLN1/PPT1 -/-* mice and age-matched wild type mice.** Incorporation rate of [2-^{3}H] mannose into LLOs was measured in normal or

CLN1/PPT1 -/- brain (A) and liver (B) microsomes in the presence of 400 µM of acceptor or non-acceptor tripeptide for oligosaccharyltransferase. (C) % discharge of oligosaccharide intermediates onto the target peptides were calculated for brain and liver of *CLN1/PPT1 -/-* and wild type mice, respectively. The results shown are typical of two independent experiments.

mannose incorporated into LLOs was counted, and assays were performed with acceptor

(Ac-Asn-Tyr-Thr-CONH$_2$) tripeptide and non-acceptor (Ac-Gln-Tyr-Thr-CONH$_2$) peptides

for oligosaccharyltransferase (OST) to measure the rate of discharge as well. OST is an ER

lumenal enzyme that transfers oligosaccharide from the mature LLO (Glc$_3$Man$_9$GlcNAc$_2$-P-

P-dolichol) to appropriate asparagine residues of newly synthesized polypeptides. OST,

however, also transfers immature LLO intermediates to the target peptide if excess acceptor

peptides are available (Gao *et al.* 2002c). As shown in Figure 4.4, there were no significant

differences in LLO synthesis between wild type and *CLN1/PPT1 -/-* brain (A) and liver (B)

microsomes.

As anticipated, liver microsomes showed higher OST activity than brain microsomes

(Figure 4.4 C). However, there were no significant differences in rates of discharge of LLOs

onto the target peptide between wild type and *CLN1/PPT1 -/-* microsomes observed. These

results suggest that LLO synthesis, extension and transfer are normal in the *CLN1/PPT1 -/-*

mouse.

4.3.4   Accumulated LLOs in *CLN1/PPT1 -/-* mouse brain are not discharged by

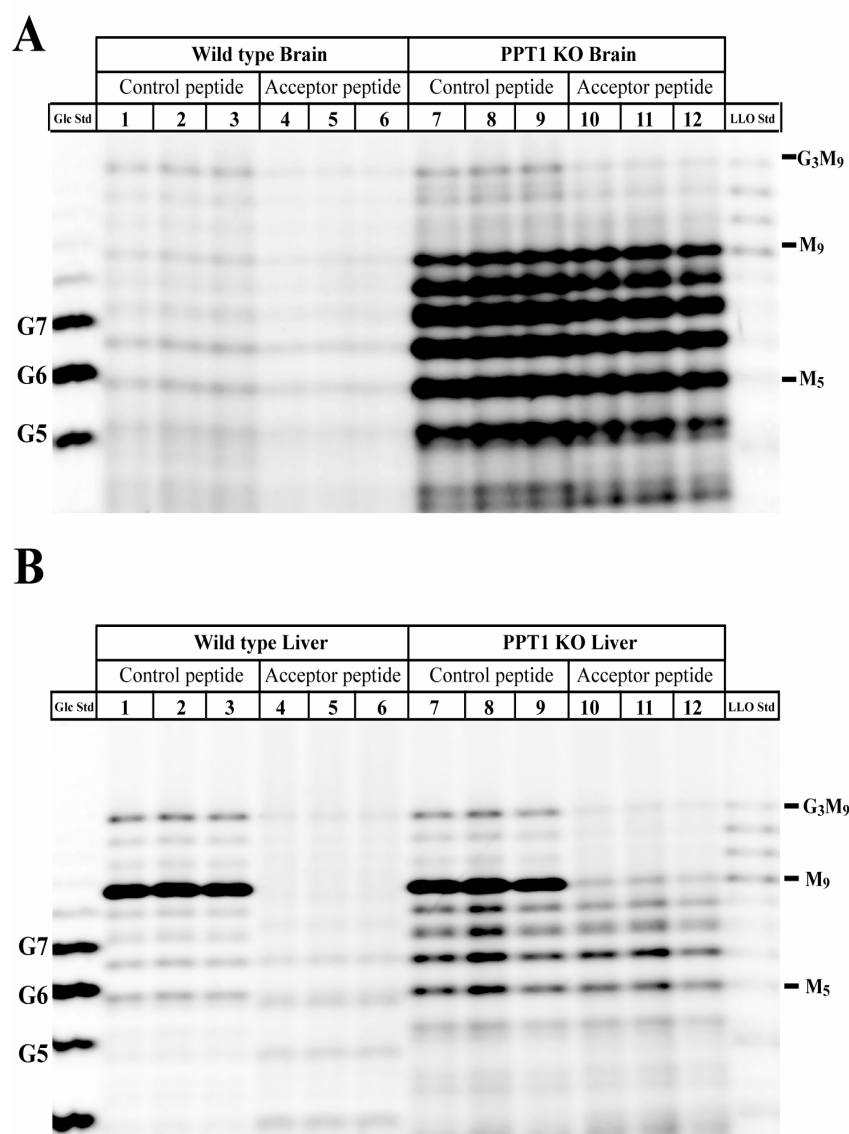**oligosaccharyltransferase (OST)**

Figure 4.5 LLOs accumulating in *CLN1/PPT1* -/- mouse are not competent for transfer to the acceptor peptide. Brain (A) and liver (B) microsomes were incubated in the presence of acceptor or control peptides for 30 min at 37˚C and the extracted LLOs were resolved and analyzed by FACE. LLOs from normal brain transfer readily to the acceptor peptide (lanes

4-6) but not control peptide (lanes 1-3), whereas the LLOs specific to the PPT1 knockout tissues do not (compare lanes 7-9 and 10-12).

The experiments presented above suggest that the accumulated LLOs in *CLN1/PPT1 -/-* mouse brain are catabolic products. Extracted LLOs from *CLN1/PPT1 -/-* brain and liver microsomes were also analyzed by FACE after treatment with acceptor and non-acceptor peptides for oligosaccharyltransferase (OST) (Figure 4.5). LLOs in wild type brain (Figure 4.5A, lanes 1-3 vs. lanes 4-6) and liver (Figure 4.5B, lanes 1-3 vs. lanes 4-6) were efficiently discharged while almost none of accumulated LLOs in both *CLN1/PPT1 -/-* brain (4.5A, lanes 7-9 and 10-12) and liver (Figure 4.5B, lanes 7-9 and 10-12) were discharged, implying that the accumulated LLOs are either not substrates for OST or that they are present in a different subcellular localization that is inaccessible to OST. As noted earlier (Camp *et al.* 1993a; Gao *et al.* 2002c), appreciable deglucosylation of pre-formed $Glc_3Man_9GlcNAc_2$-P-P-dolichol can occur during the incubation. This explains the predominance of $Man_9GlcNAc_2$-P-P-dolichol in the liver LLO samples incubated with control peptide (Figure 4.5B, lanes 1-3 and 7-9).

4.3.5   Enrichment of LLOs in autofluorescence storage material from *CLN1/PPT1 -/- mouse brain*

One of the distinctive pathological characteristics of infantile Batten disease is the accumulation of autofluorescence storage material (also known as granular osmophilic deposits, or GROD) in brain and other tissues. To determine whether LLOs are enriched in this material, storage deposits were isolated by CsCl density centrifugation and analyzed by

epifluorescence microscopy (Figure 4.6A) and FACE analysis (Figure 4.6B). The crude and

CsCl purified storage material were visualized under Nomarski optics (Figure 4.6A, *a* and *b*)

and these images were compared with images visualized under the fluorescence microscope

(Figure 4.6A, *c* and *d*). Autofluorescence in storage material purified from *CLN1/PPT1 -/-*

brain covered nearly 100% of the area the seen in the bright field (*b* and *d*), whereas in crude

homogenates it represented a minor fraction (*a* and *c*), indicating that significant enrichment

of autofluorescent material was accomplished by CsCl centrifugation. Next, LLOs were

extracted directly from the CsCl purified storage material pellet and analyzed by FACE

(Figure 4.6B). As a control, LLOs were extracted directly from the unfractionated

CLN1/PPT1 -/- brain (lane 4) and wild type brain subjected to the same procedures (lanes 1-

3). Extracts from equivalent amounts of brain (wet weight) were loaded.

As can be seen in Figure 4.6B, most of the truncated LLOs in *CLN1/PPT1 -/-* brain

present in the crude homogenate (Figure 4.6B, lane 4) were recovered in the CsCl purified

storage material (lane 5), indicating that accumulated LLOs are enriched in the storage

material in the *CLN1/PPT1 -/-* mouse (57.3-fold enrichment, see Table 4.1). Note that in

normal and PPT1 defective tissue, the mature species $Glc_3Man_9GlcNAc_2$ was not recovered

form the CsCl pellet but rather from the supernatant (compare Figure 4.6B, lanes 4 and 6 vs.

lanes 1 and 3). Taken together with the results of Figure 4.5, this confirms that the

accumulated LLOs in the storage material are associated with a subcellular compartment

distinct from those LLOs that are utilized in asparagine-linked glycosylation. Using data

similar to that presented in Figure 4.1D, we calculate that LLOs constitute 0.3% of the dry

weight of storage material from *CLN1/PPT1 -/-* mouse brain.

A

Crude | CsCl Pellet

Normarsky

Autofluorescence

B

	Wild type			PPT1 KO			
	Crude	Pellet	Sup	Crude	Pellet	Sup	
Glc Std	1	2	3	4	5	6	LLO Std

- G₃M₉

- M₉

G7
G6

- M₅

G5
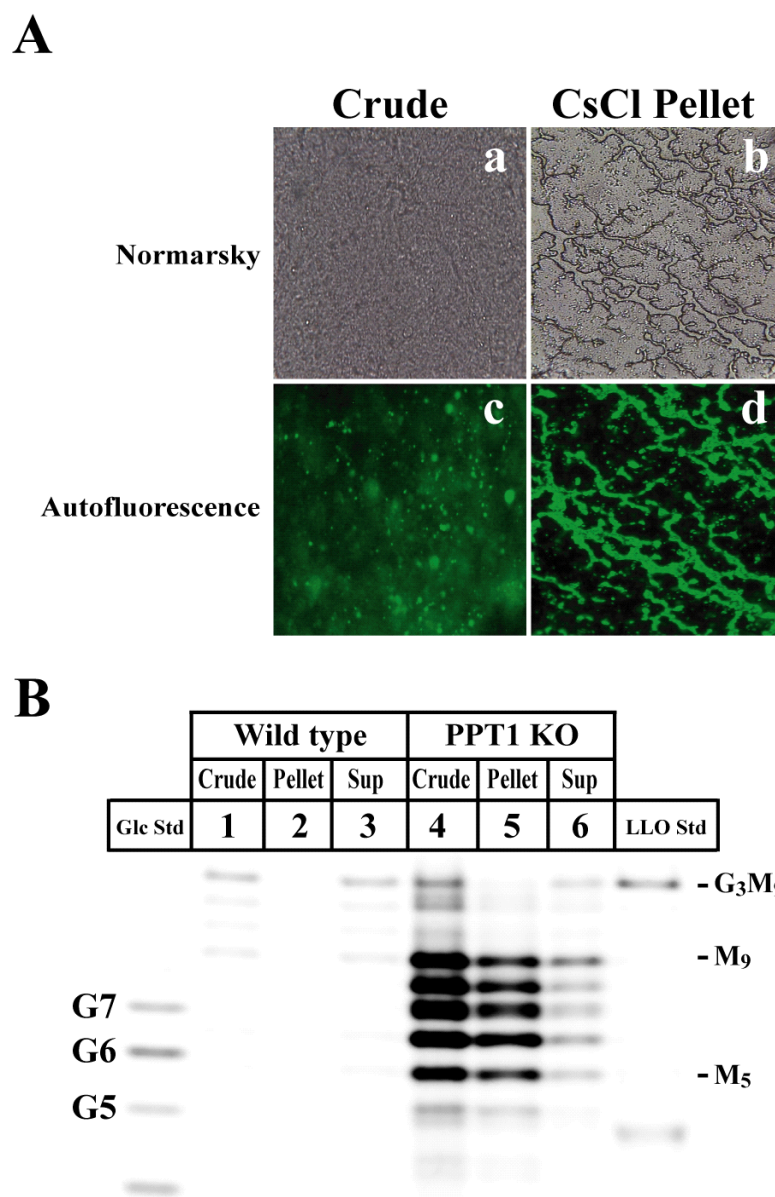
Figure 4.6 Enrichment of autofluorescent storage material and LLOs from *CLN1/PPT1 -/-* mouse brain by CsCl density gradient centrifugation. (A) Autofluorescent storage material was purified on a 16.75 % CsCl density gradient (ρ= 1.13 g/cm^3) and the resulting pellet was resuspended in Milli-Q water. A suspension of the pellet was analyzed by epifluorescence microscopy (panels c and d), and Nomarski optics (panels a and b). (B) LLOs extracted from crude unfractionated normal brain (lane 1), the CsCl purified pellet

(lane 2) and supernatant (lane 3) were analyzed by FACE. An identical purification procedure was applied to age-matched *CLN1/PPT1 -/-* brain (lanes 4-6). Extracts from equivalent amounts of brain (based on wet weight) were loaded. Results shown represent one of two independent experiments yielding similar results.

Table 4.1 LLO Composition of Mouse Brain and Purified Storage Bodies

	LLOs (nmol/g dry weight)		Enrichment of LLOs in Storage Bodies
	Crude	**CsCl purified**	
Wild type	1.2	-	-
PPT KO	19.1	1090	57.3-fold

To further elucidate the association of the LLOs with autofluorescent storage material, differential centrifugation of a homogenate of *CLN1/PPT1 -/-* brain was performed. Brain homogenates from *CLN1/PPT1 -/-* and age-matched wild type mice were centrifuged as described in Experimental Procedures and the resulting pellets were observed under Nomarski and epifluorescence microscopy (Figure 4.7A). Consistent with the known high density of the storage material, the majority of autofluorescent material sedimented at 6,000 X g or lower (Figure 4.7A, panels f, g, h), whereas the material sedimenting at higher g forces displayed little autofluorescence (Figure 4.7A, panels i and j). As shown in Figure 4.7B, the pellets from the differential centrifugation were processed and analyzed by FACE.
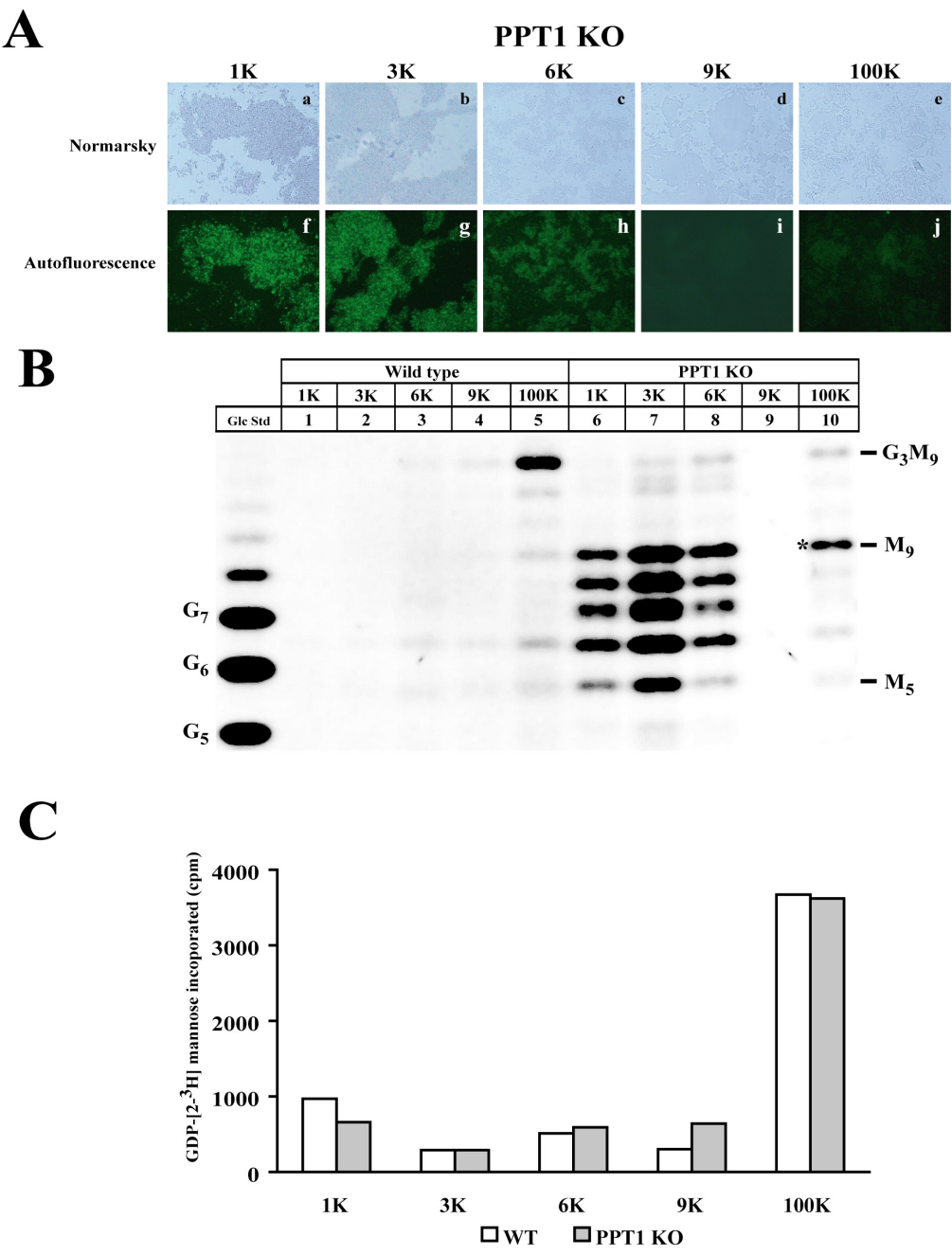
A

PPT1 KO

B

C

Figure 4.7 Co-fractionation of LLOs accumulating in *CLN1/PPT1 -/-* mouse brain with autofluorescent storage material and non-ER fractions. Brain homogenates from age-matched wild type and *CLN1/PPT1 -/-* brains were fractionated by differential centrifugation. (A) The fractionated homogenates from *CLN1/PPT1 -/-* brain were analyzed by epifluorescence microscope (lanes f-j) and Nomarski optics (lanes a-e). (B) The resulting fractions from wild type (lanes 1-5) and *CLN1/PPT1 -/-* (lanes 6-10) brains were subjected to FACE analysis. (C) An aliquot of each fraction was incubated with GDP-[2-^{3}H] mannose for 30 min at 37 °C to monitor the extent of incorporation of [2-^{3}H] mannose into LLOs. Results shown are one of two independent experiments yielding similar results. The asterisk (*) denotes $Man_9GlcNAc_2$-ANDS.

In wild type brain, the bulk of LLOs sedimented in the 100,000 X g microsomal fraction (Graham 1984) and appeared as the mature LLO, $Glc_3Man_9GlcNAc_2$-ANDS (Figure 4.7B, lane 5). However, in the *CLN1/PPT1 -/-* brain, most of the accumulated LLOs were sedimented between 1,000 X g and 6,000 X g in fractions that were also highly enriched in autofluorescent material. As a metabolic marker for each fraction, the extent of incorporation of [2-^{3}H] mannose into LLOs was monitored (Figure 4.7C). An aliquot of each fraction was incubated with GDP-[2-^{3}H] mannose for 30 min at 37ºC followed by CMW 10:10:3 (vol/vol/vol) extractions. A portion of the organic phase of the extract was counted to determine the rate of LLO synthesis. As expected, [2-^{3}H] mannose incorporation into LLO was predominantly observed in the 100,000 X g fractions from wild type and *CLN1/PPT1 -/-* brains, which is consistent with the known subcellular localization of LLO synthesis in the endoplasmic reticulum.

Interestingly, the major band observed in 100,000 X g pellet of *CLN1/PPT1 -/-* brain was $Man_9GlcNAc_2$-ANDS (asterisk) rather than $Glc_3Man_9GlcNAc_2$-ANDS, and the level of $Glc_3Man_9GlcNAc_2$-ANDS was reduced as compared with wild-type. It is possible that this

was caused by deglucosylation of pre-formed $Glc_3Man_9GlcNAc_2$-P-P-dolichol during fractionation.

4.3.6 Age-dependent accumulation of LLOs in brains of *CLN1/PPT1 -/-* mice

The accumulation of LLO intermediates was age-dependent as assessed in the brains of 2-week to 6-month-old PPT1 knockout mice (Figure 4.8). Mannosylated LLO intermediates were the predominant component of the accumulation and started to accumulate as early as 2 weeks of age. Greater than 10-fold accumulation of LLOs as compared to the wild type were observed by the age of 6 months, an age at which 50 to 75% of mice develop neurological abnormalities such as clasping and myoclonic jerks (Gupta *et al.* 2001).
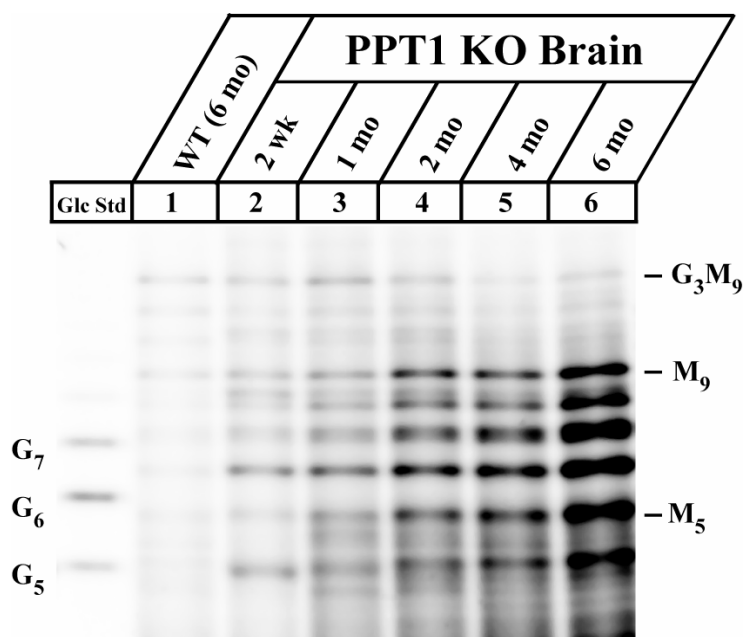

Figure 4.8 Accumulation of LLO intermediates in *CLN1/PPT1 -/-* mouse brain is age-dependent. Brains from *CLN1/PPT1* -/- mice from 2 weeks to 6 months of age were analyzed by FACE. A wild type mouse brain at 6 months of age is shown for comparison

(lane 1). Each lane represents 10% of one whole brain. The result shown is one of two yielding similar results.

4.3.7 Accumulation of LLO intermediates in mouse models of lysosomal storage disease (LSD)

In each case, brains from at least three clearly symptomatic animals were examined and representative results are shown. (Of note, all mouse models represent complete loss of function mutations, with the exception of the CLN6/*nclf*, and CLN8/*mnd*; in these two models, the impact of underlying missense mutations on protein function is unknown.) Marked LLO accumulation was observed in the brains of *CLN1/PPT1-/-* (Figure 4.9A, lane 2), *CLN6 -/-* (lane 8) and *CLN 8 -/-* (Figure 4.9B, lane 8) mice. These models have all been shown to demonstrate copious amounts of autofluorescent storage material in brain tissue (Bronson *et al.* 1993; Bronson *et al.* 1998; Ranta *et al.* 1999; Gupta *et al.* 2001; Bolivar *et al.* 2002 ; Gao *et al.* 2002a; Wheeler *et al.* 2002). Lesser but significantly increased LLOs were seen in *CLN2 -/-* (Figure 4.9C, lane 2), and *CLN3 -/-* (Figure 4.9A, lane 6) mouse brains. Accumulation of LLOs in *PPT2* knockout mice was modest (Figure 4.9B, lane 10) consistent with the scant amounts of storage material in brains of mice at this age (Gupta *et al.* 2003). Quantitation of LLOs by densitometric scanning of gels in comparison with standards revealed that brains from symptomatic mice with Niemann Pick type C (NPC), Sanfilippo syndrome type B (NAGLU) and Krabbe disease (GALC) were not significantly different from normal (Figure 4.9D). These results, taken together with the demonstration of LLOs in the autofluorescent storage material of PPT/CLN1 mice, support a relative specificity for LLO accumulation in the neuronal ceroid lipofuscinosis.

Table 4.2 Characteristics of NCL mouse mutants in this study

Disorder	Defective gene	Affected protein	Mouse phenotype	Age at this study	Ref.
Infantile NCL	*CLN1/Ppt1*	Palmitoyl protein thioesterase-1	Spasticity by age 5 months. Myoclonic jerking and seizures. Fatal by 10 months.	7-mo	(Gupta *et al.* 2001; Gupta *et al.* 2003)
Late Infantile NCL	*CLN2/Tpp1*	Tripeptidyl peptidase-I	Tremor at 7 weeks and then ataxia, median survival 4.5 months.	3.5 to 4-mo	*a*
Juvenile NCL	*CLN3*	Lysosomal transmembrane protein	Neuropathological abnormalities. Motor coordination deficits at 6 months.	6-mo and 20-mo	(Mitchison *et al.* 1999), *b*
Variant Late-Infantile NCL	*CLN6(Nclf)*	Putative transmembrane protein	Progressive retinal atrophy. Gait disturbance and weakness in limbs evident by 6 months and severe paralysis by 9 months.	6-mo	(Bronson *et al.* 1998; Gao *et al.* 2002a; Wheeler *et al.* 2002)
Epilepsy with mental retardation	*CLN8(Mnd)*	Putative transmembrane protein	Hindlimb weakness and ataxia at 6 to 7 months. Behavioral abnormalities.	7-mo	(Bronson *et al.* 1993; Ranta *et al.* 1999; Bolivar *et al.* 2002)
Unknown	*PPT2*	Palmitoyl protein thioesterase 2	Spasticity and ataxia by 13 mo. Scant neuronal storage. Bone marrow infiltration and extramedullary hematopoiesis. Death by 17 mo.	14-mo	(Gupta *et al.* 2003)

[a]Sleat, D.E. and Lobel, P., unpublished data.
[b]Weimer, J. M. and Pearce, D. A., unpublished data.

LLO profiles of five homozygous NCL mouse models (*CLN1/PPT1-/-*, *CLN2/TPPI-/-*, *CLN3 -/-*, *CLN6/nclf*, and *CLN8/mnd*), three non-NCL models (Niemann Pick Type C, designated *NPC -/-*, Sanfilippo Type B, *NAGLU -/-*, and Krabbe disease, *GALC -/-*) and the *PPT2 -/-* mouse were analyzed by FACE (Figure 4.9).

The characteristics of the animal models and the ages of mice used in the experiment are summarized in Tables 4.2 and 4.3.

Table 4.3 Characteristics of non-NCL LSD mouse mutants in this study

| Disorder	Defective gene	Affected protein	Mouse phenotype	Age at this study	Ref.
Niemann-Pick Type C	*NPC1*	Transmembrane protein with sterol-sensing domain	Weight loss, tremor and ataxia by 7 wks.	2-mo	(Miyawaki *et al.* 1982; Loftus *et al.* 1997; Patel *et al.* 1999)
Sanfilippo Type B	*NAGLU*	α-N-acetyl-glucosaminidase	Ganglioside accumulation in brain. Heparan sulfate in liver and kidney. Death at 8 to 12 mo.	9-mo	(Li *et al.* 1999)
Krabbe Disease	*GALC*	Galactocerebrosidase	Normal at birth. Progressive tremor, weakness and wasting at 3-wk. Death at 3 mo.	1-mo	(Duchen *et al.* 1980; Luzi *et al.* 2001; Biswas *et al.* 2002)
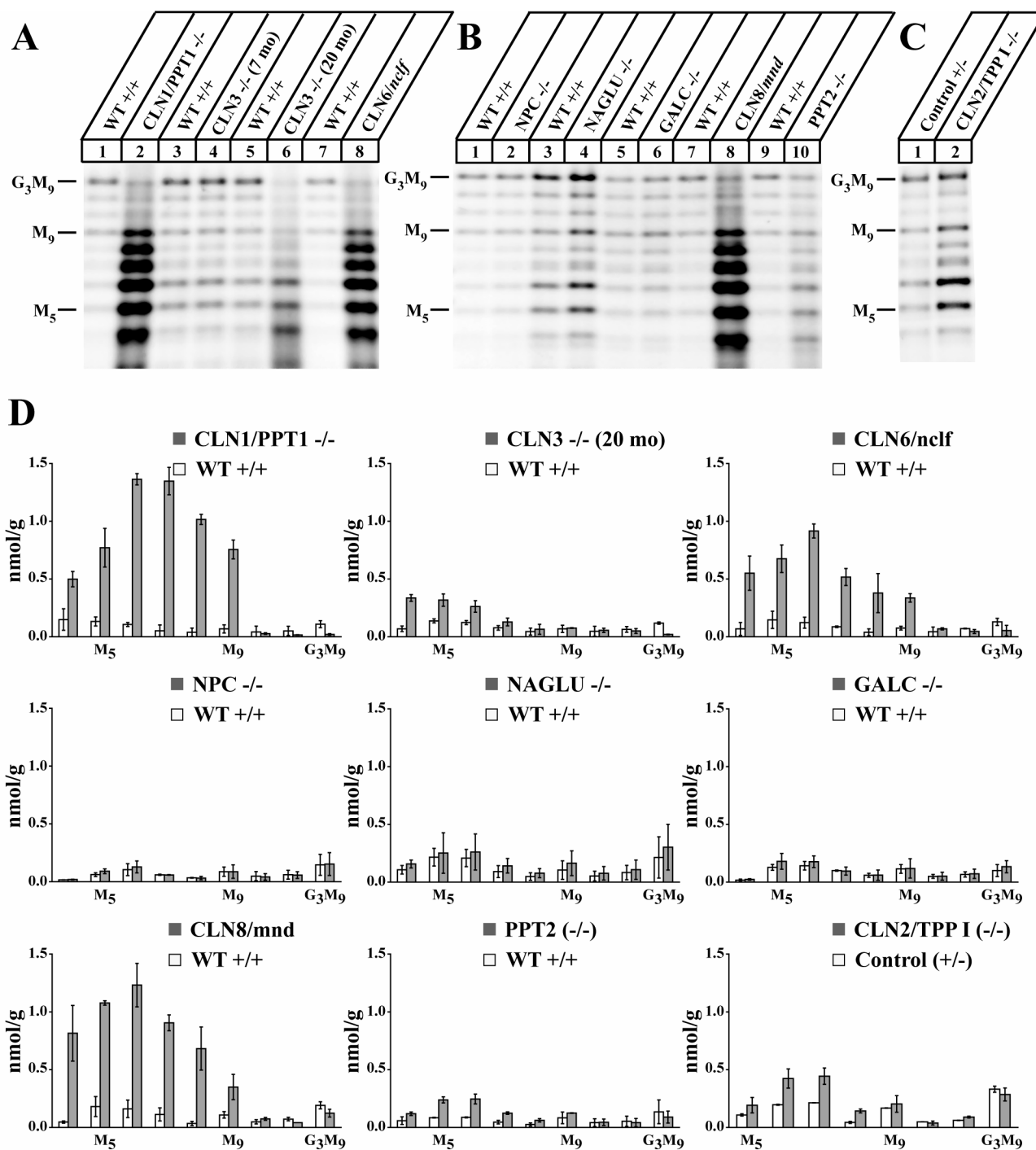
Figure 4.9 LLO profiles of brain tissue from mouse models of NCL and non-NCL lysosomal storage disorders. All mice demonstrated overt neurological signs at the time of analysis, with the exception of 7 month old CLN3 -/- mice, which are shown for comparison. Three representative gels (A, B, and C) are shown. Lanes represent paired wild-type littermate controls (odd lanes) and mouse models (even lanes) as indicated. The mouse models analyzed and their corresponding human disorders are CLN1/PPT1 -/- (infantile NCL), CLN3 -/- (juvenile NCL), CLN6/*nclf* (variant late infantile), NPC -/-(Niemann-Pick Type C), NAGLU (Sanfilippo B), GALC (Krabbe disease), CLN8/mnd (Northern epilepsy), and PPT2 -/- (unknown). In Figure 2.9C, lane 1, only heterozygous littermate controls were available for analysis (designated +/-). Each lane represents 10% of a single whole brain. Three brains from each model (and an equal number of littermate controls) were analyzed. (D) Quantitation of LLO profiles determined by densitometric scanning of FACE gels. Values shown represent mean ± standard error of the mean.

4.4 Discussion

In the present study, a 15-fold elevation of lipid-linked oligosaccharide (LLO) intermediates was demonstrated in the brains (and lesser increases in other tissues) of mice representing models of neuronal ceroid lipofuscinosis. The LLOs represent intermediates in a catabolic pathway, as determined by structural characterization through enzymatic digestion and FACE analysis. The rate of incorporation of [^{3}H] mannose into new LLO synthesis in brain and liver microsomes of *CLN1/PPT1* -/- mice was normal, as was the rate of oligosaccharide discharge from LLO to an oligosaccharyltransferase acceptor peptide, again supporting the idea that the accumulation of LLOs is related to a defect in LLO degradation rather than synthesis or transfer. Excess LLOs co-localized with autofluorescent CsCl purified storage material from *CLN1/PPT1* -/- mouse brain and sedimented in the heavy lysosome-like fraction rather than the microsomal fraction. Quantitative analysis showed that the LLOs constituted only a minor proportion of the autofluorescent storage material (0.3 %) by mass. The accumulation of LLOs was age-dependent and specific for mouse models of

NCL (CLN1, CLN2, CLN3, CLN 6 and CLN8) and not seen in three mouse models of other lysosomal storage disorders (Niemann Pick type C, Sanfilippo syndrome type B, and Krabbe disease).

In several respects, I have confirmed and extended earlier studies performed on brain material obtained at autopsy from NCL patients in the era before NCL genetics were defined. The quantitation of LLOs in the storage material measured in brain tissue from human (Daniel *et al.* 1992) and mouse (this study) were remarkably similar (13.7 nmol/g vs. 17.2 ± 1.4 nmol/g and 2.1 ± 1.9 nmol/g vs. 1.2 ± 0.7 nmol/g for infantile NCL/CLN1 and normal brain, respectively). The dolichol-phosphate content measured in two infantile NCL brain samples (0.3 and 0.37% by mass) (Hall *et al.* 1989) agree well with our estimation of LLO from CsCl purified storage material from CLN1 mouse brain (0.3%). The results in this chapter confirm that LLO does not constitute a major portion of the mass of the material.

The structural characterization of LLOs in mouse CLN1 brain was also consistent with experiments performed by others (Daniel *et al.* 1992; Hall *et al.* 1992) and support the conclusion that these LLOs represent catabolic rather than synthetic intermediates. In this study, I was, in addition, able to cleanly separate the abnormal catabolic products from the normal synthetic products by differential centrifugation, with the catabolic intermediates pelleting in the dense fraction and the normal intermediates fractionating as expected in the 100,000 X g microsomal fraction.

In a previous studies, no differences in incorporation of [^{3}H]-mannose or oligosaccharidyl transferase (OST) activity were found in cells derived from JNCL as compared to control cells (Hall *et al.* 1992; Van Dessel *et al.* 1992). The results in this

chapter have confirmed the normal incorporation of [^{3}H] mannose into brain and liver

microsomes prepared from CLN1 mice. In addition, it has been shown that there was no

block in transfer of the oligosaccharide from dolichol-PP to nascent protein, because the

discharge rate of LLOs onto an acceptor peptide was normal. Thus, the failure to transfer as a

mechanism for accumulation of LLO is ruled out in this form of NCL.

Why might catabolic LLOs accumulate in NCL tissues? Any model must account for

the appearance of LLOs in the dense fraction, the complete absence of glucosyl residues, and

the partial loss of mannosyl residues. A potential explanation for the appearance of LLOs in

dense membranes may be autophagocytosis. The lipofuscin pigments and residual storage

bodies observed in NCL have structural properties reminiscent of autophagolysosomes,

sometimes containing clear morphological evidence of partially autolyzed mitochondria or

other organelles. These 'tertiary lysosomes' are believed to form from the fusion of

autophagosomes and mature lysosomes as a late step in the process of autophagy (Dunn

1990; Cuervo *et al.* 1998; Kim *et al.* 2000). In the NCLs, the metabolism or removal of these

autophagolysosomes appears to be inhibited. Although the origin of autophagocytic

membrane is not yet clear (Dunn 1990; Klionsky *et al.* 2000), it has been suggested that the

formation of autophagic vacuoles is initiated from the membranes of rough endoplasmic

reticulum (RER) (Dunn 1990) which is also the site of LLO synthesis and transfer to

proteins. Therefore, it is likely that 'catabolic' LLOs accumulating in NCLs are derived from

autophagocytic membranes, and that the accumulation of LLO in the NCLs may result from

their over-representation in membranes (such as RER) destined for autophagocytic removal.

An alternative explanation may be that a small fraction of the LLO pool is always missorted

to lysosomes and rapidly degraded. However, due to a lysosomal dysfunction in NCL (see below) these LLOs would accumulate as storage material.

Degradation of $Man_9GlcNAc_2$-P-P-dolichol would normally be expected to be carried out by lysosomal α-mannosidase, a housekeeping enzyme. The optimal physiological pH for lysosomal α-mannosidase is 4.5 (Merkle *et al.* 1997; Stinchi *et al.* 1999). However, it has been reported that lysosomal pH in fibroblasts derived from NCLs is elevated by as much as 1 pH unit (Holopainen *et al.* 2001). Perhaps the lysosomal pH is insufficient to ensure complete degradation of LLOs at this step. Alternatively, it is possible that the $Man_{5-9}GlcNAc_2$-P-P-dolichol forms aggregates, or are in some other way inaccessible to lysosomal α-mannosidase. It is also plausible that one of the other storage products (for example, in the case of PPT1 a palmitoylated peptide) acts as a mannosidase inhibitor.

The absence of glucosyl residues from the accumulated LLOs in PPT1 defective tissue may simply indicate that deglucosylation occurs efficiently in the dense membranes. Alternatively, for some reason the LLOs in dense membranes may be selectively derived from non-glucosylated LLOs generated from the pool of $Man_9GlcNAc_2$-P-P-dolichol that is normally present in equilibrium with $Glc_3Man_9GlcNAc_2$-P-P-dolichol as a result of the glucosytransferase-glucosidase shuttle in the ER (Spiro *et al.* 1991).

CHAPTER FIVE

Conclusions and Future Directions

In this dissertation, I have cloned and characterized *pdf1*, an ortholog of *PPT1* in *S. pombe*, by ablating the gene and determining the consequences of inactivating mutations in the Ppt1p and Dolpp1p domains independently through plasmid complementation assays. It was demonstrated that *pdf1* ablation causes lethality, and that Dolpp1p alone can rescue the lethal phenotype. It was also shown that cells containing no functional copy of Ppt1p are abnormally sensitive to sodium orthovanadate and elevated external pH, which are phenotypes associated with vacuolar dysfunction in yeast. Furthermore, I have demonstrated that Pdf1p in *S. pombe* expressed as a single polypeptide with the orthologs of human *PPT1* and mouse *DOLPP1*. However, these two proteins are post-translationally processed into two independent proteins. By immunoblotting yeast extracts with antibodies that recognize the carboxyl terminus of Pdf1p, I have provided evidence that Pdf1p is produced as a precursor protein that is cleaved to two separate polypeptides, probably as a result of a kex-related protease, Krp1. Finally, it has been shown that a human *PPT1* cDNA is able to complement the phenotypes of Ppt1p deficiency, demonstrating that *S. pombe* provides a new genetic model for the study of Batten disease.

I have also cloned mouse *DOLPP1* gene from a mouse brain cDNA library, which encodes a dolichol pyrophosphatase 1. The mouse *DOLPP1* has been confirmed to complement the defects in growth and protein *N*-glycosylation, and to correct the accumulation of Dol-P-P in the *cwh8Δ* yeast mutant. Northern blot analysis has demonstrated

a wide distribution of the *DOLPP1* mRNA in mouse tissues. In COS cells, overexpression of Dolpp1p has produced substantial increases in Dol-P-P phosphatase activity but not in dolichyl monophosphate or phosphatidic acid phosphatase activities in microsomal fractions. Subcellular fractionation and immunofluorescence studies have localized the enzyme encoded by *DOLPP1* to the endoplasmic reticulum of COS cells. The results of protease sensitivity studies with microsomal vesicles from the *lpp1Δ/dpp1Δ* yeast mutant expressing *DOLPP1* are consistent with Dolpp1p having a luminally oriented active site. The sequence of the *DOLPP1* cDNA predicts a polypeptide with 238 amino acids, and a new polypeptide corresponding to 27 kDa has been observed when *DOLPP1* is expressed in COS cells. I have presented the first identification and characterization of a cDNA clone encoding an essential component of a mammalian lipid pyrophosphate phosphatase that is highly specific for Dol-P-P.

Finally I have examined brain and tissue samples from the five well-defined genetic mouse models of the NCLs and other mouse models of lysosomal storage disorders with central nervous system neurodegenerative phenotypes using a newly developed fluorophore-assisted carbohydrate electrophoresis (FACE) technique to analyze the characteristics of the LLO in these well-defined specimens. I have confirmed that LLO accumulate to high levels in five types of NCL but not in three non-NCL lysosomal storage disorders. I have characterized these in detail in *CLN1/PPT1* -/- mice. There was an age-dependent accumulation of LLO, which are highly enriched in storage material yet constitute only a small fraction (0.3%) of its mass. Detailed structural characterization revealed that the LLO

are consistent with catabolic products, and the increase in LLOs in the *CLN1/PPT1* -/- mouse brain is confined to non-glucosylated intermediates ($Man_{5-9}GlcNAc_2$).

In conclusion, the data presented in this dissertation describe that Ppt1p and Dolpp1p are functioning as independent polypeptides, and no direct interaction between the two is evident in higher eukaryotic cells. Although the gene structure of pdf1 in *S. pombe* suggested a certain degree of interaction between Ppt1p and Dolpp1p, it was demonstrated that the two proteins are processed post-translationally and probably localized in different compartments. Furthermore, subcellular localization studies of mouse Dolpp1p demonstrated that Dolpp1p is localized in the ER membrane (PPT1 is a soluble lysosomal enzyme). Therefore, it is less likely that these two proteins are physically interacting in higher eukaryotic cells. Finally, the analysis of the accumulation of lipid linked oligosaccharides (LLOs) in infantile NCL using PPT1 knockout mouse model has revealed that those LLOs are the accumulation of 'catabolic' products rather than that of 'metabolic' intermediates, which might be caused by defects in dolichol recycling. Therefore, it is more likely that the abnormal dolichol metabolism in infantile NCL results as a secondary phenotype of lysosomal dysfunction triggered by PPT1 deficiency, rather than an effect directly from Dolpp1p function.

Future studies into the molecular mechanisms of infantile NCL could address several interesting questions. First, how do LLOs accumulate in the storage material during the neuropathogenesis of infantile NCL? As I discussed earlier, it would be worthwhile to investigate whether autophagy plays a role during the development of the disorder. Mouse embryonic fibroblasts (MEF) from PPT1 null mutant mice are an important tool for this kind of studies. It will be interesting to see whether LLOs accumulate in autophagic vacuoles that

are induced by vinblastine or other drugs that blocks autophagy in wild type and the PPT1

deficient cells.

Are LLOs substrates for Dolpp1p? And is Dolpp1p activity normal in PPT1 deficient

tissues? Preliminary data have shown that Dolpp1p activity in PPT1 deficient mouse brain

was reduced. The assays should be repeated to provide a more definitive answer for these

questions. One improvement that could be made would be to separate out the catabolic LLOs

(in the non-ER, lysosomal fraction) from the microsomal fraction by differential

centrifugation. In this way, possible interference by the accumulated LLOs can be prevented

during the enzyme assay for Dolpp1p activity.

Another question is what are the direct, physiological substrates of PPT1 *in vivo*?

PPT1 deficiency should lead to the accumulation of acylated peptides in the lysosomes of

affected brain tissues. It has been shown that [^{35}S] cysteine-labeled lipid thioesters derived

from fatty acylated proteins accumulate in lymphoblastoid cells derived from infantile NCL

patients (Lu *et al.* 1996). These metabolically radio-labeled lipids from PPT1-deficient

infantile NCL lymphoblastoid cells are separated as five distinctive bands by high-

performance thin layer chromatography (TLC). These infantile NCL specific bands are

associated with the dense lysosomal fraction and the accumulation of these infantile NCL

specific thioesters are corrected by incubating the patient's lymphoblastoid cells with

recombinant PPT1 in prior to the metabolic labeling (Lu *et al.* 1996; Lu *et al.* 2002).

There have been attempts to purify those infantile NCL specific, metabolically radio-

labeled thioesters from the patient's cells. However, the efforts are not fruitful so far mainly

because the mass of the accumulated thioesters in the cells is too low. The storage material

accumulated in infantile NCL is extremely heterogeneous. Furthermore, the major

component of the storage material has not yet been elucidated. As I have demonstrated,

accumulated LLOs constitute only a minor portion (0.3% by mass) of the autofluorescent

storage material in the PPT1 deficient mouse. Therefore, in order to identify the

physiological substrate for PPT1, it is necessary to use a method that can specifically

separate the substrate from the heterogeneous, hydrophobic storage material. One possibility

is to use of biotin-streptavidin system. Biotinylated-HPDP (hexyl-3'-(2'pyridyldithio-

propionamide)) can be useful because HPDP is able to react with the thiol groups in the

putative PPT1 substrates (acylated small peptides) in the storage material (Jaffrey *et al.*

2001a; Jaffrey *et al.* 2001b). If this works, the molecule trapped by biotin-streptavidin will be

identified by mass spectrometry.

I have shown that the mutations on dibasic motifs in the linker domain of *pdf1*, the *S.*

pombe ortholog of PPT1, completely impair the posttranslational processing. Another

question that remains to be answered is how impairment of the post-translational processing

affects the function of *pdf1*. So, it will be interesting to see whether this impairment affects

the function of Ppt1p and Dolpp1p individually. The preliminary observation was that the

cells harboring the double mutants (R344A, R354A) were significantly growth retarded

compared to the cells harboring wild type plasmid. It would be also interesting to see whether

the PPT active site mutants and the processing mutants cause any LLO accumulation in *S.*

pombe. LLO profiling by FACE analysis in yeast has not been reported and it would be

worthwhile to verify the profile of LLO intermediates in these mutants.

I have shown that the *S. pombe* system can be used as a model organism for infantile NCL. To further extend the benefit of this lower eukaryotic model system, it will be necessary to construct mutant strains that have PPT active site mutations integrated into the chromosomal allele. Once these mutant strains are constructed, then suppressor screening can be done by transforming human cDNA library to discover human gene(s) that complement the vacuolar dysfunction phenotypes of *S. pombe*. The analysis of suppressor genes may provide a clue as to the mechanism of infantile NCL.

There are many gaps to be filled understanding how PPT1 deficiency leads to neurodegeneration in affected children. I have valuable information that can be used to fill these gaps. However, more pieces are required to solve this puzzle. That effort will lead to a better understanding of the neuropathogenesis of infantile NCL and will eventually elucidate the molecular mechanisms of infantile NCL.

REFERENCES

Alfa, C. E., I. M. Gallagher and J. S. Hyams (1993). "Antigen localization in fission yeast." *Methods Cell Biol* 37: 201-22.

Allen, C. M., Jr., J. R. Kalin, J. Sack and D. Verizzo (1978). "CTP-dependent dolichol phosphorylation by mammalian cell homogenates." *Biochemistry* 17(23): 5020-6.

Anand, M., J. S. Rush, S. Ray, M. A. Doucey, J. Weik, F. E. Ware, J. Hofsteenge, C. J. Waechter and M. A. Lehrman (2001). "Requirement of the Lec35 gene for all known classes of monosaccharide-P-dolichol-dependent glycosyltransferase reactions in mammals." *Mol Biol Cell* 12(2): 487-501.

Appelkvist, E. L. and A. Kalen (1989). "Biosynthesis of dolichol by rat liver peroxisomes." *Eur J Biochem* 185(3): 503-9.

Bankaitis, V. A., L. M. Johnson and S. D. Emr (1986). "Isolation of yeast mutants defective in protein targeting to the vacuole." *Proc Natl Acad Sci U S A* 83(23): 9075-9.

Banta, L., J. Robinson, D. Klionsky and S. Emr (1988). "Organelle assembly in yeast: characterization of yeast mutants defective in vacuolar biogenesis and protein sorting." *J. Cell Biol.* 107(4): 1369-1383.

Bartlett, G. R. (1959). "Phosphorus assay in column chromatography." *J Biol Chem* 234(3): 466-8.

Beeley, J. G. (1985). Glycoprotein and proteoglycan techniques. Amsterdam, Elsevier.

Bellizzi, J. J., J. Widom, C. Kemp, J.-Y. Lu, A. K. Das, S. L. Hofmann and J. Clardy (2000). "The crystal structure of palmitoyl protein thioesterase 1 and the molecular basis of infantile neuronal ceroid lipofuscinosis." *PNAS* 97(9): 4573-4578.

Bernstein, M., F. Kepes and R. Schekman (1989). "Sec59 encodes a membrane protein required for core glycosylation in Saccharomyces cerevisiae." *Mol Cell Biol* 9(3): 1191-9.

Bible, E., P. Gupta, S. L. Hofmann and J. D. Cooper (2004). "Regional and cellular neuropathology in the palmitoyl protein thioesterase-1 null mutant mouse model of infantile neuronal ceroid lipofuscinosis." *Neurobiol Dis* 16(2): 346-59.

Blommaart, E. F., J. J. Luiken and A. J. Meijer (1997). "Autophagic proteolysis: control and specificity." *Histochem J* 29(5): 365-85.

Bolivar, V. J., J. Scott Ganus and A. Messer (2002). "The development of behavioral abnormalities in the motor neuron degeneration (mnd) mouse." *Brain Res* 937(1-2): 74-82.

Bronson, R. T., B. D. Lake, S. Cook, S. Taylor and M. T. Davisson (1993). "Motor neuron degeneration of mice is a model of neuronal ceroid lipofuscinosis (Batten's disease)." *Ann Neurol* 33(4): 381-5.

Bronson, R. T., L. R. Donahue, K. R. Johnson, A. Tanner, P. W. Lane and J. R. Faust (1998). "Neuronal ceroid lipofuscinosis (nclf), a new disorder of the mouse linked to chromosome 9." *Am J Med Genet* 77(4): 289-97.

Burda, P. and M. Aebi (1999). "The dolichol pathway of N-linked glycosylation." *Biochimica et Biophysica Acta (BBA) - General Subjects* 1426(2): 239-257.

Burke, J. D. and K. L. Gould (1994). "Molecular cloning and characterization of the Schizosaccharomyces pombe his3 gene for use as a selectable marker." *Mol Gen Genet* 242(2): 169-76.

Cacan, R., S. Duvet, O. Labiau, A. Verbert and S. S. Krag (2001). "Monoglucosylated oligomannosides are released during the degradation process of newly synthesized glycoproteins." *J Biol Chem* 276(25): 22307-12.

Calero, G., P. Gupta, M. C. Nonato, S. Tandel, E. R. Biehl, S. L. Hofmann and J. Clardy (2003). "The crystal structure of palmitoyl protein thioesterase-2 (PPT2) reveals the basis for divergent substrate specificities of the two lysosomal thioesterases, PPT1 and PPT2." *J Biol Chem* 278(39): 37957-64.

Camp, L., L. Verkruyse, S. Afendis, C. Slaughter and S. Hofmann (1994). "Molecular cloning and expression of palmitoyl-protein thioesterase." *J. Biol. Chem.* 269(37): 23212-23219.

Camp, L. A., P. Chauhan, J. D. Farrar and M. A. Lehrman (1993a). "Defective mannosylation of glycosylphosphatidylinositol in Lec35 Chinese hamster ovary cells." *J Biol Chem* 268(9): 6721-8.

Camp, L. A. and S. L. Hofmann (1993b). "Purification and properties of a palmitoyl-protein thioesterase that cleaves palmitate from H-Ras." *J Biol Chem* 268(30): 22566-74.

Carroll, K. K., N. Guthrie and K. Ravi (1992). "Dolichol: function, metabolism, and accumulation in human tissues." *Biochem Cell Biol* 70(6): 382-4.

Carson, D., B. Earles and W. Lennarz (1981). "Enhancement of protein glycosylation in tissue slices by dolichylphosphate." *J. Biol. Chem.* 256(22): 11552-11557.

Casey, P. J. (1995). "Protein lipidation in cell signaling." *Science* 268(5208): 221-5.

Cataldo, A., P. Paskevich, E. Kominami and R. Nixon (1991). "Lysosomal Hydrolases of Different Classes are Abnormally Distributed in Brains of Patients with Alzheimer Disease." *PNAS* 88(24): 10998-11002.

Cha, J.-H., J. S. Brooke, K. N. Ivey and L. Eidels (2000). "Cell Surface Monkey CD9 Antigen Is a Coreceptor That Increases Diphtheria Toxin Sensitivity and Diphtheria Toxin Receptor Affinity." *J. Biol. Chem.* 275(10): 6901-6907.

Chattopadhyay, S., N. E. Muzaffar, F. Sherman and D. A. Pearce (2000). "The yeast model for batten disease: mutations in btn1, btn2, and hsp30 alter pH homeostasis [In Process Citation]." *J Bacteriol* 182(22): 6418-23.

Cho, S. K. and S. L. Hofmann (2004). "pdf1, a palmitoyl protein thioesterase 1 Ortholog in Schizosaccharomyces pombe: a yeast model of infantile Batten disease." *Eukaryot Cell* 3(2): 302-10.

Clarke, P. G. (1990). "Developmental cell death: morphological diversity and multiple mechanisms." *Anat Embryol (Berl)* 181(3): 195-213.

Cohen, L. H., M. Griffioen, C. W. van Roermund and R. J. Wanders (1992). "Subcellular localization of squalene synthase in human hepatoma cell line Hep G2." *Biochim Biophys Acta* 1126(1): 114-8.

Cottone, C. D., S. Chattopadhyay and D. A. Pearce (2001). "Searching for interacting partners of CLN1, CLN2 and Btn1p with the two-hybrid system." *Eur J Paediatr Neurol* 5 Suppl A: 95-8.

Crick, D. C., J. R. Scocca, J. S. Rush, D. W. Frank, S. S. Krag and C. J. Waechter (1994a). "Induction of dolichyl-saccharide intermediate biosynthesis corresponds to increased long chain cis-isoprenyltransferase activity during the mitogenic response in mouse B cells." *J Biol Chem* 269(14): 10559-65.

Crick, D. C. and C. J. Waechter (1994b). "Long-chain cis-isoprenyltransferase activity is induced early in the developmental program for protein N-glycosylation in embryonic rat brain cells." *J Neurochem* 62(1): 247-56.

Cuervo, A. M. and J. F. Dice (1998). "Lysosomes, a meeting point of proteins, chaperones, and proteases." *J Mol Med* 76(1): 6-12.

Daniel, P. F., D. L. Sauls and R. M. Boustany (1992). "Evidence for processing of dolichol-linked oligosaccharides in patients with neuronal ceroid-lipofuscinosis." *Am J Med Genet* 42(4): 586-92.

Danilov, L. L., T. N. Druzhinina, N. A. Kalinchuk, S. D. Maltsev and V. N. Shibaev (1989). "Polyprenyl phosphates: synthesis and structure-activity relationship for a biosynthetic system of Salmonella anatum O-specific polysaccharide." *Chem Phys Lipids* 51(3-4): 191-203.

Das, A. K., C. H. Becerra, W. Yi, J. Y. Lu, A. N. Siakotos, K. E. Wisniewski and S. L. Hofmann (1998). "Molecular genetics of palmitoyl-protein thioesterase deficiency in the U.S." *J Clin Invest* 102(2): 361-70.

Das, A. K., J. Y. Lu and S. L. Hofmann (2001). "Biochemical analysis of mutations in palmitoyl-protein thioesterase causing infantile and late-onset forms of neuronal ceroid lipofuscinosis." *Hum Mol Genet* 10(13): 1431-9.

Davey, J., K. Davis, Y. Imai, M. Yamamoto and G. Matthews (1994). "Isolation and characterization of krp, a dibasic endopeptidase required for cell viability in the fission yeast Schizosaccharomyces pombe." *EMBO J.* 13(24): 5910-5921.

Davis, L. and G. R. Smith (2001). "Meiotic recombination and chromosome segregation in Schizosaccharomyces pombe." *PNAS* 98(15): 8395-8402.

Dunn, W. A., Jr. (1990). "Studies on the mechanisms of autophagy: formation of the autophagic vacuole." *J Cell Biol* 110(6): 1923-33.

Dunn, W. A., Jr. (1994). "Autophagy and related mechanisms of lysosome-mediated protein degradation." *Trends Cell Biol* 4(4): 139-43.

Dunphy, P. J., J. D. Kerr, J. F. Pennock, K. J. Whittle and J. Feeney (1967). "The plurality of long chain isoprenoid alcohols (polyprenols) from natural sources." *Biochim Biophys Acta* 136(1): 136-47.

Eggens, I., L. C. Eriksson, T. Chojnacki and G. Dallner (1984). "Role of dolichyl phosphate in regulation of protein glycosylation in 2-acetylaminofluorene-induced carcinogenesis in rat liver." *Cancer Res* 44(2): 799-805.

Faulkner, A., X. Chen, J. Rush, B. Horazdovsky, C. J. Waechter, G. M. Carman and P. C. Sternweis (1999). "The LPP1 and DPP1 Gene Products Account for Most of the Isoprenoid Phosphate Phosphatase Activities in Saccharomyces cerevisiae." *J. Biol. Chem.* 274(21): 14831-14837.

Fernandez, F., J. S. Rush, D. A. Toke, G.-s. Han, J. E. Quinn, G. M. Carman, J.-Y. Choi, D. R. Voelker, M. Aebi and C. J. Waechter (2001). "The CWH8 Gene Encodes a Dolichyl Pyrophosphate Phosphatase with a Luminally Oriented Active Site in the Endoplasmic Reticulum of Saccharomyces cerevisiae." *J. Biol. Chem.* 276(44): 41455-41464.

Fernandez, F., P. Shridas, S. Jiang, M. Aebi and C. J. Waechter (2002). "Expression and characterization of a human cDNA that complements the temperature-sensitive defect in dolichol kinase activity in the yeast sec59-1 mutant: the enzymatic phosphorylation of dolichol and diacylglycerol are catalyzed by separate CTP-mediated kinase activities in Saccharomyces cerevisiae." *Glycobiology* 12(9): 555-562.

Gao, H., R. M. Boustany, J. A. Espinola, S. L. Cotman, L. Srinidhi, K. A. Antonellis, T. Gillis, X. Qin, S. Liu, L. R. Donahue, R. T. Bronson, J. R. Faust, D. Stout, J. L. Haines, T. J. Lerner and M. E. MacDonald (2002a). "Mutations in a Novel CLN6-Encoded Transmembrane Protein Cause Variant Neuronal Ceroid Lipofuscinosis in Man and Mouse." *Am J Hum Genet* 70(2): 324-35.

Gao, N. and M. A. Lehrman (2002b). "Analyses of dolichol pyrophosphate-linked oligosaccharides in cell cultures and tissues by fluorophore-assisted carbohydrate electrophoresis." *Glycobiology* 12(5): 353-60.

Gao, N. and M. A. Lehrman (2002c). "Coupling of the dolichol-P-P-oligosaccharide pathway to translation by perturbation-sensitive regulation of the initiating enzyme, GlcNAc-1-P transferase." *J Biol Chem* 277(42): 39425-35.

Gao, N. and M. A. Lehrman (2003). "Alternative and sources of reagents and supplies of fluorophore-assisted carbohydrate electrophoresis(FACE)." *Glycobiology* 13(1): 1G-3G.

Glaser, R. L., A. J. Hickey, H. L. Chotkowski and Q. Chu-LaGraff (2003). "Characterization of Drosophila palmitoyl-protein thioesterase 1." *Gene* 312: 271-9.

Goebel, H. H. (1995). "The neuronal ceroid-lipofuscinoses." *J Child Neurol* 10(6): 424-37.

Graham, J. (1984). Isolation of subcellular organelles and membranes. Centrifugation: A practical approach. D. Rickwood. Oxford, IRL Press**:** 161-182.

Grunler, J., J. Ericsson and G. Dallner (1994). "Branch-point reactions in the biosynthesis of cholesterol, dolichol, ubiquinone and prenylated proteins." *Biochim Biophys Acta* 1212(3): 259-77.

Gupta, P., A. A. Soyombo, A. Atashband, K. E. Wisniewski, J. M. Shelton, J. A. Richardson, R. E. Hammer and S. L. Hofmann (2001). "Disruption of PPT1 or PPT2 causes neuronal ceroid lipofuscinosis in knockout mice." *Proc Natl Acad Sci U S A* 98(24): 13566-71.

Gupta, P., A. A. Soyombo, J. M. Shelton, I. G. Wilkofsky, K. E. Wisniewski, J. A. Richardson and S. L. Hofmann (2003). "Disruption of PPT2 in mice causes an unusual

lysosomal storage disorder with neurovisceral features." *Proc Natl Acad Sci U S A* 100(21): 12325-30.

Hall, N. A. and A. D. Patrick (1985). "Dolichol and phosphorylated dolichol content of tissues in ceroid-lipofuscinosis." *J Inherit Metab Dis* 8(4): 178-83.

Hall, N. A. and A. D. Patrick (1987). "Accumulation of phosphorylated dolichol in several tissues in ceroid-lipofuscinosis (Batten disease)." *Clin Chim Acta* 170(2-3): 323-30.

Hall, N. A. and A. D. Patrick (1988). "Accumulation of dolichol-linked oligosaccharides in ceroid-lipofuscinosis (Batten disease)." *Am J Med Genet Suppl* 5: 221-32.

Hall, N. A., B. D. Lake, D. N. Palmer, R. D. Jolly and A. D. Patrick (1989). "Glycoconjugates in storage cytosomes from ceroid-lipofuscinosis (Batten's disease) and in lipofuscin from old-age brain." *Adv Exp Med Biol 266:225-41*.

Hall, N. A., J. E. Thomas-Oates, A. Dell, M. Haltia, B. D. Lake and A. D. Patrick (1992). "Stored dolichyl pyrophosphoryl oligosaccharides in Batten disease." *Am J Med Genet* 42(4): 580-5.

Harford, J. B., C. J. Waechter and F. L. Earl (1977). "Effect of exogenous dolichyl monophosphate on a developmental change in mannosylphosphoryldolichol biosynthesis." *Biochem Biophys Res Commun* 76(4): 1036-43.

Harford, J. B. and C. J. Waechter (1980). "A developmental change in dolichyl phosphate mannose synthase activity in pig brain." *Biochem J* 188(2): 481-90.

Helenius, J., D. T. Ng, C. L. Marolda, P. Walter, M. A. Valvano and M. Aebi (2002). "Translocation of lipid-linked oligosaccharides across the ER membrane requires Rft1 protein." *Nature* 415(6870): 447-50.

Heller, L., P. Orlean and W. L. Adair, Jr. (1992). "Saccharomyces cerevisiae sec59 cells are deficient in dolichol kinase activity." *Proc Natl Acad Sci U S A* 89(15): 7013-6.

Hellsten, E., J. Vesa, V. M. Olkkonen, A. Jalanko and L. Peltonen (1996). "Human palmitoyl protein thioesterase: evidence for lysosomal targeting of the enzyme and disturbed cellular routing in infantile neuronal ceroid lipofuscinosis." *EMBO J.* 15(19): 5240-5.

Hemming, F. W. (1992). "Dolichol: a curriculum cognitionis." *Biochem Cell Biol* 70(6): 377-81.

Herscovics, A. and P. Orlean (1993). "Glycoprotein biosynthesis in yeast." *FASEB J.* 7(6): 540-550.

Hochstrasser, M. (1996). "Ubiquitin-dependent protein degradation." *Annu Rev Genet* 30: 405-39.

Hofmann, S. L., L. A. Lee, J. Y. Lu and L. A. Verkruyse (1997). "Palmitoyl-protein thioesterase and the molecular pathogenesis of infantile neuronal ceroid lipofuscinosis." *Neuropediatrics* 28(1): 27-30.

Hofmann, S. L., A. K. Das, W. Yi, J. Y. Lu and K. E. Wisniewski (1999). "Genotype-Phenotype Correlations in Neuronal Ceroid Lipofuscinosis Due to Palmitoyl-Protein Thioesterase Deficiency." *Mol Genet Metab* 66(4): 234-239.

Hofmann, S. L., A. K. Das, J. Y. Lu, K. E. Wisniewski and P. Gupta (2001a). "Infantile neuronal ceroid lipofuscinosis: no longer just a 'Finnish' disease." *Europ J Paediatr Neurol* 5(Suppl A): 47-51.

Hofmann, S. L. and L. Peltonen (2001b). The Neuronal Ceroid Lipofuscinoses. <u>The Metabolic and Molecular Bases of Inherited Disease</u>. C. R. Scriver, A. L. Beaudet, W. S. Sly, B. Childs and B. Vogelstein. New York, McGraw-Hill. 8.

Hofmann, S. L. (2002). Batten Disease. <u>Fundamental Neuroscience</u>. L. R. Squire. San Diego, Academic Press**:** ?

Hofmann, S. L., A. Atashband, S. K. Cho, A. K. Das, P. Gupta and J. Y. Lu (2002). "Neuronal ceroid lipofuscinoses caused by defects in soluble lysosomal enzymes (CLN1 and CLN2)." *Curr Mol Med* 2(5): 423-37.

Holopainen, J. M., J. Saarikoski, P. K. Kinnunen and I. Jarvela (2001). "Elevated lysosomal pH in neuronal ceroid lipofuscinoses (NCLs)." *Eur J Biochem* 268(22): 5851-6.

Humaloja, K., R. P. Roine, K. Salmela, E. Halmesmaki, K. Jokelainen and M. Salaspuro (1991). "Serum dolichols in different clinical conditions." *Scand J Clin Lab Invest* 51(8): 705-9.

Humphrey, T. (2000). "DNA damage and cell cycle control in Schizosaccharomyces pombe." *Mutation Research/Fundamental and Molecular Mechanisms of Mutagenesis* 451(1-2): 211-226.

Imperiali, B. and T. L. Hendrickson (1995). "Asparagine-linked glycosylation: specificity and function of oligosaccharyl transferase." *Bioorg Med Chem* 3(12): 1565-78.

Inoue, S., H. Sano and M. Ohta (2000). "Growth suppression of Escherichia coli by induction of expression of mammalian genes with transmembrane or ATPase domains." *Biochem Biophys Res Commun* 268(2): 553-61.

Iwaki, T., F. Osawa, M. Onishi, T. Koga, Y. Fujita, A. Hosomi, N. Tanaka, Y. Fukui and K. Takegawa (2003). "Characterization of vps33+, a gene required for vacuolar biogenesis and protein sorting in Schizosaccharomyces pombe." *Yeast* 20(10): 845-55.

Jaffrey, S. R., H. Erdjument-Bromage, C. D. Ferris, P. Tempst and S. H. Snyder (2001a). "Protein S-nitrosylation: a physiological signal for neuronal nitric oxide." *Nat Cell Biol* 3(2): 193-7.

Jaffrey, S. R. and S. H. Snyder (2001b). "The biotin switch method for the detection of S-nitrosylated proteins." *Sci STKE* 2001(86): PL1.

Jarvela, I. (1991). "Infantile neuronal ceroid lipofuscinosis (CLN1): linkage disequilibrium in the Finnish population and evidence that variant late infantile form (variant CLN2) represents a nonallelic locus." *Genomics* 10(2): 333-7.

Jokelainen, K., K. S. Salmela, K. Humaloja, R. Roine, S. Autio, M. Arvio, I. Jarvela, I. Nykanen, J. Palo and M. Salaspuro (1992). "Blood dolichol in lysosomal diseases." *Biochem Cell Biol* 70(6): 481-5.

Kato, K., C. J. Der and J. E. Buss (1992). "Prenoids and palmitate: lipids that control the biological activity of Ras proteins." *Semin Cancer Biol* 3(4): 179-88.

Katz, M. L., H. Shibuya, P. C. Liu, S. Kaur, C. L. Gao and G. S. Johnson (1999). "A mouse gene knockout model for juvenile ceroid-lipofuscinosis (batten disease) [In Process Citation]." *J Neurosci Res* 57(4): 551-6.

Keller, R. K., D. Armstrong, F. C. Crum and N. Koppang (1984). "Dolichol and dolichyl phosphate levels in brain tissue from English setters with ceroid lipofuscinosis." *J Neurochem* 42(4): 1040-7.

Kerr, J. F., A. H. Wyllie and A. R. Currie (1972). "Apoptosis: a basic biological phenomenon with wide-ranging implications in tissue kinetics." *Br J Cancer* 26(4): 239-57.

Khalfan, W. A. and D. J. Klionsky (2002). "Molecular machinery required for autophagy and the cytoplasm to vacuole targeting (Cvt) pathway in S. cerevisiae." *Current Opinion in Cell Biology* 14(4): 468-475.

Kim, J. and D. J. Klionsky (2000). "Autophagy, cytoplasm-to-vacuole targeting pathway, and pexophagy in yeast and mammalian cells." *Annu Rev Biochem* 69: 303-42.

Kitamoto, K., K. Yoshizawa, Y. Ohsumi and Y. Anraku (1988). "Mutants of Saccharomyces cerevisiae with defective vacuolar function." *J Bacteriol* 170(6): 2687-91.

Klionsky, D. J., P. K. Herman and S. D. Emr (1990). "The fungal vacuole: composition, function, and biogenesis." *Microbiol Rev* 54(3): 266-92.

Klionsky, D. J. and S. D. Emr (2000). "Autophagy as a regulated pathway of cellular degradation." *Science* 290(5497): 1717-21.

Kopacek, J., S. Sakaguchi, K. Shigematsu, N. Nishida, R. Atarashi, R. Nakaoke, R. Moriuchi, M. Niwa and S. Katamine (2000). "Upregulation of the genes encoding lysosomal hydrolases, a perforin-like protein, and peroxidases in the brains of mice affected with an experimental prion disease." *J Virol* 74(1): 411-7.

Korey, C. A. and M. E. MacDonald (2003). "An over-expression system for characterizing Ppt1 function in Drosophila." *BMC Neurosci* 4(1): 30.

Kornfeld, R. and S. Kornfeld (1985). "Assembly of asparagine-linked oligosaccharides." *Annu Rev Biochem* 54: 631-64.

Kufs, H. (1925). "Uber eine spatform der amaurotischcen idiotie and ihre heredofamiliaren grundlagen." *Z. Ges. Neurol Psychiartr.* 95: 169-188.

Lerner, T. J., R. N. Boustany, J. W. Anderson, K. D. D'Arigo, K. Schlumpf, A. J. Buckler, J. F. Gusella, J. L. Haines, G. Kremmidiotis, I. L. Lensink, G. R. Sutherland, D. F. Callen, P. E. M. Taschner, N. deVos, G.-J. B. van Ommen, M. H. Breuning, N. A. Doggett, L. J. Meincke, Z.-Y. Liu, L. A. Goodwin, J. G. Tesmer, H. M. Mitchison, A. M. O'Rawe, P. B. Munroe, I. E. Jarvela, R. M. Gardiner and S. E. Mole (1995). "Isolation of a novel gene underlying Batten disease, CLN3 (The International Batten Disease Consortium)." *Cell* 82: 949-957.

Li, H. H., W. H. Yu, N. Rozengurt, H. Z. Zhao, K. M. Lyons, S. Anagnostaras, M. S. Fanselow, K. Suzuki, M. T. Vanier and E. F. Neufeld (1999). "Mouse model of Sanfilippo syndrome type B produced by targeted disruption of the gene encoding alpha-N-acetylglucosaminidase." *Proc Natl Acad Sci U S A* 96(25): 14505-10.

Liang, D. T. and S. L. Forsburg (2001). "Characterization of Schizosaccharomyces pombe mcm7(+) and cdc23(+) (MCM10) and interactions with replication checkpoints." *Genetics* 159(2): 471-86.

Loftus, S. K., J. A. Morris, E. D. Carstea, J. Z. Gu, C. Cummings, A. Brown, J. Ellison, K. Ohno, M. A. Rosenfeld, D. A. Tagle, P. G. Pentchev and W. J. Pavan (1997). "Murine model of Niemann-Pick C disease: mutation in a cholesterol homeostasis gene." *Science* 277(5323): 232-5.

Lu, J. Y., L. A. Verkruyse and S. L. Hofmann (1996). "Lipid thioesters derived from acylated proteins accumulate in infantile neuronal ceroid lipofuscinosis: correction of the

defect in lymphoblasts by recombinant palmitoyl-protein thioesterase." *Proc Natl Acad Sci U S A* 93(19): 10046-50.

Lu, J. Y., L. A. Verkruyse and S. L. Hofmann (2002). "The effects of lysosomotropic agents on normal and INCL cells provide further evidence for the lysosomal nature of palmitoyl-protein thioesterase function." *Biochim Biophys Acta* 1583(1): 35-44.

Lucas, J. J. and E. Levin (1977). "Increase in the lipid intermediate pathway of protein glycosylation during hen oviduct differentiation." *J Biol Chem* 252(12): 4330-6.

Luzi, P., M. A. Rafi, M. Zaka, M. Curtis, M. T. Vanier and D. A. Wenger (2001). "Generation of a mouse with low galactocerebrosidase activity by gene targeting: a new model of globoid cell leukodystrophy (Krabbe disease)." *Mol Genet Metab* 73(3): 211-23.

Merkle, R. K., Y. Zhang, P. J. Ruest, A. Lal, Y. F. Liao and K. W. Moremen (1997). "Cloning, expression, purification, and characterization of the murine lysosomal acid alpha-mannosidase." *Biochim Biophys Acta* 1336(2): 132-46.

Mitchell, W. A., R. B. Wheeler, J. D. Sharp, S. L. Bate, R. M. Gardiner, U. S. Ranta, L. Lonka, R. E. Williams, A. E. Lehesjoki and S. E. Mole (2001). "Turkish variant late infantile neuronal ceroid lipofuscinosis (CLN7) may be allelic to CLN8." *Europ J Paediatr Neurol* 5(Suppl A): 21-7.

Mitchison, H. M., D. J. Bernard, N. D. Greene, J. D. Cooper, M. A. Junaid, R. K. Pullarkat, N. de Vos, M. H. Breuning, J. W. Owens, W. C. Mobley, R. M. Gardiner, B. D. Lake, P. E. Taschner and R. L. Nussbaum (1999). "Targeted disruption of the Cln3 gene provides a mouse model for Batten disease." *Neurobiol Dis* 6(5): 321-34.

Mitchison, H. M. and S. E. Mole (2001). "Neurodegenerative disease: the neuronal ceroid lipofuscinoses (Batten disease)." *Curr Opin Neurol* 14(6): 795-803.

Mitchison, H. M., M. J. Lim and J. D. Cooper (2004). "Selectivity and types of cell death in the neuronal ceroid lipofuscinoses." *Brain Pathol* 14(1): 86-96.

Monti, J. A., S. T. Christian and J. S. Schutzbach (1987). "Effects of dolichol on membrane permeability." *Biochim Biophys Acta* 905(1): 133-42.

Moreno, S., A. Klar and P. Nurse (1991). "Molecular genetic analysis of fission yeast Schizosaccharomyces pombe." *Methods Enzymol* 194: 795-823.

Mortimore, G. E. and A. R. Poso (1987). "Intracellular protein catabolism and its control during nutrient deprivation and supply." *Annu Rev Nutr* 7: 539-64.

Munafo, D. B. and M. I. Colombo (2001). "A novel assay to study autophagy: regulation of autophagosome vacuole size by amino acid deprivation." *J Cell Sci* 114(20): 3619-3629.

Munafo, D. B. and M. I. Colombo (2002). "Induction of Autophagy Causes Dramatic Changes in the Subcellular Distribution of GFP-Rab24." *Traffic* 3(7): 472-482.

Nelson, H. and N. Nelson (1990). "Disruption of genes encoding subunits of yeast vacuolar H(+)-ATPase causes conditional lethality." *Proc Natl Acad Sci U S A* 87(9): 3503-7.

Ng Ying Kin, N. M., J. Palo, M. Haltia and L. S. Wolfe (1983). "High levels of brain dolichols in neuronal ceroid-lipofuscinosis and senescence." *J Neurochem* 40(5): 1465-73.

Oluwatosin, Y. E. and P. M. Kane (1998). "Mutations in the yeast KEX2 gene cause a Vma(-)-like phenotype: a possible role for the Kex2 endoprotease in vacuolar acidification." *Mol Cell Biol* 18(3): 1534-43.

Palmer, D. N., G. Barns, D. R. Husbands and R. D. Jolly (1986). "Ceroid lipofuscinosis in sheep. II. The major component of the lipopigment in liver, kidney, pancreas, and brain is low molecular weight protein." *J Biol Chem* 261(4): 1773-7.

Pan, Y. T. and A. D. Elbein (1990). "Control of N-linked oligosaccharide synthesis: cellular levels of dolichyl phosphate are not the only regulatory factor." *Biochemistry* 29(35): 8077-84.

Pearce, D. A. and F. Sherman (1997). "BTN1, a yeast gene corresponding to the human gene responsible for Batten's disease, is not essential for viability, mitochondrial function, or degradation of mitochondrial ATP synthase." *Yeast* 13(8): 691-7.

Pearce, D. A. and F. Sherman (1998). "A yeast model for the study of Batten disease." *Proc Natl Acad Sci U S A* 95(12): 6915-8.

Pearce, D. A., C. J. Carr, B. Das and F. Sherman (1999a). "Phenotypic reversal of the btn1 defects in yeast by chloroquine: a yeast model for Batten disease." *Proc Natl Acad Sci U S A* 96(20): 11341-5.

Pearce, D. A., T. Ferea, S. A. Nosel, B. Das and F. Sherman (1999b). "Action of BTN1, the yeast orthologue of the gene mutated in Batten disease." *Nat Genet* 22(1): 55-8.

Pearce, D. A. (2000). "Localization and processing of CLN3, the protein associated to Batten disease: where is it and what does it do?" *J Neurosci Res* 59(1): 19-23.

Pennock, J. F., F. W. Hemming and R. A. Morton (1960). "Dolichol: a naturally occurring isoprenoid alcohol." *Nature* 186: 470-2.

Powner, D. and J. Davey (1998). "Activation of the kexin from Schizosaccharomyces pombe requires internal cleavage of its initially cleaved prosequence." *Mol Cell Biol* 18(1): 400-8.

Pullarkat, R. K. and H. Reha (1982). "Accumulation of dolichols in brains of elderly." *J Biol Chem* 257(11): 5991-3.

Pullarkat, R. K., H. Reha and P. S. Pullarkat (1984). "Age-associated increase of free dolichol levels in mice." *Biochim Biophys Acta* 793(3): 494-6.

Ranta, S., Y. Zhang, B. Ross, L. Lonka, E. Takkunen, A. Messer, J. Sharp, R. Wheeler, K. Kusumi, S. Mole, W. Liu, M. B. Soares, M. F. Bonaldo, A. Hirvasniemi, A. de la Chapelle, T. C. Gilliam and A. E. Lehesjoki (1999). "The neuronal ceroid lipofuscinoses in human EPMR and mnd mutant mice are associated with mutations in CLN8." *Nat Genet* 23(2): 233-6.

Rickwood, D., T. Ford and J. Graham (1982). "Nycodenz: a new nonionic iodinated gradient medium." *Anal Biochem* 123(1): 23-31.

Robinson, J. S., D. J. Klionsky, L. M. Banta and S. D. Emr (1988). "Protein sorting in Saccharomyces cerevisiae: isolation of mutants defective in the delivery and processing of multiple vacuolar hydrolases." *Mol Cell Biol* 8(11): 4936-48.

Rodriguez-Vico, F., M. Martinez-Cayuela, E. Garcia-Peregrin and H. Ramirez (1989). "A procedure for eliminating interferences in the lowry method of protein determination." *Anal Biochem* 183(2): 275-8.

Rothman, J. H. and T. H. Stevens (1986). "Protein sorting in yeast: mutants defective in vacuole biogenesis mislocalize vacuolar proteins into the late secretory pathway." *Cell* 47(6): 1041-51.

Rush, J. and C. Waechter (1998). "Topological studies on the enzymes catalyzing the biosynthesis of Glc-P- dolichol and the triglucosyl cap of Glc3Man9GlcNAc2-P-P-dolichol in microsomal vesicles from pig brain: use of the processing glucosidases I/II as latency markers." *Glycobiology* 8(12): 1207-1213.

Rush, J. S., S. K. Cho, S. Jiang, S. L. Hofmann and C. J. Waechter (2002). "Identification and characterization of a cDNA encoding a dolichyl pyrophosphate phosphatase located in the endoplasmic reticulum of mammalian cells." *J Biol Chem* 277(47): 45226-34.

Sakai, Y., A. Koller, L. K. Rangell, G. A. Keller and S. Subramani (1998). "Peroxisome degradation by microautophagy in Pichia pastoris: identification of specific steps and morphological intermediates." *J Cell Biol* 141(3): 625-36.

Sakakihara, Y., T. Imabayashi, Y. Suzuki and S. Kamoshita (1994). "Elevated levels of dolichol in the brains of mucopolysaccharidosis and related disorders." *Mol Chem Neuropathol* 22(2): 97-103.

Salonen, T., E. Hellsten, N. Horelli-Kuitunen, L. Peltonen and A. Jalanko (1998). "Mouse palmitoyl protein thioesterase: gene structure and expression of cDNA." *Genome Res* 8(7): 724-30.

Sambrook, J., E. F. Fritsch and T. Maniatis (1989). <u>Molecular Cloning: A Laboratory Manual</u>. Cold Spring Harbor, NY, Cold Spring Harbor Laboratory Press.

Sato, T. K., P. Rehling, M. R. Peterson and S. D. Emr (2000). "Class C Vps protein complex regulates vacuolar SNARE pairing and is required for vesicle docking/fusion." *Mol Cell* 6(3): 661-71.

Savukoski, M., M. Kestila, R. Williams, I. Jarvela, J. Sharp, J. Harris, P. Santavuori, M. Gardiner and L. Peltonen (1994). "Defined chromosomal assignment of CLN5 demonstrates that at least four genetic loci are involved in the pathogenesis of human ceroid lipofuscinoses." *Am J Hum Genet* 55(4): 695-701.

Savukoski, M., T. Klockars, V. Holmber, P. Santavuori, E. S. Lander and L. Peltonen (1998). "CLN5, a novel gene encoding a putative transmembrane protein mutated in the Finnish variant late infantile neuronal ceroid lipofuscinosis (vLINCL)." *Nature Genetics* 19: 286-288.

Schedin, S., P. G. Pentchev, U. Brunk and G. Dallner (1995). "Changes in the Levels of Dolichol and Dolichyl Phosphate in a Murine Model of Niemann-Pick's Type C Disease." *J Neurochem* 65(2): 670-676.

Schenk, B., F. Fernandez and C. J. Waechter (2001). "The ins(ide) and out(side) of dolichyl phosphate biosynthesis and recycling in the endoplasmic reticulum." *Glycobiology* 11(5): 61R-70R.

Scher, M. and C. Waechter (1984a). "Brain dolichyl pyrophosphate phosphatase. Solubilization, characterization, and differentiation from dolichyl monophosphate phosphatase activity." *J. Biol. Chem.* 259(23): 14580-14585.

Scher, M. G., G. H. Devries and C. J. Waechter (1984b). "Subcellular sites of enzymes catalyzing the phosphorylation-dephosphorylation of dolichol in the central nervous system." *Arch Biochem Biophys* 231(2): 293-302.

Schiestl, R. H. and R. D. Gietz (1989). "High efficiency transformation of intact yeast cells using single stranded nucleic acids as a carrier." *Curr Genet* 16(5-6): 339-46.

Schriner, J. E., W. Yi and S. L. Hofmann (1996). "cDNA and genomic cloning of human palmitoyl-protein thioesterase (PPT), the enzyme defective in infantile neuronal ceroid lipofuscinosis [published erratum appears in Genomics 1996 Dec 15;38(3):458]." *Genomics* 34(3): 317-22.

Schweichel, J. U. and H. J. Merker (1973). "The morphology of various types of cell death in prenatal tissues." *Teratology* 7(3): 253-66.

Seals, D. F., G. Eitzen, N. Margolis, W. T. Wickner and A. Price (2000). "A Ypt/Rab effector complex containing the Sec1 homolog Vps33p is required for homotypic vacuole fusion." *Proc Natl Acad Sci U S A* 97(17): 9402-7.

Seglen, P. O. and P. Bohley (1992). "Autophagy and other vacuolar protein degradation mechanisms." *Experientia* 48(2): 158-72.

Sharp, J. D., R. B. Wheeler, B. D. Lake, M. Savukoski, I. E. Jarvela, L. Peltonen, R. M. Gardiner and R. E. Williams (1997). "Loci for classical and a variant late infantile neuronal ceroid lipofuscinosis map to chromosomes 11p15 and 15q21-23." *Hum Mol Genet* 6(4): 591-5.

Sherman, M. Y. and P. J. Muchowski (2003). "Making yeast tremble: yeast models as tools to study neurodegenerative disorders." *Neuromolecular Med* 4(1-2): 133-46.

Silberstein, S. and R. Gilmore (1996). "Biochemistry, molecular biology, and genetics of the oligosaccharyltransferase." *FASEB J.* 10(8): 849-858.

Sleat, D. E., R. J. Donnelly, H. Lackland, C. G. Liu, I. Sohar, R. K. Pullarkat and P. Lobel (1997). "Association of mutations in a lysosomal protein with classical late-infantile neuronal ceroid lipofuscinosis." *Science* 277(5333): 1802-5.

Spiro, M. and R. Spiro (1986). "Control of N-linked carbohydrate unit synthesis in thyroid endoplasmic reticulum by membrane organization and dolichyl phosphate availability." *J. Biol. Chem.* 261(31): 14725-14732.

Spiro, M. J. and R. G. Spiro (1991). "Potential regulation of N-glycosylation precursor through oligosaccharide-lipid hydrolase action and glucosyltransferase-glucosidase shuttle." *J Biol Chem* 266(8): 5311-7.

Spiro, M. J. and R. G. Spiro (2000). "Use of recombinant endomannosidase for evaluation of the processing of N-linked oligosaccharides of glycoproteins and their oligosaccharide-lipid precursors." *Glycobiology* 10(5): 521-9.

Stamellos, K., J. Shackelford, I. Shechter, G. Jiang, D. Conrad, G. Keller and S. Krisans (1993). "Subcellular localization of squalene synthase in rat hepatic cells. Biochemical and immunochemical evidence." *J. Biol. Chem.* 268(17): 12825-12836.

Stengel, C. (1826). Account of a singular illness among four siblings in the vicinity of Roraas. Ceroid-Lipofuscinosis (Batten's Disease). e. a. D. Armstrong. Amsterdam, Elsevier Biomedical Press 1982**:** 17-19. Translated from: Beretning om et maerkeligt Sygdomstilfoelde hos fire Sodskende I Naeheden af Rorass, Eyr et medicinsk Tidskrift 1, 347-352.

Stinchi, S., R. Lullmann-Rauch, D. Hartmann, R. Coenen, T. Beccari, A. Orlacchio, K. von Figura and P. Saftig (1999). "Targeted disruption of the lysosomal alpha-mannosidase gene results in mice resembling a mild form of human alpha-mannosidosis." *Hum Mol Genet* 8(8): 1365-72.

Studdert, V. P. and R. W. Mitten (1991). "Clinical features of ceroid lipofuscinosis in border collie dogs." *Aust Vet J* 68(4): 137-40.

Stukey, J. and G. M. Carman (1997). "Identification of a novel phosphatase sequence motif." *Protein Sci* 6(2): 469-472.

Takegawa, K., D. B. DeWald and S. D. Emr (1995). "Schizosaccharomyces pombe Vps34p, a phosphatidylinositol-specific PI 3-kinase essential for normal cell growth and vacuole morphology." *J Cell Sci* 108 (Pt 12): 3745-56.

Takeshige, K., M. Baba, S. Tsuboi, T. Noda and Y. Ohsumi (1992). "Autophagy in yeast demonstrated with proteinase-deficient mutants and conditions for its induction." *J Cell Biol* 119(2): 301-11.

Thumm, M., R. Egner, B. Koch, M. Schlumpberger, M. Straub, M. Veenhuis and D. H. Wolf (1994). "Isolation of autophagocytosis mutants of Saccharomyces cerevisiae." *FEBS Lett* 349(2): 275-80.

Toke, D. A., W. L. Bennett, D. A. Dillon, W.-I. Wu, X. Chen, D. B. Ostrander, J. Oshiro, A. Cremesti, D. R. Voelker, A. S. Fischl and G. M. Carman (1998). "Isolation and Characterization of the Saccharomyces cerevisiae DPP1 Gene Encoding Diacylglycerol Pyrophosphate Phosphatase." *J. Biol. Chem.* 273(6): 3278-3284.

Toke, D. A., M. L. McClintick and G. M. Carman (1999). "Mutagenesis of the phosphatase sequence motif in diacylglycerol pyrophosphate phosphatase from Saccharomyces cerevisiae." *Biochemistry* 38(44): 14606-13.

Trumpower, B. L., R. M. Houser and R. E. Olson (1974). "Studies on Ubiquinone. DEMONSTRATION OF THE TOTAL BIOSYNTHESIS OF UBIQUINONE-9 IN RAT LIVER MITOCHONDRIA." *J. Biol. Chem.* 249(10): 3041-3048.

Tsukada, M. and Y. Ohsumi (1993). "Isolation and characterization of autophagy-defective mutants of Saccharomyces cerevisiae." *FEBS Letters* 333(1-2): 169-174.

Tyynela, J., D. N. Palmer, M. Baumann and M. Haltia (1993). "Storage of saposins A and D in infantile neuronal ceroid-lipofuscinosis." *FEBS Lett* 330(1): 8-12.

Tyynela, J., I. Sohar, D. E. Sleat, R. M. Gin, R. J. Donnelly, M. Baumann, M. Haltia and P. Lobel (2000). "A mutation in the ovine cathepsin D gene causes a congenital lysosomal storage disease with profound neurodegeneration." *Embo J* 19(12): 2786-92.

Valtersson, C., G. van Duyn, A. J. Verkleij, T. Chojnacki, B. de Kruijff and G. Dallner (1985). "The influence of dolichol, dolichol esters, and dolichyl phosphate on phospholipid polymorphism and fluidity in model membranes." *J Biol Chem* 260(5): 2742-51.

van Berkel, M., M. Rieger, S. te Heesen, A. Ram, H. van den Ende, M. Aebi and F. Klis (1999). "The Saccharomyces cerevisiae CWH8 gene is required for full levels of dolichol-linked oligosaccharides in the endoplasmic reticulum and for efficient N-glycosylation." *Glycobiology* 9(3): 243-253.

Van Dessel, G., A. Lagrou, H. Hilderson and W. Dierick (1992). "Dolichyl-pyrophosphoryloligosaccharide protein oligosaccharide transferase in neuronal ceroid-lipofuscinosis." *Biochem Cell Biol* 70(6): 515-8.

Verkruyse, L. A. and S. L. Hofmann (1996). "Lysosomal Targeting of Palmitoyl-protein Thioesterase." *J. Biol. Chem.* 271(26): 15831-15836.

Verkruyse, L. A., M. R. Natowicz and S. L. Hofmann (1997). "Palmitoyl-protein thioesterase deficiency in fibroblasts of individuals with infantile neuronal ceroid lipofuscinosis and I-cell disease." *Biochimica et Biophysica Acta* 1361: 1-5.

Vesa, J., E. Hellsten, L. A. Verkruyse, L. A. Camp, J. Rapola, P. Santavuori, S. L. Hofmann and L. Peltonen (1995). "Mutations in the palmitoyl protein thioesterase gene causing infantile neuronal ceroid lipofuscinosis." *Nature* 376(6541): 584-7.

Voet, D. and J. G. Voet (1990). Lpid Metabolism. Biochemistry. New York, Chichester, Brisbane, Toronto, Singapore, John Wiley and Sons. Chapter 23**:** 618-677.

Wheeler, R. B., J. D. Sharp, R. A. Schultz, J. M. Joslin, R. E. Williams and S. E. Mole (2002). "The gene mutated in variant late-infantile neuronal ceroid lipofuscinosis (CLN6)

and in nclf mutant mice encodes a novel predicted transmembrane protein." *Am J Hum Genet* 70(2): 537-42.

Wisniewski, K. E. and N. Zhong (2001a). "Batten Disease: Diagnosis, Treatment and Research (Appendix: Batten Support Groups)." *Advances in Genetics* 45: 225-236.

Wisniewski, K. E., E. Kida, A. A. Golabek, W. Kaczmarski and N. Zhong (2001b). Neuronal Ceroid Lipofuscinoses: Classification and Diagnosis. Batten Disease: Diagnosis, Treatment, and Research. K. E. Wisniewski, Zhong, N. San Diego, San Francisco, New York, Boston, London, Sydney, Tokyo, Academic Press**:** 1-34.

Wolf, M., J. Rush and C. Waechter (1991). "Golgi-enriched membrane fractions from rat brain and liver contain long- chain polyisoprenyl pyrophosphate phosphatase activity." *Glycobiology* 1(4): 405-410.

Wolfe, L., N. Ng Ying Kin, J. Palo and M. Haltia (1983). "Dolichols in brain and urinary sediment in neuronal ceroid lipofuscinosis." *Neurology* 33(1): 103-106.

Wolfe, L. S., S. Gauthier, M. Haltia and J. Palo (1988). "Dolichol and dolichyl phosphate in the neuronal ceroid-lipofuscinoses and other diseases." *Am J Med Genet* Suppl 5: 233-242.

Wong, T., G. Decker and W. Lennarz (1982a). "Localization of dolichol in the lysosomal fraction of rat liver." *J. Biol. Chem.* 257(11): 6614-6618.

Wong, T. and W. Lennarz (1982b). "The site of biosynthesis and intracellular deposition of dolichol in rat liver." *J. Biol. Chem.* 257(11): 6619-6624.

Wood, V., R. Gwilliam, M.-A. Rajandream, M. Lyne, R. Lyne, A. Stewart, J. Sgouros, N. Peat, J. Hayles, S. Baker, D. Basham, S. Bowman, K. Brooks, D. Brown, S. Brown, T. Chillingworth, C. Churcher, M. Collins, R. Connor, A. Cronin, P. Davis, T. Feltwell, A. Fraser, S. Gentles, A. Goble, N. Hamlin, D. Harris, J. Hidalgo, G. Hodgson, S. Holroyd, T. Hornsby, S. Howarth, E. J. Huckle, S. Hunt, K. Jagels, K. James, L. Jones, M. Jones, S. Leather, S. McDonald, J. McLean, P. Mooney, S. Moule, K. Mungall, L. Murphy, D. Niblett, C. Odell, K. Oliver, S. O'Neil, D. Pearson, M. A. Quail, E. Rabbinowitsch, K. Rutherford, S. Rutter, D. Saunders, K. Seeger, S. Sharp, J. Skelton, M. Simmonds, R. Squares, S. Squares, K. Stevens, K. Taylor, R. G. Taylor, A. Tivey, S. Walsh, T. Warren, S. Whitehead, J. Woodward, G. Volckaert, R. Aert, J. Robben, B. Grymonprez, I. Weltjens, E. Vanstreels, M. Rieger, M. Schafer, S. Muller-Auer, C. Gabel, M. Fuchs, C. Fritzc, E. Holzer, D. Moestl, H. Hilbert, K. Borzym, I. Langer, A. Beck, H. Lehrach, R. Reinhardt, T. M. Pohl, P. Eger, W. Zimmermann, H. Wedler, R. Wambutt, B. Purnelle, A. Goffeau, E. Cadieu, S. Dreano, S. Gloux, V. Lelaure, S. Mottier, F. Galibert, S. J. Aves, Z. Xiang, C. Hunt, K. Moore, S. M. Hurst, M. Lucas, M. Rochet, C. Gaillardin, V. A. Tallada, A. Garzon, G. Thode, R. R. Daga, L. Cruzado, J. Jimenez, M. Sanchez, F. del

Rey, J. Benito, A. Dominguez, J. L. Revuelta, S. Moreno, J. Armstrong, S. L. Forsburg, L. Cerrutti, T. Lowe, W. R. McCombie, I. Paulsen, J. Potashkin, G. V. Shpakovski, D. Ussery, B. G. Barrell and P. Nurse (2002). "The genome sequence of Schizosaccharomyces pombe." *Nature* 415(6874): 871-880.

Wood, W. G., C. Gorka, L. S. Williamson, R. Strong, A. Y. Sun, G. Y. Sun and F. Schroeder (1986). "Dolichol alters dynamic and static properties of mouse synaptosomal plasma membranes." *FEBS Lett* 205(1): 25-8.

Yoshida, S. and Y. Anraku (2000). "Characterization of staurosporine-sensitive mutants of Saccharomyces cerevisiae: vacuolar functions affect staurosporine sensitivity." *Mol Gen Genet* 263(5): 877-88.

Yuan, J. and B. A. Yankner (2000). "Apoptosis in the nervous system." *Nature* 407(6805): 802-9.

Yuan, W., D. L. Tuttle, Y. J. Shi, G. S. Ralph and W. A. Dunn, Jr. (1997). "Glucose-induced microautophagy in Pichia pastoris requires the alpha-subunit of phosphofructokinase." *J Cell Sci* 110 (Pt 16): 1935-45.

Zeman, W. and P. Dyken (1969). "Neuronal ceroid-lipofuscinosis (Batten's disease). Relationship to amaurotic familial idiocy?" *Pediatrics* 44: 570-583.

Zeng, Y. C. and M. A. Lehrman (1990). "A block at Man5GlcNAc2-pyrophosphoryldolichol in intact but not disrupted castanospermine and swainsonine-resistant Chinese hamster ovary cells." *J Biol Chem* 265(4): 2296-305.

Vitae

Steve Kyungrae Cho was born in Busan, Korea, on September 4th, 1968, the first son of Dr. In Jae Cho and Mrs. Jung Soon Cho. After graduating from Young Dong High School in Seoul, Korea in 1987, he entered Han Yang University in Seoul, Korea. After completing the first two years of college, in 1989, he decided to pursue his education further in the United States. He received the degree of Bachelor of Science with a major in Biochemistry from University of California at Los Angeles in June, 1994. During his senior year, he joined the laboratory of Dr. H. Philip Koeffler at UCLA School of Medicine (Division of Hematology-Oncology, Cedars-Sinai Medical Center) as a student research fellow. After receiving his B.S. degree, he continued to work as a research associate in Dr. Koeffler's lab for two more years. In August, 1996, he entered the Graduate School of Biomedical Sciences at the University of Texas Southwestern Medical Center at Dallas. After one year of study at the division of cell and molecular biology, he joined the laboratory of Dr. Sandra Hofmann, a professor of Internal Medicine and Molecular Genetics, for his dissertation work and received the Ph.D. degree in August 2004. In 1996, he married to Judy Cho and they have two children, Timothy and Rachel. Timothy was born in April 1997 and Rachel was born in September 2001.

Permanent Address: 9220 Forest Hills Drive, Irving, TX 75063

This dissertation was typed by Steve K. Cho.